UCLouvain

AGRO LOUVAIN

Faculté des bioingénieurs

Maize (*Zea mays*) hydraulic responses to water deficit in controlled conditions

Author: Francis MULLIGAN
Supervisor: Valentin COUVREUR
Co-supervisor: Mathieu JAVAUX
Readers: Guillaume LOBET, Muriel QUINET
Academic year: 2023-2024

Master's thesis presented to obtain the Bioengineer diploma in agronomic science

Acknowledgments

I would like to begin by expressing my deepest gratitude to my supervisor, Valentin Couvreur, for the opportunity to contribute to his research. His guidance, insightful feedback, patience, and encouragement have been invaluable throughout this journey. His leadership and kindness in supervising this thesis have made this experience both enriching and enjoyable. I am also thankful to my co-supervisor, Mathieu Javaux, for his essential support in providing the necessary materials and for the assistance offered by his PhD students.

My sincere thanks go to the readers, Guillaume Lobet and Muriel Quinet, for agreeing to review this master's thesis. Your willingness to engage with this work and the time you have given is deeply appreciated, and I wish you an enjoyable read.

A heartfelt thank you to Thomas Dagbert for his support and companionship during the preparation of the experiment and data collection. Your help, along with the moments shared over discussions and jokes, made this process much more enjoyable; as a result, you certainly deserve that I keep the "carnet" to myself. I also want to thank Sébastien François and Olivier Lebbe for their assistance, kindness, and advice. My gratitude goes to Marc Migon for his availability and support, particularly in adjusting the settings of the phytotron amidst numerous requests.

I am grateful to Adrien Heymans for his help during the experiment preparation—despite the unfortunate incident of the spilled plant, everything turned out well in the end, and no hard feelings were held. Thanks to Marco D'Agostino for his assistance and friendly presence, and to Moustapha Kolawole for stepping in during the measurements and taking over the second experiment.

My gratitude extends to Lei Ding for teaching me how to use the HPFM and for his assistance during the measurements, and to Tianjiao Wei for her help and explanations regarding the psychrometers. I also want to thank Andrea Cecere for her guidance and support, and to Salomé Lengrand for providing the soil that was crucial for launching the experiment. I am thankful to François Chaumont's lab for their generous donation of maize seeds, and to Xavier Draye for his valuable discussions and advice regarding the experiment.

I want to acknowledge the entire Pepa team for creating a pleasant and supportive atmosphere in the lab. Your remarks, advice, and shared moments, whether in seminars, the cafeteria, or solving puzzles together, have been greatly appreciated.

On a more personal note, I wish to thank all my siblings for their support: Marie, Anthony, Nell, Sophie, Philomène, Brigitte, Joseph, and Jacinthe. A special thanks to Marie Mulligan and Rone Rodrigues for hosting me when I needed a change of scenery. My gratitude also goes to Philomène Mulligan for being a listening ear and for the vacations spent together, and to Joseph Mulligan for his motivating projects and for keeping me on track with my to-do list. As recommended in the Ten Commandments, I shall honour my father and mother: thank you to my mother, Christine Pieters, for her encouragement and support, and to my father, Stephen Mulligan, and his wife, Omayma Abu El Khair Masoud, for their warm hospitality and presence.

Finally, I extend my heartfelt thanks to my chosen family—my friends. Thank you to Renaud Bulpa, Alexis Fanchon, Justine Bourgois, Xavier Belin, Sophie Lecop, Aline Fockedey, and Margot Beelaert, for their encouragement, moral support, and the moments of distraction.

Thank you all, and to all those who have directly or indirectly helped me and are not named here.

Table of contents

List of figures

1. Introduction

Agriculture is vital to human survival, providing essential food and resources that sustain our global population. Approximately 37% of the world's land is dedicated to agriculture, contributing around 80% of the calories consumed globally (FAO et al., 2024). Water is crucial for agriculture, with about 70% of global water withdrawals used for this purpose (UNESCO World Water Assessment Programme, 2024). It plays key roles in plant growth, including photosynthesis, nutrient transport, and maintaining cell turgor pressure for structural support (Taiz et al., 2015). Water deficit, which occurs when there is an imbalance between soil water availability and evaporative demand, results in reduced carbon accumulation, diminished tissue expansion, and fewer cells (Tardieu et al., 2011).

Drought is a climatic phenomenon characterized by prolonged periods of abnormally low rainfall, leading to water shortages. This results in a significant decline in the availability of water in soil, groundwater, and surface water, impacting ecosystems, agriculture, and human societies. Water scarcity occurs when there is a prolonged imbalance between the demand for water and its available supply (WMO, 2022). Plants suffer from water deficit when the available water is insufficient to meet their needs for transpiration and growth (Draye et al., 2010).

Drought severely affects agriculture by reducing soil moisture, impairing plant growth, and diminishing crop yields. Given that agriculture heavily depends on water, drought can lead to widespread crop failures and threaten food security (FAO, 2023a). Drought is one of the costliest natural disasters, with approximately 1.4 billion people affected between 2002 and 2021 (UNESCO World Water Assessment Programme, 2024). Its consequences extend beyond agriculture, leading to food shortages, increased prices, economic instability, exacerbated hunger, malnutrition, and even triggering population displacement, violence, and political instability (FAO, 2023a).

Climate change is expected to exacerbate the occurrence and intensity of droughts, posing an even greater threat to agriculture and communities worldwide. Rising global temperatures are likely to alter precipitation patterns, leading to more frequent and severe droughts. According to the Intergovernmental Panel on Climate Change (IPCC, 2023), the increase in greenhouse gases is expected to intensify the hydrological cycle, causing more extreme weather events, including prolonged droughts. Changes in seasonal precipitation and higher evaporation rates due to warmer temperatures are projected to reduce water availability, especially in vulnerable regions. This shift presents a significant challenge to agriculture, potentially resulting in decreased crop productivity, more frequent crop failures, and heightened food insecurity (IPCC, 2023).

Understanding how plants respond to water deficits is crucial as droughts become more prevalent and severe. Water deficit impacts plants at multiple levels, from cellular processes to whole-plant physiology, affecting growth, development, and yield (Chaves et al., 2003). A comprehensive understanding of these responses is essential for developing crops that can better withstand drought conditions, thereby ensuring food security in a changing climate. By studying mechanisms of water uptake, transport, and conservation, researchers can identify traits that confer drought resilience, facilitating the breeding or engineering of crops with enhanced drought tolerance (Tardieu, 2012).

Maize (*Zea mays*) is one of the most widely cultivated crops globally, serving as a staple food for millions and a critical component of livestock feed. It is grown on over 197 million hectares of

land, making it one of the most significant cereal crops worldwide (FAO, 2023b). Understanding how maize adapts to water deficits can provide valuable insights into improving its drought tolerance and inform broader agricultural practices and crop management strategies.

A deeper understanding of the mechanisms of water absorption and hydraulic adaptations in maize is crucial for developing crop varieties that are more resilient to water deficits. This knowledge will be a key element in selecting and breeding varieties that can better withstand the increasing challenges posed by climate change and ensure sustainable food production.

2. State of the art

2.1. The Soil-Plant-Atmosphere Continuum (SPAC)

2.1.1. Introduction of the SPAC

The Soil-Plant-Atmosphere Continuum (SPAC) is a model describing the movement of water from the soil, through the plant, and into the atmosphere. This movement is driven by a gradient in water potential, a measure of the potential energy of water, which decreases from the soil, through the plant, and into the atmosphere (Kramer & Boyer, 1995).

Water absorption begins in the soil, where it enters the plant roots primarily through root hairs. The water then moves across root cells and into the xylem, the plant's specialised tissue for long-distance water transport (Tyree & Zimmermann, 2013). Within the xylem, the movement of water is facilitated by cohesion and adhesion forces, as well as the tension created by water evaporating from the leaves (Taiz et al., 2015). This process, often described by the cohesion-tension theory, explains how water is pulled upward against gravity (Brown, 2013). Once in the xylem, water travels upwards towards the leaves, where it is eventually lost to the atmosphere through stomata—small openings on the leaf surface that regulate gas exchange and water vapour loss. This loss of water to the atmosphere, known as transpiration, creates negative pressure within the xylem, further pulling water from the roots to the leaves (Kramer & Boyer, 1995). The rate of transpiration is influenced by several factors, including humidity, temperature, wind, and the plant's stomatal conductance, which is the ability of stomata to open and close (Chaves et al., 2003).

The SPAC can be understood as a series of water potentials, where water moves from one point to another by crossing membranes or travelling through tissues that exhibit a certain level of conductance or resistance. Conductance refers to the ease with which water can move through these pathways, while resistance, being the inverse of conductance, indicates the degree of resistance to water flow (Nobel, 2009).

2.1.2. Component of the SPAC

2.1.2.1. Water potential

Understanding water flow in plants and their surrounding environment requires grasping the concept of water potential, often symbolised by Ψ. Water potential measures the free energy of water per unit volume and determines both the direction and flow rate of water movement within the SPAC (De Swaef et al., 2022).

Water potential is measured in pressure units, typically megapascals (MPa), with pure water at 25°C and atmospheric pressure having a water potential of 0 MPa (H. Jones, 2013). Any deviation from this standard reflects a change in the water's free energy and indicates the potential for water movement.

Water potential represents the combined pressures of water within a system, comprising osmotic potential ($\Psi\pi$), matrix potential (Ψm), hydrostatic or turgor potential ($\Psi\rho$), and gravitational potential (Ψg) (De Swaef et al., 2022).

Osmotic potential (Ψπ) is always negative, as water moves from areas of low to high solute concentration. Matrix potential (Ψm) arises from charged surfaces like soil particles and cell walls, often dominating water potential in soils. Hydrostatic pressure (Ψρ) can be positive, as in turgid cells, or negative, as seen in stressed xylem vessels. Gravitational potential (Ψg), though often ignored, significantly impacts water flow in tall plants, decreasing water potential by 0.1 MPa for every 10 metres of height (Chavarria & dos Santos, 2012).

A. Soil water potential

The soil water potential (SWP) reflects the amount of water in the soil and its availability to plants. It represents the potential energy of water within the soil matrix and determines the direction and rate of water movement between the soil, plants, and the atmosphere (Hillel, 2013).

SWP is primarily influenced by two factors: matric potential (Ψm) and osmotic potential (Ψπ). The total SWP (Ψs) is the sum of these two components:

$\Psi s = \Psi m + \Psi \pi$

Water potential in the soil varies spatially and temporally due to its physical properties and the soil water balance. This balance is affected by inputs such as precipitation and irrigation, and outputs including drainage, evaporation, and root absorption (Hillel, 2013). Soil water potential reflects the combined effects of these factors, influencing water availability to plants and overall soil moisture content.

The water content available for the plants is the water situated between two key points, field capacity and wilting point.

Field capacity (FC) refers to the maximum amount of soil moisture or water content that the soil can hold after being saturated and allowed to drain freely. At FC, the soil retains water against gravitational forces, with excess water having drained away. This measure is essential for understanding the soil's capacity to supply water to plants under typical conditions, and it corresponds to a soil water potential of approximately -0.03 MPa. In natural field conditions, FC describes the water held in the soil profile. In greenhouse pots, where there is no deep soil profile, "pot capacity" is used instead. This term refers to the amount of water remaining in the pot after irrigation and visible drainage have ceased (Kirkham, 2005).

The wilting point (WP) is the soil moisture level at which plants can no longer extract water, leading to irreversible wilting without additional water supply. At this point, the soil water potential is so low that plants cannot maintain turgor pressure, typically estimated at -1.5 MPa (Rai et al., 2017). The WP is influenced by the soil's physical and chemical properties, as well as the specific plant species. Plant species vary in their ability to cope with low soil water content due to factors such as root anatomy, depth, osmotic adjustment capacity, and other drought resistance mechanisms (Chavarria & dos Santos, 2012).

Soil water potential is typically measured using a variety of methods, with tensiometers being among the most common. Tensiometers are devices that measure the matric potential (Ψm) of soil by determining the tension with which soil water is held. They consist of a porous ceramic cup connected to a vacuum gauge or manometer. When the soil dries, water is pulled from the ceramic cup, creating a negative pressure that is recorded by the gauge. The tension in the soil

water can then be directly related to the soil water potential (Hillel, 2013). Tensiometers are particularly useful for measuring soil moisture in the field and are relatively straightforward to use, although their accuracy can be affected by soil texture and calibration.

B. Leaf water potential

Leaf water potential (LWP) is a crucial parameter in plant physiology that reflects the water status within the leaves, influencing the plant's overall water balance and physiological functions. It represents the potential energy of water in the leaf and is a key determinant of water movement from the plant's xylem into the leaf cells and, subsequently, to the atmosphere through transpiration (Taiz et al., 2015). LWP is influenced by several factors, including turgor pressure, osmotic potential, and the water content of the leaf (Tyree & Zimmermann, 2013).

The relationship between these potentials determines the leaf's overall water potential and thus its ability to maintain physiological processes such as photosynthesis and stomatal function. Monitoring leaf water potential provides insights into how plants cope with water stress and can be used to assess plant health and drought resilience (Chaves et al., 2003).

Leaf water potential is commonly measured using two primary techniques: the Scholander pressure chamber and psychrometers. The Scholander pressure chamber, also known as a pressure bomb, is a widely used method that measures turgor pressure directly. In this technique, a leaf or a segment of a stem is placed in a pressure chamber, and the pressure is gradually increased until the sap begins to exude from the cut surface. The pressure applied at this point is equivalent to the leaf's turgor pressure, and the leaf water potential can be calculated by adding this pressure to the leaf's osmotic potential (Scholander et al., 1965). This method is advantageous for its simplicity and ability to provide rapid, direct measurements of the leaf water potential.

Alternatively, psychrometers measure water potential indirectly by assessing the water vapour pressure within the leaf tissue. This method involves placing a small sample of leaf tissue in a sealed chamber and measuring the relative humidity or water vapour pressure. The leaf water potential is inferred from the difference between the water vapour pressure in the leaf tissue and the surrounding air (H. G. Jones & Corlett, 1992). Psychrometers, particularly those based on thermocouple or chilled mirror technology, are useful for obtaining detailed and precise measurements of leaf water potential under varying environmental conditions.

C. Atmosphere water potential

Atmospheric water potential (Ψa) is determined by the vapour pressure of the air, reflecting the moisture content in the atmosphere. Higher vapour pressure indicates higher atmospheric water potential (Buck, 1981). This potential is related to Vapour Pressure Deficit (VPD), the difference between saturated vapour pressure and actual vapour pressure. VPD drives water loss from plants; a high VPD increases transpiration rates and lowers atmospheric water potential (Monteith & Unsworth, 2013).

2.1.2.2. Hydraulic conductance and resistance in plants

Hydraulic conductance (K) is a critical parameter in understanding water movement within plants, soil, and across interfaces between them. It quantifies the ease with which water moves through a given system, whether it be soil, plant tissues, or the xylem. Conversely, hydraulic resistance (R) is the inverse of hydraulic conductance and represents the difficulty of water flow through a system. The relationship between conductance and resistance can be expressed as:

$$K = \frac{1}{R}$$

In plants, hydraulic conductance is a key parameter that describes the efficiency of water transport from the soil through the plant to the atmosphere. This can be assessed at various levels, each providing insight into different aspects of water movement. At the whole plant level, hydraulic conductance reflects the overall efficiency of water transport across all tissues. More specific measures include root conductance, which indicates how well the root system absorbs and transfers water to the plant's vascular system. Xylem conductance focuses on the efficiency of water movement through the plant's long-distance transport tissues, essential for maintaining water flow to the leaves. Finally, stomatal conductance pertains to the regulation of water loss through leaf stomata, influencing transpiration rates and overall plant water balance.

Hydraulic conductance in plants is influenced by several factors including xylem anatomy, the presence of embolisms or air bubbles that can obstruct water flow, and the plant's ability to adjust its stomatal opening in response to environmental conditions. Plants can actively regulate hydraulic conductance through mechanisms such as adjusting the diameter of xylem vessels, closing stomata to reduce water loss, and increasing root growth to enhance water uptake (Tyree & Zimmermann, 2013).

Hydraulic conductance in plant tissues can be measured using the High-Pressure Flow Meter (HPFM) method (Tyree et al., 1995). This technique involves using compressed air to push water through plant tissue until the flow stabilises.

Hydraulic conductivity is often calculated as the ratio of hydraulic conductance to the cross-sectional area through which water flows. Conversely, hydraulic conductance is typically calculated as the ratio of water flow through a sample to the water potential gradient across that sample (Flexas et al., 2013). Therefore, hydraulic conductivity provides a measure of how easily water can move through a given medium, while hydraulic conductance reflects the efficiency of water transport in relation to the area and water potential gradient.

2.1.3. Water fluxes in and out the plant

Water fluxes in and out the plants occur at the root-soil interface, where water is absorbed from the soil, and the leaf-atmosphere interface, where water evaporates through stomata during transpiration (Kramer & Boyer, 1995).

2.1.3.1. Water absorption by roots

Water absorption by roots is the initial step in the SPAC, where water is taken up from the soil and transported through the plant's vascular system. This process is primarily driven by the water potential gradient between the rhizosphere and the root xylem. Two main mechanisms establish

this gradient: a gradient in solute concentration, which induces osmosis, and a gradient in pressure, which drives passive absorption (Kramer & Boyer, 1995).

Passive absorption dominates in plants with high transpiration rates, where the negative pressure created by water loss through the leaves generates tension in the xylem vessels, effectively "pulling" water from the soil into the roots (Mullins et al., 1992). However, some studies challenge this traditional view, reporting instances where roots absorb water even when the water potential in the xylem is higher than at the root surface (Bai et al., 2007; Enns et al., 2000; Rowan et al., 2000; Schenk et al., 2021). These observations suggest that plants might absorb more water than predicted by existing theories. Additionally, recent modeling studies propose that non-uniform osmotic potentials within the symplastic pathway could further complicate traditional theories of root water absorption, leading to deviations from expected radial flow rates (Couvreur et al., 2018). Mathematical findings by Couvreur et al. (2021) together with the experimental observations by Enns et al. (2000), suggest that a hidden osmotic gradient within living cells may drive water flow in a manner previously considered impossible under the current paradigm of water uptake by plant roots.

2.1.3.2. Transpiration

Transpiration is the process through which plants lose water vapor to the atmosphere, primarily through the stomata on their leaves. This process begins when water in the plant's xylem moves into the leaf's intercellular spaces and evaporates into the air. The evaporation creates a water potential gradient, drawing more water from the xylem and roots, thereby maintaining a continuous flow of water from the soil through the plant to the atmosphere. Transpiration is a crucial component of the SPAC, as it influences the water potential gradient between the soil and the plant, regulating water uptake and maintaining plant hydration. Factors such as stomatal conductance, relative humidity, and wind speed affect the rate of transpiration. Stomata regulate water loss by opening and closing in response to environmental conditions, while the boundary layer resistance around the leaf surface also plays a role (Chaves et al., 2003; Nobel, 2009).

Transpiration rates can be measured using a gravimetric method, which involves continuously weighing the plant and its pot. In this method, the plant is grown in a pot with a sensitive scale that records changes in weight over time. The loss of weight corresponds to the amount of water lost through transpiration (Cirelli et al., 2012).

2.2. Water stress

Water stress in plants arises when water availability is insufficient to meet physiological needs. The causes of water stress include water deficit, drought, or high soil salinity, leading to a significant impact on plant growth and productivity Drought, in particular, has always been a major limiting factor for agriculture, threatening food security and economic stability in many regions of the world (King-Okumu, 2021).

2.2.1. Effect of water stress on plants

Water stress affects plants at both the cellular and whole-plant levels, disrupting normal physiological processes and leading to a range of adverse effects. A primary consequence of water stress is the reduction in photosynthesis due to stomatal closure, which limits carbon dioxide intake and thereby decreases the production of photosynthates necessary for plant growth and development (Flexas et al., 2004). Additionally, water stress impairs nutrient uptake from the soil, further exacerbating growth limitations. At the cellular level, dehydration induces osmotic stress, leading to the accumulation of reactive oxygen species (ROS), which can damage vital cellular components such as proteins, lipids, and DNA (Mittler, 2002).

The effects of water stress are also evident at the morphological level. Under water-limited conditions, plants typically exhibit reduced leaf area, fewer and smaller leaves, and inhibited root growth (Farooq et al., 2009). While these morphological changes can be adaptive in reducing water loss, they come at the cost of diminished photosynthetic capacity and overall plant vigour (Lisar et al., 2012).

2.2.2. Plant responses to water stress

Plants have developed various strategies to cope with drought stress, broadly classified into escape, avoidance, and tolerance mechanisms (Seleiman et al., 2021). Escape strategies involve rapid development to complete growth before severe drought conditions (Tadesse & Anteneh, 2018). Avoidance strategies maintain high water potential through reduced transpiration and enhanced water uptake (Dobra et al., 2010). Tolerance strategies allow plants to endure water deficits by adjusting physiological and morphological traits, including changes in leaf area, root system characteristics, and other adaptive mechanisms (Seleiman et al., 2021).

2.2.2.1. Cellular and tissue adjustments

Under water stress, plants experience reduced cell turgor and volume. This leads to an increase in solute concentration, which helps maintain osmotic potential and turgor pressure but can also slow cell growth and expansion. Reduced turgor pressure affects leaf growth, leading to smaller leaf areas, which in turn limits photosynthesis and transpiration, ultimately impacting productivity (Hsiao & Acevedo, 1974; Taiz et al., 2015).

2.2.2.2. Root system adaptations

Plants often develop deeper root systems to access moisture from lower soil layers during drought. Initial root growth is concentrated near the surface, but as the upper soil dries, roots grow deeper to find water. In severe stress, resources may be reallocated from root growth to reproductive structures, potentially reducing water absorption efficiency and affecting plant health (Taiz et al., 2015).

2.2.2.3. Stomatal regulation

Stomatal closure is a primary response to conserve water during drought. While this reduces transpiration and water loss, it also limits gas exchange, affecting photosynthesis and carbon fixation. As soil water potential decreases, stomatal conductance typically decreases as well,

helping to maintain leaf water potential and minimize further water loss (Pirasteh-Anosheh et al., 2016).

2.2.2.4. Isohydric and anisohydric strategies

Plants are categorized into isohydric and anisohydric types based on their water regulation strategies. Isohydric plants maintain a relatively constant leaf water potential by tightly regulating stomatal conductance, helping to prevent excessive dehydration under varying conditions (Tardieu & Simonneau, 1998). In contrast, anisohydric plants allow their leaf water potential to fluctuate with soil water availability, which helps them tolerate variable conditions but can lead to greater stress during prolonged droughts (Tardieu & Simonneau, 1998).

2.3. Maize

Maize, also known as corn (*Zea mays*), is a vital cereal crop and a major staple in global agriculture. Its high production volume underscores its importance for food, livestock feed, and various industrial uses (Erenstein et al., 2022).

As a C4 plant, maize is exceptionally well-adapted to hot and arid environments. This classification enables it to perform photosynthesis efficiently even under intense sunlight and high temperatures. The C4 photosynthetic pathway is notably more water-efficient than the C3 pathway found in many other crops, making maize an ideal subject for studying drought responses (Sage, 2004).

Additionally, research by has shown that maize roots adjust osmotically in response to water deficit. This osmotic adjustment is part of a broader suite of physiological and morphological adaptations maize employs to manage water scarcity. Typically, maize displays isohydric behaviour, maintaining relatively stable leaf water potential despite variations in soil moisture (Tardieu & Simonneau, 1998).

3. Objectives

This master's thesis was conducted as part of the European Research Council (ERC) project "The Plant Water Pump," under the supervision of Prof. Valentin Couvreur. A central aim of this project is to explore the diversity of hydraulic and osmotic responses to water deficit across various crops and trees. Within this broader framework, this thesis specifically focuses on investigating the hydraulic traits of maize under water deficit conditions during its vegetative stage.

This research endeavours to address key questions:

(i) **"How does maize respond to water deficit under controlled conditions during the vegetative stage?"**. This primary question aims to measure various variables related to the plant's water status, such as water potential, transpiration, and conductance. The goal is to capture the dynamic nature of these responses and assess whether these adjustments are sustained after a rewatering phase. This initial experiment also serves as a pilot study, intended to refine the experimental protocol for subsequent research.

(ii) **"How can we effectively manage and process large volumes of data generated from these experiments?".** Given the substantial amount of data produced, especially regarding root surface area measurements and transpiration, this research also aims to develop efficient data management pipelines. These pipelines are designed to facilitate the handling and analysis of complex datasets, which are crucial for accurately interpreting the experimental outcomes.

Thus, the core objective of this thesis is twofold: first, to quantify maize's response to water deficit through an experimental protocol, and second, to establish robust data management pipelines. The insights gained from this initial experiment will not only deepen our understanding of plant responses to water deficit but will also guide the refinement and improvement of protocols for future experiments. This iterative approach aims to ensure that subsequent research is conducted with greater precision and effectiveness, ultimately leading to a more accurate and comprehensive understanding of maize's hydraulic behaviour under water stress.

4. Material and method

As part of this master's thesis, an initial experiment was conducted. The protocol for this experiment is detailed in this section, followed by the presentation and discussion of the results. A second experiment, with a slightly adapted protocol, was subsequently carried out by PhD student Moustapha Kolawole. The modified protocol is detailed in "10.1. Annex 1: Experiment 2 methodology", but the results of this second experiment are not analysed in this thesis.

4.1. Experimental design

The experiment followed a randomized arrangement of plants in two treatments: well-watered (control treatment) and stress (water deficit) treatment. The methodology for the experimental design is described as follows:

Treatments:

Well-Watered Treatment (Control Treatment): Plants in this group were maintained under regular watering conditions, ensuring that the soil water potential remained close to pot capacity, comparable to field capacity. The exact amount of water required was determined as follows: Pot capacity was established using three pots, each containing 1,030 grams of soil saturated with water. These pots were placed on a scale for 48 hours, allowing excess water to drain off the scale plate. Data from the scales indicated that pot capacity was reached after 24 hours, with a stable weight corresponding to 330 ml/pot, as no significant weight change was observed beyond this point.

Stress Treatment: Plants in this treatment were subjected to reduced watering, resulting in a soil water potential of approximately -400 kPa.

Replication and Sample Size:

In this experiment, a total of eight plants were assigned to each treatment. The figure 1 display the plants after 3 weeks.

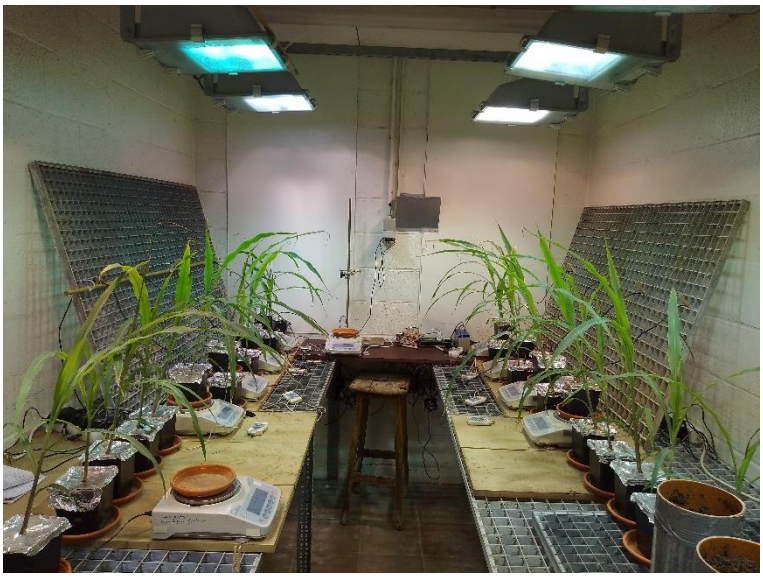

Figure 1: The maize plants in the phytotron.

The replication and sample size were distributed as follows:

- Destructive measurements before treatment:
  Four plants were grown specifically for conducting destructive measurements before the application of the treatment.
- Fully monitored plants during treatment:
  Four plants from each treatment were selected for full monitoring throughout the treatment period and the subsequent rewatering phase. The destructive measurement were taken after the rewatering phase.
- Destructive measurements after treatment:
  Additionally, four plants from each treatment were designated for destructive measurements after the treatment application.

Randomization:

The plants were arranged in two lines, with the treatments alternated to minimize potential spatial effects.

Experimental Timeline:

The experiment can be divided into three phases :

1) The growing phase : All plants were grown for approximately six weeks, until reaching the sixth leaf stage. During this period, all plants received the same regular watering regime (April 18th - May 25th, 2023).

2) The treatment phase : After the six-week growth period, the well-watered and stress treatments were applied to their respective plant groups for two weeks (May 25th – June 8th, 2023).

3) The rewatering phase : Following two weeks of treatment, the plants underwent a rewatering period to alleviate the stress conditions and restore adequate soil moisture (June 8th – June 16th, 2023).

4.2. Plant material

The plants used are Maize B104, the seeds were obtained from the Louvain Institute of Biomolecular Science and Technology.

The germination of the seeds was carried out in a Petri dish that was maintained vertically in dark conditions. Two wet filter papers were placed on either side of the seeds to provide moisture. The germination process was conducted at a temperature of 20°C.

Before the germination process, the seeds were subjected to sterilization. This was done by immersing the seeds in a 50% bleach solution for a duration of 5 minutes. Following the bleach treatment, the seeds were rinsed in water five times, with each rinsing step being interrupted by sponging to remove any residual bleach. This ensured that the seeds were adequately sterilized and ready for germination.

After a period of 3 days, the germinated maize seeds were transplanted into pots for further growth and development.

4.3. Environment

The experiment was conducted in a phytotron. The temperature was set to be 26°C during the day and 20°C during the night with a photoperiod of 16 hours. The relative humidity was set to be of 55%. However, as shown in Figure 2, the actual relative humidity was higher than the target level.

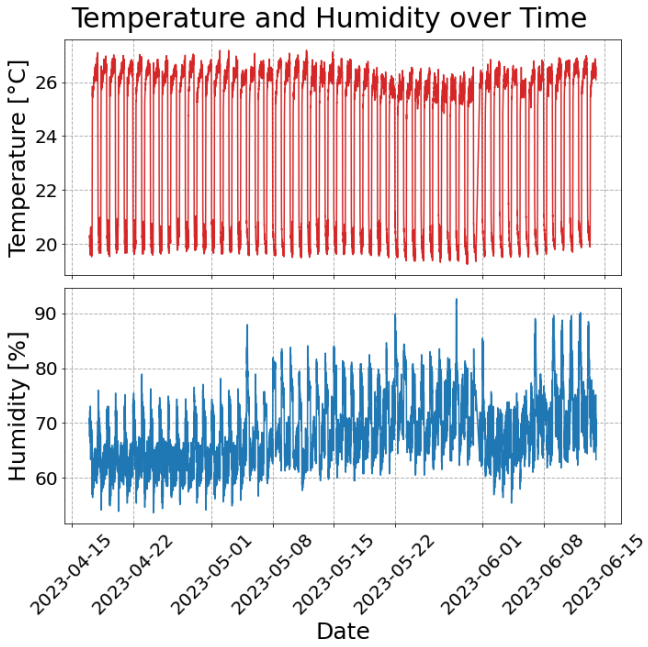

Figure 2: Temperature and humidity in the phytotron.

4.4. Substrate

The soil used for this experiment was repurposed from soil originally collected from a field in Saint-Amand, Fleurus, Belgium (50°30'N, 4°33'E), a region with an oceanic temperate climate. This soil, obtained from the top layer (0-30 cm) of potato mounds during harvest, had been stored outdoors for two years before being used in this study. The soil was initially collected by Salomé Lengrand, a PhD student at the Earth and Life Institute, Applied Microbiology Laboratory, UCL. Although it was intended for another experiment that was ultimately not conducted, it had undergone some treatments and was therefore reused for this study.

After collection, the soil was dried in a greenhouse. Once dried, it was crushed using a cement mixer and then sieved through three screens with mesh sizes of 6 mm, 4 mm, and 2 mm. The resulting fractions from this process were stored in the greenhouse for an additional two years.

To achieve the desired granulometric distribution, the three soil fractions (6 mm, 4 mm, and 2 mm) were mixed with siliceous sand from Mol (M32) to approximate a sand content of 15% in the overall mixture, the goals of this process was to make the soil textural fractions similar to the loam substrate characterised by Vetterlein et al. (2021). The proportions used were 3.916 kg of the 6 mm fraction, 13.152 kg of the 4 mm fraction, 7.930 kg of the 2 mm fraction, and 2.215 kg of M32 sand. The specified quantities of each fraction and the sand were carefully measured and mixed in a cement mixer for 5 minutes.

4.5. Pots

The pots used in this experiment were TEKU pots manufactured by Pöppelmann. Specifically, the pots had dimensions of 11 cm x 11 cm x 12 cm (length x width x height) with approximate 1-liter capacity.

Each pot was filled with 1030 grams of soil. To minimize direct evaporation, an aluminium sheet was placed over the top of each pot. The sheet had a hole cut out to accommodate the plant, allowing it to grow through while still providing coverage for the majority of the soil surface.

4.6. Watering

The plant were watered with a Hoagland solution. During the growing period, each plant was weighted and brought back to its pot capacity weight. After the growing period (6 weeks), an estimated weight was used to correct the amount of water given to the plants, the estimated weight corresponded to the average weight of the 4 plants that were used for the destructive measurements.

The watering occurred every 2 to 3 days during the first 3 weeks of the experiment, then once a day for the 3 following weeks and then twice a day until the end of the experiment.

During the treatment period, the stressed plant were watered with the target of keeping the soil water potential around -400 kPa which is around pF 3.6. The weight to which each stressed plant was brought back was the weight registered by the scale the first time the soil water potential dropped below -400 kPa.

4.7. Measurements

4.7.1. Continuous measurements

4.7.1.1. Transpiration rate – scale

To monitor total transpiration and transpiration rates, some plants were placed on weighing scales. The scales used were the FX-3000i model, and the data loggers were the AD-1688, both from A&D Company. Each scale was connected to a data logger that recorded the weight every 15 minutes. The collected data were then processed to determine the transpiration rate. Details of the data analysis pipeline developed for this purpose are described in section “5.2.2”.

4.7.1.2. Soil matric water potential – TEROS 21

The soil matric water potential was monitored as an indicator of hydric stress as it reflects the ease with which the water is extracted from the soil by the plant. The tensiometer used in this experiment are Teros 21 from the Meter group.

The head of the Teros 21 sensor consist of two ceramic discs that are in contact with the soil thus in equilibrium with it in terms of water potential. The water matric potential is deducted from the electrical conductivity of the ceramic is given in kPa (*TEROS 21,* 2021).

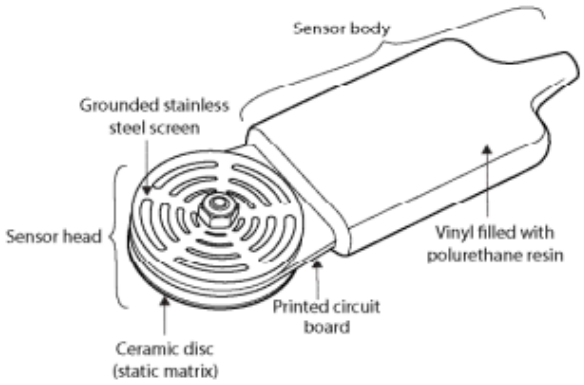

Figure 3: TEROS 21 sensor (from the manual Teros 21 Gen2 Meter group).

The Teros 21 were used with a CR1000 data logger from Campbell Scientific (*CR1000 - Measurement and Control Datalogger,* n.d.). The data logger was programmed to collect data every 15 minutes. The obtained data were processed and converted into pF values for better visualisation.

$$pF = log10(10 * |\psi_{Soil}|)$$

Where ,
- pF: Lognormal transformation of the soil matric potential
- $|\psi_{Soil}|$: The absolute value of the soil matric potential [kPa]

All plants in the stressed treatment, as well as the monitored plants in the control treatment, were equipped with a Teros 21 sensor. The Teros 21 sensor was placed at a depth of approximately half the pot height, slightly off-centre to accommodate plant growth.

4.7.1.3. Leaf water potential - Psychrometer

The leaf water potential, which is the sum of pressure potential and osmotic potential, was measured using a psychrometer to gauge plant water stress. For this experiment, we used the PSY1-Stem psychrometers, kindly lent by Prof. Javaux from the UCLouvain soil physics lab.

The Psychrometer head (shown on figure 4) includes two joined chromel-constantan thermocouples within a chromium-plated brass chamber, forming a significant insulating thermal mass ('Psychrometer PSY1 for Plant Water Potential and Water Stress', n.d.). The Psychrometer's thermocouples are strategically placed: one touches the plant tissue upon installation, while the other measures chamber air temperature. Applying a Peltier cooling current creates a temperature gradient between the sample and the dew point, determining the psychrometric depression. Automatic temperature correction accounts for errors induced by temperature gradients in the chamber, ensuring precise and consistent plant water potential measurements (*ICT - PSY1 - Plants - Stem Psychrometers By ICT International,* n.d.).

*Figure 4: Photo of an ICT international Psychrometer (*PSY1-Chamber-Parts*, n.d.).*

The psychrometers were used with the corresponding data logger during the treatment and the rewatering phases. They were placed on the sixth or seventh fully ligulated leaves.

4.7.2. Destructive measurements :

After each phase of the experiment destructive measurement were conducted. For the first experiment the date of the destructive measurement were the 26th of May 2023 for the end of the growing phase, the 8th of June 2023 for the end of the treatment phase and the 14th of June 2023 for the end of the rewatering phase.

4.7.2.1. Leaf water potential – Scholander pressure bomb

The Scholander pressure chamber, also called Scholander bomb, was used to get punctual leaf water potential data at the end of each phase of the experiment.

Figure 5: A commercially available pressure chamber. The pressure chamber is designed for either laboratory or field use. A safety valve on the lug cover ensures that pressure can be applied to the chamber only when the cover is properly and completely secured.

The Scholander pressure chamber used is a model 1000 from PMS Instrument. The chamber connects to a pressurised nitrogen cylinder that allow to measure the leaf water potential in a range from 0 to -4 MPa.

The chamber exerts air pressure on a leaf that is placed mostly in the chamber with only the end or the petiole outside passing through a seal. When the first droplet of water appears it means that the pressure in the chamber equals the tension that the leaf experiences. The higher is the pressure in the bomb, the higher is the tension and so the higher is the water stress (Shackel, 2022).

The measurements with the Scholander pressure chamber were conducted in the morning with two repetitions. For each plant of maize the last and the penultimate ligulated leaves were cut with a razor blade then used for the measurement.

4.7.2.2. Root conductance – Hydraulic Conductance Flow Meter (HCFM)

The Hydraulic Conductance Flow Meter (HCFM), also known as the High Pressure Flow Metre (HPFM), was used to assess the root conductance.

Figure 6: The Hydraulic Conductance Flow Meter.

The HCFM-XP Generation 3 model from Dynamax was used in this experiment. The device is connected to a pressurised nitrogen cylinder and pushes water into the root system. The transient analysis of the hydraulic conductance consists of measuring the flow of water forced into the root system by the increasing pressure applied. Then the HPFM-GEN3 Software (*Software & Downloads - Dynamax,* n.d.) calculate the slope of the increased flow and pressure corresponding to the hydraulic conductance of the root system (*HCFM-XP Gen 3 Hydraulic Conductance Flow Meter - Dynamax,* n.d.).

The HCFM measurement were conducted just after the Scholander bomb measurements. For each plant three transient analysis were conducted, then the K25 (conductance at the standard temperature of 25°C) were used for comparison.

4.7.2.3. Root surface – Scanner

The root surface was determined in order to normalised the conductance values obtained with the HCFM. The root surface was measured thanks to a scanner and the software ImageJ. The scanner used was an Epson Perfection V850 Pro model.

The process involved washing the roots from the pots, cutting them to fit a transparent container filled with water, and then scanning them. The resulting images were analysed with ImageJ software to determine the total root surface area. To ensure quick and accurate measurements, a dedicated pipeline and protocol was developed. Details of the pipeline can be found in section “5.2.1” and the protocol is provided in 10.5 .

5. Result

In this section, we will present and analyse the results obtained from our experiments. We will begin by evaluating the accuracy and success of the measurements conducted. Subsequently, we will compare the results across different treatments to identify any significant variations. Furthermore, we will introduce two specialised pipelines designed to efficiently handle the large datasets generated from root scans and transpiration estimations.

5.1. Experiment results

5.1.1. Soil water potential

The soil water potential was measured using TEROS21 sensors on 12 pots, divided as follows:

- 4 pots with control treatment, undergoing the 3 stages of the experiment.
- 4 pots with stress treatment, undergoing the 3 stages of the experiment.
- 4 pots with stress treatment, undergoing the first 2 stages of the experiment.

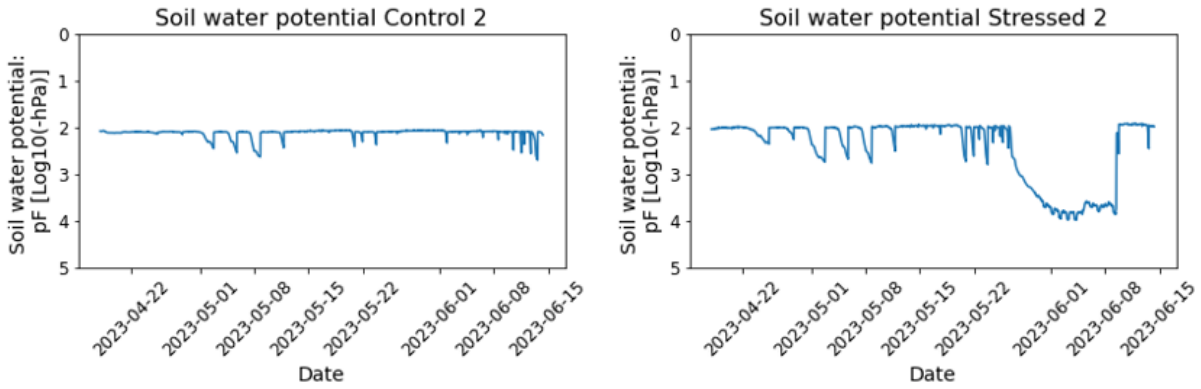

Figure 7: Time series plots of the soil water potential for control and stressed treatments.

Measurements were logged every 15 minutes throughout the entire duration of the experiment, or until the plant in the pot was harvested for destructive measurements. The soil water potential for a plant in the control treatment and a plant in the stressed treatment throughout the experiment is illustrated in the figure below.

The two graphs presented in the figure display the measurement of soil water potential, converted into pF units, over the entire duration of the experiment. The measurements are depicted continuously, allowing for easy observation of trends over time. Notably, distinct patterns emerge between the two treatments. All the graphs are available in “10.2. Annex 2: Experiment 1 Soil water potential graphs”.

In the graph on the left, representing one of the pots in the control treatment, soil water potential remains relatively stable throughout the experiment, staying around pF = 2. During both the growing phase and the rewatering phase, the soil water potential for the control and stressed treatments appears similar.

However, in the graph on the right, which corresponds to one of the pots in the stress treatment, a noticeable decrease in soil water potential is observed during the treatment phase. During the stress period, the pF value decreases significantly, reaching around pF = 4. This decline indicates the impact of water deficit stress on soil water potential.

The clear differentiation between the control and stress treatments during the treatment phase underscores the effectiveness of the experimental conditions in inducing water deficit stress.

The figure below shows the soil water potential measurements during the treatment stage for the four plants in the control group and the eight plants in the stress group, as well as the target stress level (pF 3.6).

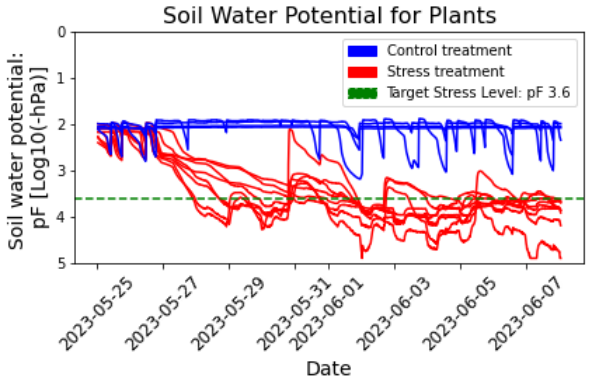

Figure 8: Soil water potential measurements during the treatment stage with the target stress level indicated at pF 3.6.

During the treatment stage, the soil water potential for the control group (represented by the blue lines) generally remains around pF = 2. However, there are brief instances where some values drop slightly, approaching pF = 3.

For the stress group (represented by the red lines), measurements show a gradual decline in soil water potential at the beginning of the treatment stage as stress is applied. The target stress level was reached in approximately 3 days for the quickest plants and approximately 7 days for the slowest ones. After reaching the target stress level some values remained close to the target, while others dropped significantly reaching almost pF = 5. Additionally, some values rose nearly to the control levels before declining again. Generally, the soil water potential in the stress group was lower than in the control group, but the values varied widely, deviating considerably from the desired stress level.

The next figure displays the soil water potential during the rewatering stage for the four remaining plants in each treatment group.

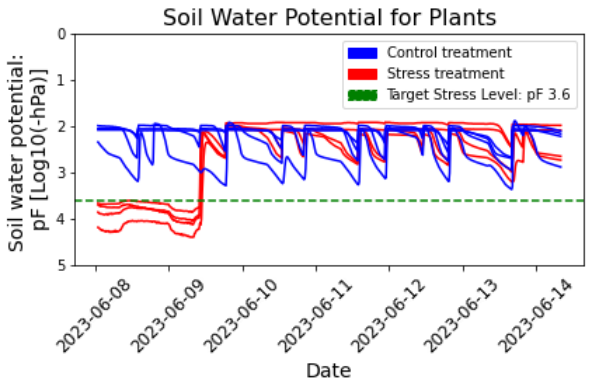

Figure 9: Soil water potential measurements during the rewatering stage with the target stress level indicated at pF 3.6.

From the graph representing the soil water potential during the rewatering stage, it seems that the plants in the stress group saw their soil water potential rise quickly to levels similar to those in the control group. However, there are noticeable fluctuations during this rewatering phase, with pF values dropping to around 3 for all plants.

5.1.2. Leaf water potential with Psychrometer

We aimed to measure the water potential of maize leaves continuously using psychrometers, in complement to the destructive measurements made with the Scholander chamber. Our plan was to conduct these measurements every 15 minutes over a period of approximately two to three weeks during the treatment stage and the rewatering stage of the experiment, initially with eight psychrometers. However, we only had six available. Due to equipment malfunctions and handling issues, we were unable to obtain conclusive data. In the following sections, we will present the data we collected and the types of problems we encountered. All the graphs of the psychrometer measurements are available in "10.3. Annex 3: Experiment 1 Leaf water potential measured with psychrometer graphs".

In reviewing the data from our psychrometers, several key issues were identified:

1) Zero Water Potential Readings:

Many of the graphs show water potential readings that are consistently zero. This issue indicates potential problems with sensor calibration or malfunction. The following figure illustrates this issue.

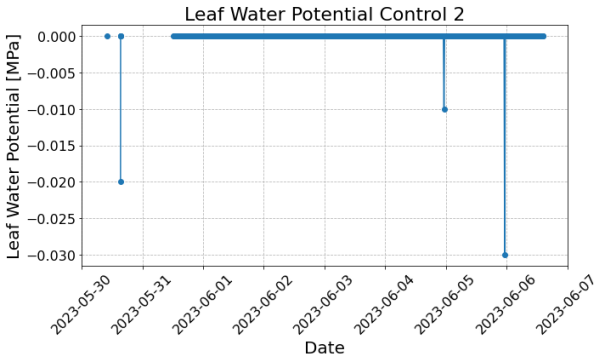

Figure 10: Example of psychrometer data showing consistent zero water potential readings.

2) Data Logger Interruptions:

We experienced interruptions in data logging, leading to gaps in our data. These interruptions could be due to connectivity issues or power failures. The following figure visualises the data logging interruptions we encountered.

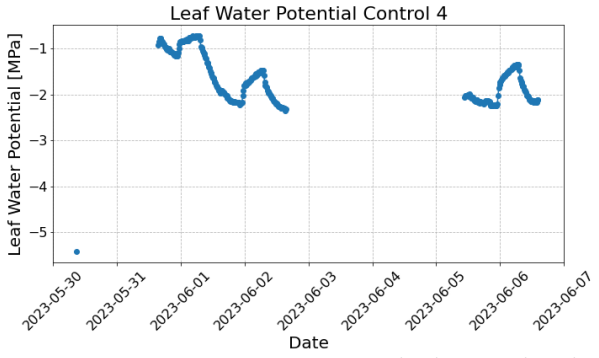

Figure 11: Example of psychrometer data showing interruptions in data logging.

Observations:

Despite the issues encountered, one of the psychrometers provided relatively consistent data throughout the measurement period. These measurements are shown in the next figure.

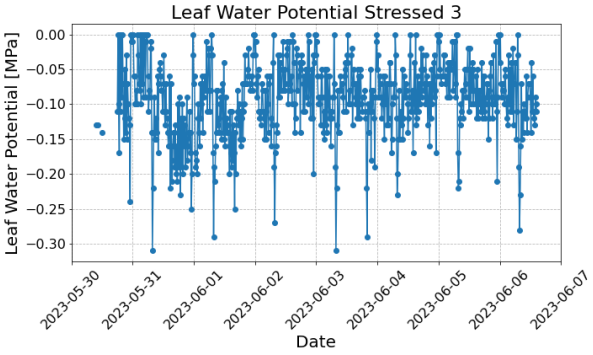

Figure 12: : Example of psychrometer data with no constant reading at zero and no interruptions in data logging.

The measured leaf water potential varied between 0 MPa and -0.3 MPa. The data seems to have a diurnal cycle but there is a lot of noise.

To better illustrate the underlying trends and reduce the impact of noise, we present a smoothed version of the same data. The data was smoothed using a moving average over five data points. This visualization aims to provide a clearer view of the overall trend in leaf water potential.

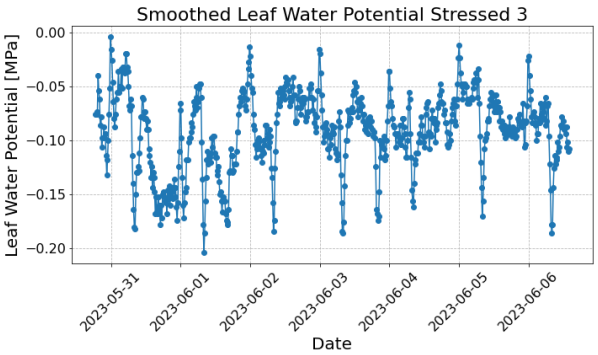

Figure 13: Smoothed data showing the trend with reduced noise.

The daily variations are clearer on this graph. The data seem to go up every night and decrease every morning, suggesting that the psychrometer successfully captured the general trend of leaf water potential changes.

5.1.3. Transpiration

Transpiration was measured using plants equipped with scales, which recorded the weight every 15 minutes. By calculating the difference between consecutive weight measurements, the change in weight can be determined, which corresponds to the amount of transpiration.

The data for transpiration was obtained through a comprehensive pipeline. This pipeline extracts data from the scales and corrects it for various factors, including watering events, outliers, and potential measurement errors. The detailed explanation of this pipeline and the data correction methods will be provided in a subsequent section.

Below, we present two graphs: one showing the transpiration of a plant from the control group and another from the stressed treatment group. These graphs illustrate the variation in transpiration over the course of the experiment. All the transpiration graphs for each plant are included in "10.4. Annex 4: Experiment 1 Transpiration graphs".

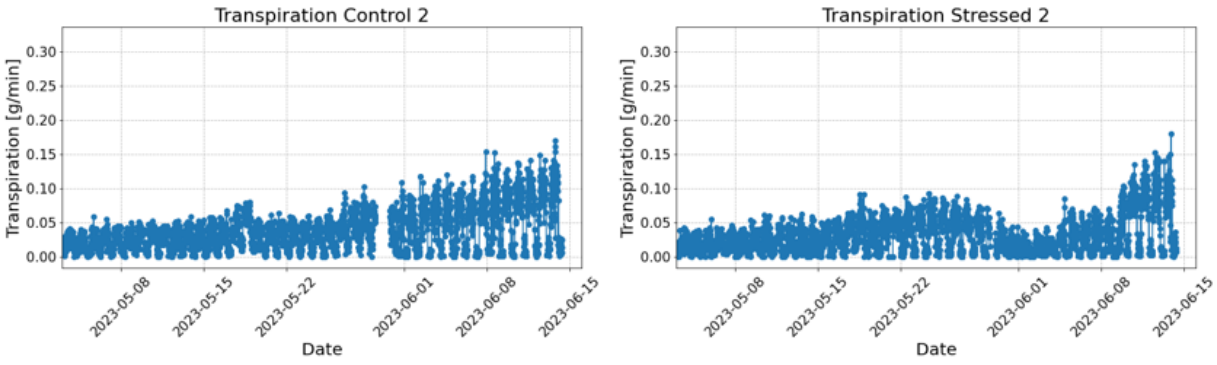

Figure 14 : Time series plots of transpiration for control and stressed treatments.

The graphs present continuous measurements of transpiration from two weeks after the experiment's start date until its conclusion. However, the data is not entirely continuous. In the left graph, representing the control group, there is an interruption in data recording due to a data logger issue.

In the control group's graph, we observe that transpiration fluctuates daily but generally increases over time. This is reflected in the gradual rise in the transpiration rate, measured in grams per minute.

In contrast, the right graph, representing the stressed treatment group, shows a similar increase in transpiration during the growth phase. However, during the stress period, transpiration decreases significantly, only to rise again during the rewatering phase.

To provide a clearer view of these patterns, we will include zoomed-in graphs for each phase. These examples illustrate that the transpiration measurements were successfully recorded and are reflective of the expected trends. As the data was logged every 15 minutes, resulting in a substantial amount of data, we will use smoothed data over a 5-value mean to present clearer trends.

On the next figure is presented the total transpiration per day per plant.

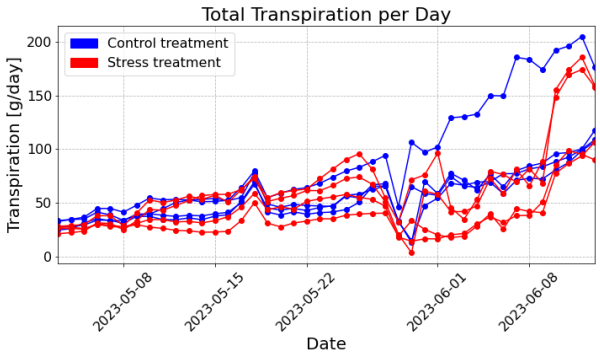

Figure 15: Total transpiration per day for all the monitored plants.

Initially, the total daily transpiration is similar across all plants. However, significant differences emerge towards the end of the experiment, even among plants within the same treatment group. This variation will be further analysed by looking at total daily transpiration across different phases of the experiment.

On the two following graphs, the transpiration rates for two plants during the growing phase are displayed. We can observe that the transpiration rate values are similar between the two plants during this phase. Additionally, we can clearly see the daily fluctuations in the transpiration rates, rising in the morning and decreasing at night, reaching zero.

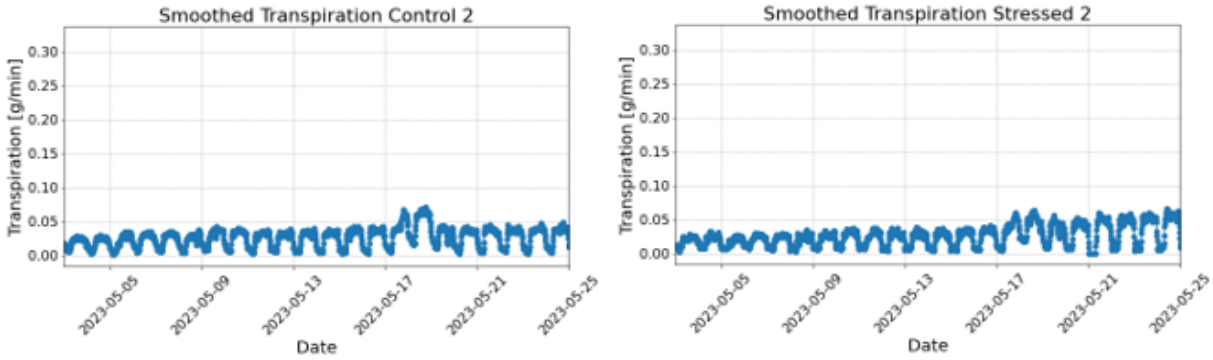

Figure 17: Transpiration rate for two plants during the growing phase.

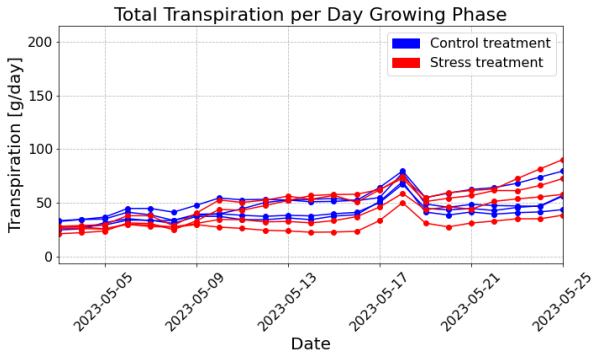

Figure 16: Total transpiration per day during the growing phase.

In the figure displaying total daily transpiration during the growing phase, we observe that all monitored plants start with similar transpiration rates. As the growing phase progresses, the range of total transpiration widens with value going from 38.5 g/day to 90.5 g/day.

Next, we will present two graphs showing the transpiration rates for plants from different treatment groups during the treatment phase.

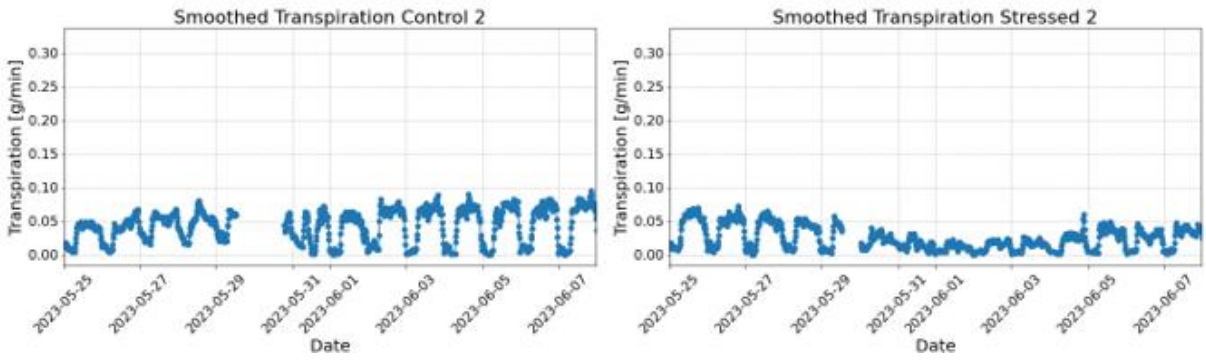

Figure 18: Transpiration rate for two plants during the treatment phase.

We can observe that the transpiration rate for the control plant maintains a similar trend throughout the treatment phase, with daily fluctuations still visible. In contrast, the transpiration rate for the stressed plant shows a noticeable decrease, and the daily fluctuations become almost imperceptible.

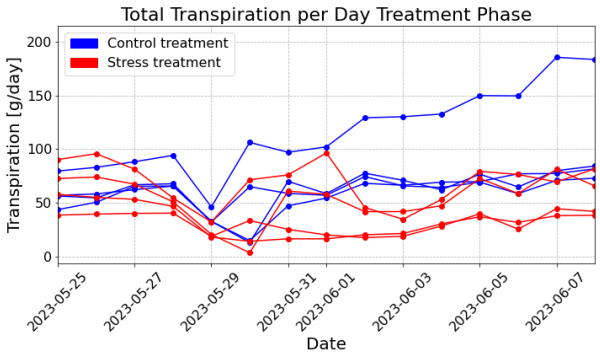

Figure 19: Total transpiration per day during the treatment phase.

The figure illustrating total daily transpiration during the treatment phase shows an initial decrease in transpiration for all plants between the 4th and 5th day. For control plants, transpiration increases again after this dip. In contrast, two plants in the stress treatment exhibit a significant and sustained decrease in transpiration. The other two stressed plants show an initial decrease followed by an increase and then a second decrease. Notably, one control plant's transpiration reaches nearly 200 g/day by the end of the treatment phase, while the others remain below 100 g/day.

The next figure displays the transpiration rates for two plants during the rewatering phase.

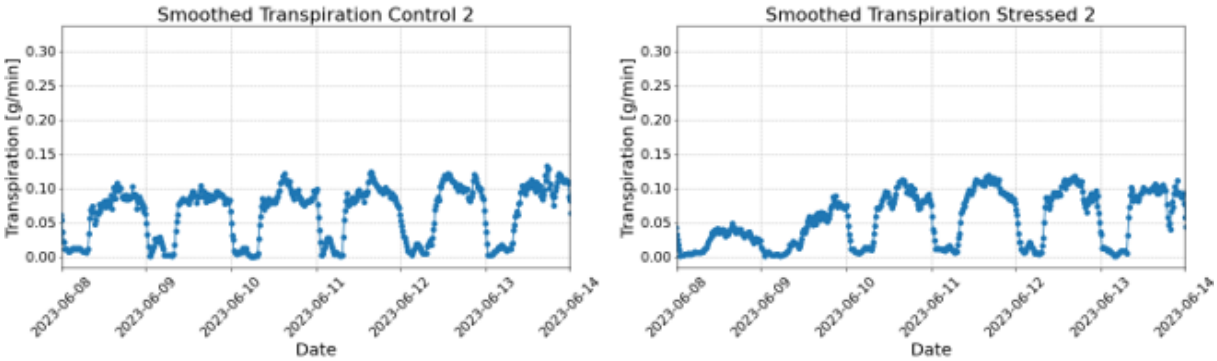

Figure 20: Transpiration rate for two plants during the rewatering phase.

The rewatering to a soil water potential close to the water capacity of the pot happened in the morning of the 9th June. We can observe that, after one day of rewatering, the transpiration rate of the stressed plant recovers to levels similar to those of the control plant.

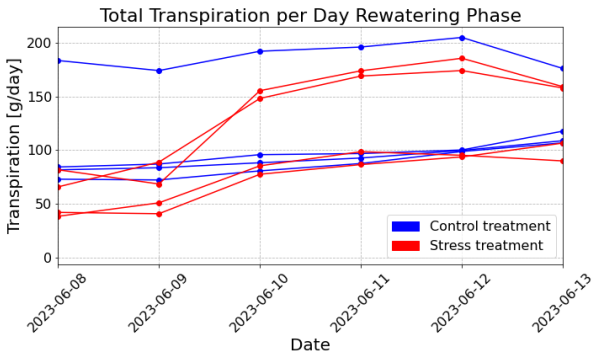

Figure 21: Total transpiration per day during the rewatering phase.

The final figure shows total daily transpiration during the rewatering phase. On June 10th, plants previously subjected to water deficit exhibit an increase in transpiration compared to earlier days. The two plants with lower transpiration during the treatment phase reach levels similar to the control plants (excluding one with exceptionally high values). The other two stressed plants achieve transpiration rates above 150 g/day, approaching the high-transpiration control plant.

5.1.4. Root conductance

Root conductance was measured using the High-Pressure Flow Meter (HCFM) transient measurement method, which assesses the flow in response to applied pressure. The slope of the resulting measurement points represents the conductance. Measurements were taken at the end of each stage of the experiment: after the growth phase, after the treatment phase, and after the rewatering phase. The following box plot illustrates root conductance at these three time points, allowing for a detailed assessment of changes in response to water deficit and subsequent rewatering.

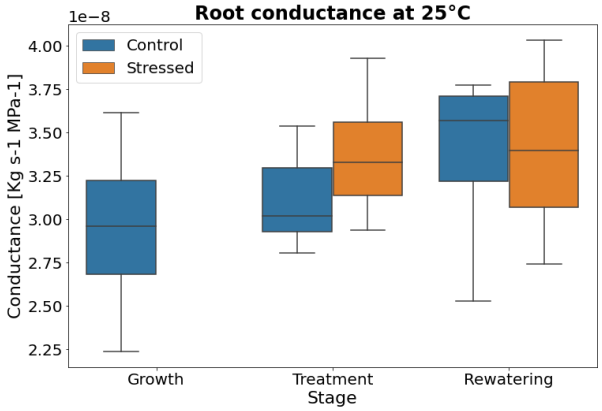

Figure 22: Box plot of root conductance measured at the end of each phase of the experiment.

The table below displays the main statistics for each group.

Table 1: Summary Statistics by Group for Root Conductance

Statistic	Growth Control	Treatment Control	Treatment Stressed	Rewatering Control	Rewatering Stressed
Mean	2.97e-08	3.09e-08	3.38e-08	3.62e-08	3.52e-08
Standard Deviation	4.16e-09	3.08e-09	3.14e-09	6.24e-09	7.08e-09
Min	2.24e-08	2.32e-08	2.94e-08	2.53e-08	2.74e-08
Max	3.61e-08	3.54e-08	3.93e-08	4.79e-08	5.71e-08
Count	12.00	16.00	16.00	16.00	16.00

From the box plot, we observe that the median value for conductance appears to increase over time. This trend is supported by the mean value and standard deviation in the table. Further statistical analysis will determine if there are significant differences between treatments and across stages.

ANOVA Analysis

The following ANOVA model was used to analyse the Conductance:

*Conductance ~ C(Treatment) * C(Stage)*

This model includes the main effects of the treatment and stage factors, as well as their interaction effect. To ensure the validity of the ANOVA results, we first assessed the assumptions of normality and homoscedasticity.

The next figure shows the distribution of residuals from the model on a Q-Q plot.

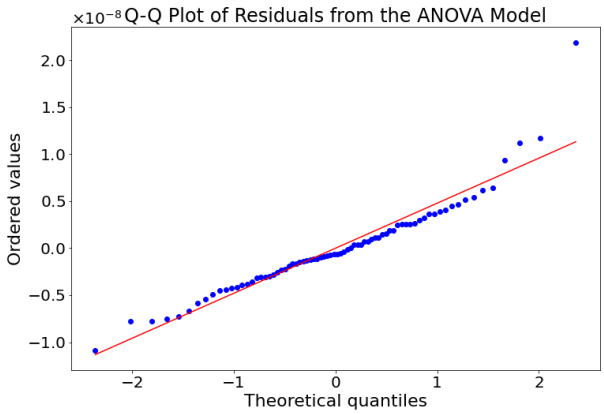

Figure 23: Q-Q plot of the residuals from the ANOVA model for conductance, used to check the normality assumption.

In the Q-Q plot, most residuals are fairly close to the normal distribution, although there are more pronounced deviations at the extremes.

Shapiro-Wilk Test for Normality:

- **Statistic:** 0.925
- **p-value:** 2.33×10^{-4}

Since the p-value (2.33×10^{-4}) is less than the significance level of 0.05, the Shapiro-Wilk test indicates that the residuals are not normally distributed. Given this result, a Box-Cox transformation was applied to the conductance data to stabilise variance and approximate a normal distribution more closely.

Following the Box-Cox transformation, an ANOVA model was fitted to the transformed data to evaluate the effects of treatment and stage on conductance. The ANOVA model used was:

*Transformed Conductance ~ C(Treatment) * C(Stage)*

This model includes the main effects of the treatment and stage factors, as well as their interaction effect. To validate the assumptions of the ANOVA model, we first examined the distribution of residuals. The Q-Q plot below illustrates the distribution of residuals from the ANOVA model applied to the transformed conductance data.

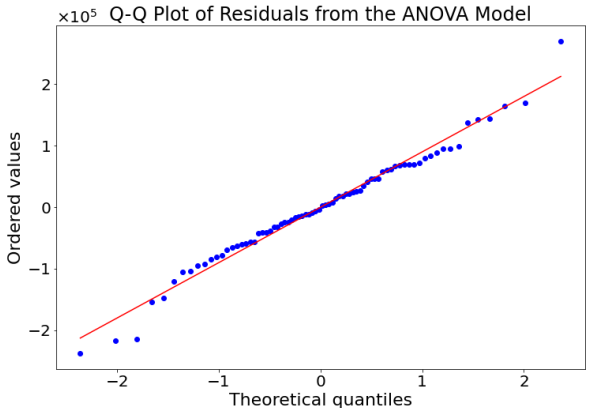

Figure 24: Q-Q plot of the residuals from the ANOVA model for the transformed conductance, used to check the normality assumption.

The Q-Q plot demonstrates that the residuals closely follow a normal distribution, though there are some deviations at the extremes.

Shapiro-Wilk Test for Normality:

- **Statistic:** 0.983
- **p-value:** 0.425

Since the p-value (0.425) exceeds the significance level of 0.05, we do not reject the null hypothesis. This suggests that the residuals from the transformed data approximate a normal distribution, indicating that the Box-Cox transformation effectively addressed the normality assumption required for the ANOVA.

With the normality assumption now satisfied, we next evaluated the assumption of homogeneity of variances, which is also crucial for the validity of the ANOVA results.

Levene's Test for Homogeneity of Variances:

- **Statistic:** 1.63
- **p-value:** 0.203

Given that the p-value (0.203) exceeds the significance level of 0.05, the null hypothesis is not rejected. This suggests that there is no significant evidence of variance differences across the groups, confirming that the homogeneity of variances assumption is met for the ANOVA model.

With both the normality and homogeneity of variances assumptions satisfied, we proceeded with the ANOVA analysis. The results for the ANOVA model applied to the transformed conductance data are summarised in the table below:

Table 2: ANOVA Results for Transformed Root Conductance Data

Source	Sum of Squares	Degrees of Freedom	F-Value	p-Value
C(Treatment)	-6.61e-05	1.000	-7.84e-15	1.000
C(Stage)	1.30e+11	2.00	7.73	9.18e-04
C(Treatment):C(Stage)	3.43e+10	2.00	2.03	0.138
Residual	5.99e+11	71.00		

Main Effect of Treatment (C(Treatment)): The p-value for the treatment effect is 1, which is above the significance level of 0.05. This indicates that there are no significant differences in root conductance among the different treatment groups.

Main Effect of Stage (C(Stage)): The p-value for the stage effect is 9.18×10^{-4}, which is below the significance level of 0.05. This suggests that there are significant differences in root conductance across the different stages of the experiment.

Interaction Effect (C(Treatment):C(Stage)): The p-value for the interaction between treatment and stage is 0.138, which is above 0.05. This indicates that there is no significant interaction effect between treatment and stage on root conductance.

Overall, the ANOVA results suggest that while the stage of the experiment has a significant impact on root conductance, neither the treatment alone nor the interaction between treatment and stage significantly affects conductance.

Following the ANOVA, which highlighted significant effects of the experimental stage, we conducted Tukey's Honestly Significant Difference (HSD) test to pinpoint which specific stages differed significantly in terms of root conductance. The results of Tukey's HSD test are summarised in the table below:

Table 3: Tukey's HSD Test Results for Pairwise Comparisons of Experimental Stages

Comparison	Mean difference	p-Value (adj)	95% Confidence interval
Control Growth vs Control Rewatering	1.28e+05	0.004	3.02e+04 to 2.26e+05
Control Growth vs. Control Treatment	3.43e+04	0.849	-6.38e+04 to 1.32e+05
Control Growth vs. Stressed Rewatering	1.09e+05	0.023	1.05e+04 to 2.07e+05
Control Growth vs. Stressed Treatment	9.68e+04	0.055	-1.36e+03 to 1.95e+05
Control Rewatering vs. Control Treatment	-9.40e+04	0.039	-1.85e+05 to -3.10e+03
Control Rewatering vs. Stressed Rewatering	-1.97e+04	0.900	-1.11e+05 to 7.12e+04
Control Rewatering vs. Stressed Treatment	-3.15e+04	0.854	-1.22e+05 to 5.94e+04
Control Treatment vs. Stressed Rewatering	7.43e+04	0.161	-1.66e+04 to 1.65e+05
Control Treatment vs. Stressed Treatment	6.24e+04	0.315	-2.84e+04 to 1.53e+05
Stressed Rewatering vs. Stressed Treatment	-1.18e+04	0.900	-1.03e+05 to 7.90e+04

Tukey's HSD test provides pairwise comparisons among all groups, allowing us to identify significant differences between pairs. A p-value less than or equal to 0.05 indicates a significant difference in means between the compared groups.

Significant Findings:

- **Control Growth vs. Control Rewatering:** Significant difference (p = 0.004), with root conductance being higher in the Control Rewatering stage compared to Control Growth.
- **Control Growth vs. Stressed Rewatering:** Significant difference (p = 0.023), suggesting that root conductance is higher in the Stressed Rewatering stage compared to Control Growth.
- **Control Rewatering vs. Control Treatment:** Significant difference (p = 0.039), with root conductance being lower in the Control Treatment compared to Control Rewatering.

5.1.5. Root surface

Root surface area was measured using scans performed after washing the roots at the end of each stage of the experiment, as part of the destructive sampling process. These measurements facilitate the comparison of how different treatments and stages affect root development. Additionally, these measurements help in normalising root conductance data, which allows for a more accurate estimation of root conductivity. The box plot below illustrates the root surface area measurements across the experimental conditions.

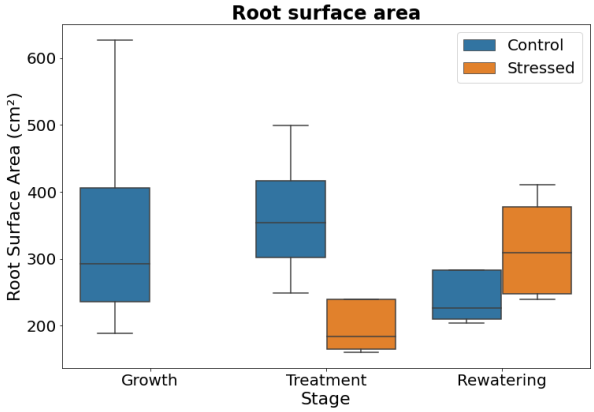

Figure 25: Box plot of root surface area measured at the end of each phase of the experiment.

The table below displays the main statistics for each group.

Table 4: Summary Statistics by Group for Root Surface area

Statistic	Growth Control	Treatment Control	Treatment Stressed	Rewatering Control	Rewatering Stressed
Mean	349.97	363.95	221.31	266.22	316.90
Standard Deviation	193.86	106.78	93.30	95.73	84.80
Min	188.98	248.39	159.84	203.79	239.45
Max	627.03	498.83	358.80	407.65	410.19
Count	4.00	4.00	4.00	4.00	4.00

The box plot shows significant variability in root surface area for the Growth Control group, while the Stressed Treatment group exhibits lower values, hinting at possible reductions in root surface area. Although no clear trend emerges across all conditions, the summary statistics indicate that the standard deviation of root surface area decreases over time. To further investigate these observations and assess the statistical significance of the differences, a detailed ANOVA analysis was conducted.

ANOVA Analysis

The following ANOVA model was used to analyse the root surface area:

*Root Surface ~ C(Treatment) * C(Stage)*

This model incorporates the main effects of the treatment and stage factors, as well as their interaction effect. To validate the ANOVA model, we first evaluated the assumptions of normality and homogeneity of variances.

The next figure shows the distribution of residuals from the model on a Q-Q plot.

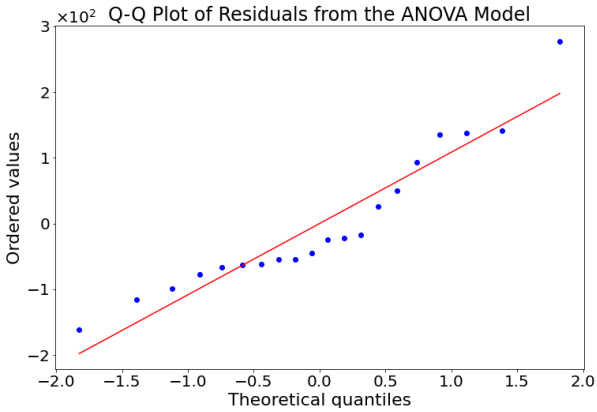

Figure 26: Q-Q plot of the residuals from the ANOVA model for root surface area, used to check the normality assumption.

The Q-Q plot indicates that the residuals seem reasonably close to the normality line, although there are some deviations.

Shapiro-Wilk Test for Normality:

- **Statistic:** 0.911
- **p-value:** 0.066

Since the p-value (0.066) is greater than the significance level of 0.05, the Shapiro-Wilk test suggests that the residuals are approximately normally distributed.

With the normality assumption now satisfied, we next evaluated the assumption of homogeneity of variances.

Levene's Test for Homogeneity of Variances:

- **Statistic:** 0.803
- **p-value:** 0.464

Given that the p-value (0.464) exceeds the significance level of 0.05, the null hypothesis is not rejected. This suggests that there is no significant evidence of variance differences across the groups, confirming that the homogeneity of variances assumption is met for the ANOVA model.

With both the normality and homogeneity of variances assumptions satisfied, we proceeded with the ANOVA analysis. The results for the ANOVA model applied to the root surface area data are summarised in the table below:

Table 5: ANOVA Results for Root Surface Area Data

Source	Sum of Squares	Degrees of Freedom	F-Value	p-Value
C(Treatment)	-2.10e-11	1.000	-1.42e-15	1.000
C(Stage)	1.07e+04	2.00	0.362	0.702
C(Treatment):C(Stage)	4.58e+04	2.00	1.55	0.245
Residual	2.22e+05	15.00		

Main Effect of Treatment (C(Treatment)): The p-value for the treatment effect is 1, which is above the significance level of 0.05. This indicates that there are no significant differences in root surface area among the different treatment groups.

Main Effect of Stage (C(Stage)): The p-value for the stage effect is 0.702, which is above the significance level of 0.05. This suggests that there are no significant differences in root surface area across the different stages of the experiment.

Interaction Effect (C(Treatment):C(Stage)): The p-value for the interaction between treatment and stage is 0.245, which is above 0.05. This indicates that there is no significant interaction effect between treatment and stage on root surface area.

Overall, the ANOVA results suggest that neither the stage of the experiment nor the treatment alone significantly impacts root surface area. Additionally, there is no significant interaction effect between treatment and stage on root surface area.

5.1.6. Root conductivity

Root conductivity was calculated by normalising root conductance with root surface area. This parameter provides a more accurate assessment of the root's ability to conduct water, as it accounts for differences in root size. By evaluating root conductivity, we can gain insights into how different treatments and stages of the experiment affect the efficiency of water transport through the roots. The box plot below illustrates the root conductivity across the experimental conditions.

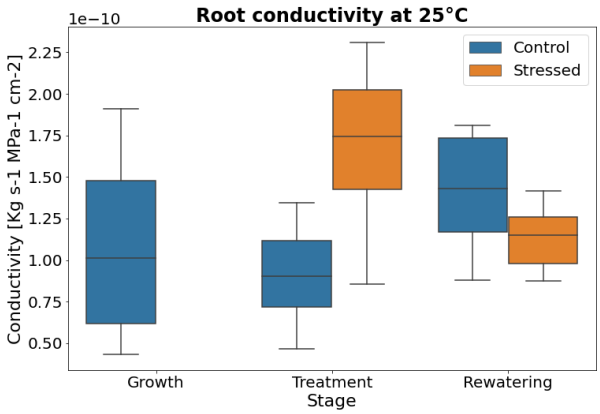

Figure 27: Box plot of root conductivity at the end of each phase of the experiment.

The table below displays the main statistics for each group.

Table 6: Summary Statistics by Group for Root Conductivity

Statistic	Growth Control	Treatment Control	Treatment Stressed	Rewatering Control	Rewatering Stressed
Mean	1.06e-10	9.10e-11	1.68e-10	1.43e-10	1.14e-10
Standard Deviation	5.33e-11	2.60e-11	4.74e-11	3.00e-11	1.78e-11
Min	4.32e-11	4.65e-11	8.57e-11	8.77e-11	8.76e-11
Max	1.91e-10	1.34e-10	2.31e-10	1.81e-10	1.41e-10
Count	12.00	16.00	16.00	16.00	16.00

From the box plot, we can observe that the root conductivity for the stressed treatment group appears to be higher than that of the other groups. However, the summary statistics table does not reveal a clear trend in the mean, range, or standard deviation across the different groups. While there seems to be an indication that conductivity might be higher for stressed plants during the treatment phase, a more in-depth ANOVA analysis is necessary to determine if there are significant differences across treatments and stages.

ANOVA Analysis

To analyse the root conductivity data, we used the following ANOVA model:

*Conductivity ~ C(Treatment) * C(Stage)*

This model includes the main effects of the treatment and stage factors, as well as their interaction effect. Before using this ANOVA model we had to check the assumptions of normality and homogeneity of the variance.

The next figure shows the distribution of residuals from the model on a Q-Q plot.

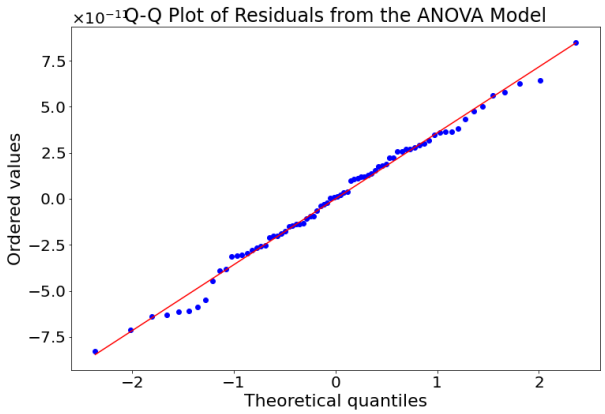

Figure 28: Q-Q plot of the residuals from the ANOVA model for root conductivity, used to check the normality assumption.

On the Q-Q plot, we can see that the residuals appear to follow a normal distribution reasonably well.

Shapiro-Wilk Test for Normality:

- **Statistic:** 0.991
- **p-value:** 0.871

Since the p-value (0.871) is greater than the significance level of 0.05, the Shapiro-Wilk test suggests that the residuals are approximately normally distributed.

After the normality assumption, we next evaluated the assumption of homogeneity of variances.

Levene's Test for Homogeneity of Variances:

- **Statistic:** 6.81
- **p-value:** 0.002

Since the p-value for Levene's test (0.002) is less than 0.05, the assumption of homogeneity of variances was not met. To address this, a Box-Cox transformation was applied to the data.

Following the transformation, an ANOVA model was fitted to the adjusted data to assess the effects of treatment and stage on root conductivity. The model used was:

*Transformed Conductivity ~ C(Treatment) * C(Stage)*

This model's assumptions were also checked. The Q-Q plot below shows the residuals from the ANOVA model on the transformed conductivity data.

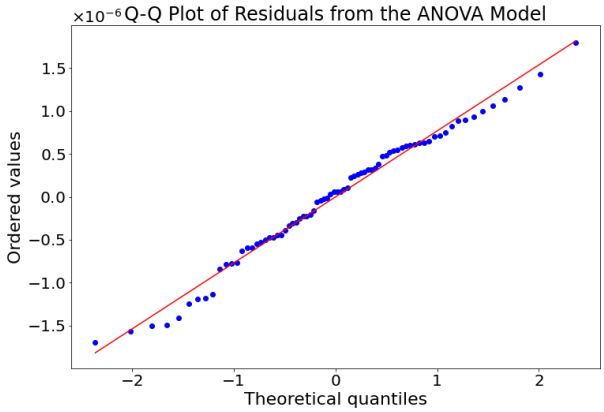

Figure 29: Q-Q plot of the residuals from the ANOVA model for the transformed conductivity, used to check the normality assumption.

The Q-Q plot for the residuals of the transformed conductivity data shows good alignment with the normal distribution. Despite some deviations at the extremes, the plot confirms that the normality assumption is reasonably satisfied, consistent with the pre-transformation assessment.

Shapiro-Wilk Test for Normality:

- **Statistic:** 0.985
- **p-value:** 0.487

Since the p-value (0.487) is greater than the significance level of 0.05, the Shapiro-Wilk test indicates that the residuals are normally distributed.

Levene's Test for Homogeneity of Variances:

- **Statistic:** 9.25
- **p-value:** 2.63×10^{-4}

Since the p-value (2.63×10^{-4}) is less than the significance level of 0.05, the Levene's test indicates that variances are not homogeneous across the groups.

Given that the assumption of homogeneity of variances was not met for the ANOVA on the transformed conductivity data, we applied the Kruskal-Wallis test to the original data. This non-parametric test does not require homogeneity of variances and allows for the evaluation of differences between groups without this assumption.

Kruskal-Wallis Test:

- **H-statistic:** 26.91
- **p-value:** 2.08×10^{-5}

The p-value (2.08×10^{-5}) is less than the significance level of 0.05, indicating that there are significant differences between the medians of the groups.

Given these significant differences, a post-hoc analysis using Dunn's Test was conducted to identify which specific groups differ. The results of this analysis are detailed in the table below.

Table 7: Post-hoc Analysis with Dunn's Test on conductivity data

Comparison	Growth Control	Treatment Control	Treatment Stressed	Rewatering Control	Rewatering Stressed
Growth Control	1.000	1.000	0.019	0.270	1.000
Treatment Control	1.000	1.000	5.24e-05	0.003	1.000
Treatment Stressed	0.019	5.24e-05	1.000	1.000	0.028
Rewatering Control	0.270	0.003	1.000	1.000	0.437
Rewatering Stressed	1.000	1.000	0.028	0.437	1.000

Dunn's Test, conducted as a post-hoc analysis following the significant Kruskal-Wallis Test, identifies which specific groups differ in their medians. A p-value ≤ 0.05 signifies a statistically significant difference between the medians of the compared groups. The results of Dunn's Test reveal the following significant differences:

- **Growth Control vs. Treatment Stressed:** Significant difference ($p = 0.019$)
- **Treatment Control vs. Treatment Stressed:** Significant difference ($p = 5.24 \times 10^{-5}$)
- **Treatment Control vs. Rewatering Control:** Significant difference ($p = 0.003$)
- **Treatment Stressed vs. Rewatering Stressed:** Significant difference ($p = 0.028$)

No significant differences were found between the other pairs of groups. These findings indicate that specific treatments have distinct effects on root conductivity, with notable differences between certain treatment combinations.

5.1.7. Leaf water potential with Scholander pressure chamber

Leaf water potential was assessed using the Scholander pressure chamber at each occurrence of destructive measurements, which took place at the end of each experimental stage. This technique provides critical information on the plant's water status, which is integral for understanding how different treatments and stages affect leaf hydration. The box plot below illustrates the distribution of leaf water potential across the experimental groups.

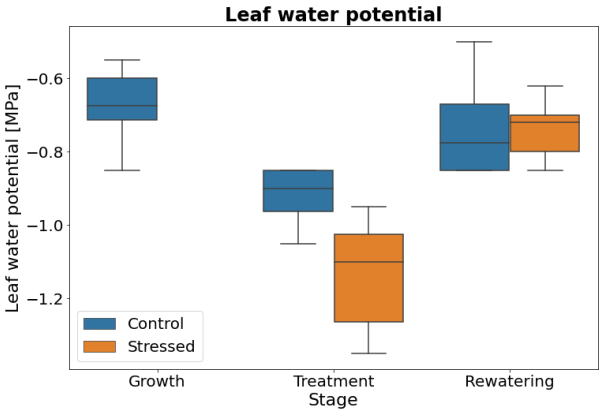

Figure 30: Box plot of leaf water potential at the end of each phase of the experiment.

The table below displays the main statistics for each group.

Table 8: Summary Statistics by Group for Leaf Water Potential

Statistic	Growth Control	Treatment Control	Treatment Stressed	Rewatering Control	Rewatering Stressed
Mean	-0.692	-0.919	-1.13	-0.735	-0.739
Standard Deviation	0.129	0.075	0.153	0.133	0.073
Min	-1.000	-1.05	-1.35	-0.850	-0.850
Max	-0.550	-0.850	-0.950	-0.500	-0.620
Count	12.00	8.00	8.00	8.00	8.00

The box plot reveals that during the treatment phase, both the Control and Stress treatments exhibit lower leaf water potential compared to the Growth Control and Rewatering groups. This trend is consistent with the statistical summary table. To further investigate these differences, we will conduct a detailed ANOVA analysis.

ANOVA Analysis

The ANOVA model used to analyse the leaf water potential was:

*Leaf Water Potential ~ C(Treatment) * C(Stage)*

his model assesses the main effects of treatment and stage, as well as their interaction. To ensure the validity of the ANOVA results, we checked the assumptions of normality and homogeneity of variances.

The next figure shows the distribution of residuals from the model on a Q-Q plot.

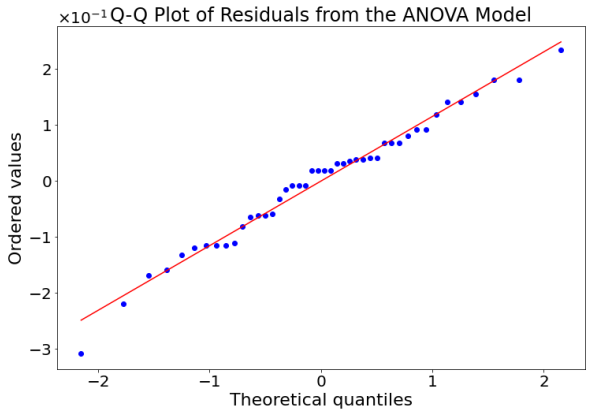

Figure 31: Q-Q plot of the residuals from the ANOVA model for leaf water potential, used to check the normality assumption.

At first glance, the Q-Q plot of the residuals suggests that they follow the normal distribution quite well. The normality assumption was further validated using the Shapiro-Wilk test.

Shapiro-Wilk Test for Normality:

- **Statistic:** 0.984
- **p-value:** 0.787

Since the p-value (0.787) is greater than the significance level of 0.05, the Shapiro-Wilk test suggests that the residuals are normally distributed.

After confirming normality, we next evaluated the assumption of homogeneity of variances with Levene's test.

Levene's Test for Homogeneity of Variances:

- **Statistic:** 1.04
- **p-value:** 0.362

Given that the p-value (0.362) exceeds the significance level of 0.05, the null hypothesis is not rejected. This suggests that there is no significant evidence of variance differences across the groups, confirming that the homogeneity of variances assumption is met for the ANOVA model.

With both the normality and homogeneity of variances assumptions satisfied, we proceeded with the ANOVA analysis. The results for the ANOVA model applied to the leaf water potential data are summarised in the table below:

Table 9: ANOVA Results for Leaf Water Potential Data

Source	Sum of Squares	Degrees of Freedom	F-Value	p-Value
C(Treatment)	-1.40e-16	1.000	-9.92e-15	1.000
C(Stage)	0.977	2.00	34.58	2.30e-09
C(Treatment):C(Stage)	0.181	2.00	6.40	0.004
Residual	0.551	39.00		

Main Effect of Treatment (C(Treatment)): The p-value for the treatment effect is 1, which is above the significance level of 0.05. This indicates that there are no significant differences in leaf water potential among the different treatment groups.

Main Effect of Stage (C(Stage)): The p-value for the stage effect is 2.30×10^{-9}, which is below the significance level of 0.05. This suggests that there are significant differences in leaf water potential across the different stages of the experiment.

Interaction Effect (C(Treatment):C(Stage)): The p-value for the interaction between treatment and stage is 0.004, which is below 0.05. This indicates that there is a significant interaction effect between treatment and stage on leaf water potential.

Overall, the ANOVA results suggest that while the stage of the experiment significantly impacts leaf water potential, the treatment alone does not. Additionally, there is a significant interaction effect between treatment and stage, indicating that the impact of treatment on leaf water potential varies depending on the stage of the experiment.

Following the ANOVA analysis, which revealed significant effects of treatment and stage on leaf water potential, we performed Tukey's Honestly Significant Difference (HSD) test to determine which specific group comparisons were significant. The results of Tukey's HSD test are summarized in the table below:

Table 10: Tukey's HSD Test Results for Pairwise Comparisons of Leaf Water Potential

Comparison	Mean difference	p-Value (adj)	95% Confidence interval
Control Growth vs Control Rewatering	-0.043	0.900	-0.199 to 0.112
Control Growth vs. Control Treatment	-0.227	0.001	-0.382 to -0.072
Control Growth vs. Stressed Rewatering	-0.047	0.900	-0.202 to 0.108
Control Growth vs. Stressed Treatment	-0.440	0.001	-0.595 to -0.284
Control Rewatering vs. Control Treatment	-0.184	0.028	-0.354 to -0.014
Control Rewatering vs. Stressed Rewatering	-0.004	0.900	-0.174 to 0.166
Control Rewatering vs. Stressed Treatment	-0.396	0.001	-0.566 to -0.226
Control Treatment vs. Stressed Rewatering	0.180	0.033	0.010 to 0.350
Control Treatment vs. Stressed Treatment	-0.212	0.008	-0.382 to -0.043
Stressed Rewatering vs. Stressed Treatment	-0.393	0.001	-0.562 to -0.223

Significant Findings:

- **Control Growth vs. Control Treatment**: A significant difference (p = 0.001) indicates that leaf water potential is lower in the Control Treatment compared to Control Growth.
- **Control Growth vs. Stressed Treatment**: A significant difference (p = 0.001) suggests that leaf water potential is lower in the Stressed Treatment compared to Control Growth.
- **Control Rewatering vs. Control Treatment**: A significant difference (p = 0.028) reveals that leaf water potential is lower in the Control Treatment compared to Control Rewatering.
- **Control Rewatering vs. Stressed Treatment**: A significant difference (p = 0.001) indicates that leaf water potential is lower in the Stressed Treatment compared to Control Rewatering.
- **Control Treatment vs. Stressed Rewatering**: A significant difference (p = 0.033) shows that leaf water potential is higher in the Control Treatment compared to Stressed Rewatering.
- **Stressed Rewatering vs. Stressed Treatment**: A significant difference (p = 0.001) suggests that leaf water potential is lower in the Stressed Treatment compared to Stressed Rewatering.

These results highlight notable differences in leaf water potential, with significant changes observed between the groups in the treatment phase compared to the others phases.

5.2. Pipeline results

One of the objectives of this research was to develop a method for reliable and efficient data processing, especially for large datasets like root surface measurements and transpiration rate calculations. To achieve this, two distinct data processing pipelines were created. These pipelines not only aimed to accelerate the data processing but also introduced a systematic approach for effectively managing and analysing substantial volumes of data, ensuring that the process was both quick and reliable.

For the pipeline concerning root scans, a detailed protocol was established to ensure accurate data tracking (see" 10.5. Annex 5: Pipeline 1 protocol"). This protocol encompasses the entire process, from the proper cleaning and collection of roots to obtaining surface area measurements in square centimetres. In the first part, we will explain the developed pipeline for scanning roots and obtaining root surface areas, detailing the procedural steps involved. Subsequently, we will describe the pipeline created to derive transpiration rates from the balance data, showcasing the steps taken to ensure accuracy and efficiency in the data analysis process.

5.2.1. Pipeline 1 Root surface pipeline

The developed protocol for measuring root surface area from scans can be divided into four main stages:

1) Extraction and Cleaning of Roots: This initial step involves carefully extracting the roots from the soil and thoroughly cleaning them to remove any adhering soil particles. Proper cleaning ensures that the scans are accurate and free from artifacts caused by debris.
2) Scanning of Roots and Calibration: In this stage, ensure accuracy in the conversion into surface area, calibration scans are also performed alongside the root scans.
3) Image Processing with ImageJ: The scanned images are then processed using the ImageJ software. This step involves analysing the images to detect and measure the root surface areas.
4) Data Conversion and Aggregation with Python: The final step involves converting the image-derived data into surface area measurements in square centimetres. This includes summing the root surface areas for each plant to provide a total root surface area per plant. A specialized Python script, executed in a Jupyter Notebook, matches the scans to the corresponding plants, ensuring that the data is accurately aggregated and reported.

Once the two first steps are completed, we have our images in an 8-bit grayscale format. Using the ImageJ software, we proceed to analyse the images and the fraction of the area covered by the roots. The process involves several key steps:

Opening the Program and Preparing the measurements: First, we open ImageJ and ensure that the measurement settings are configured to measure the area and the fraction of the area, and that the display options include labels as shown on the figure below.

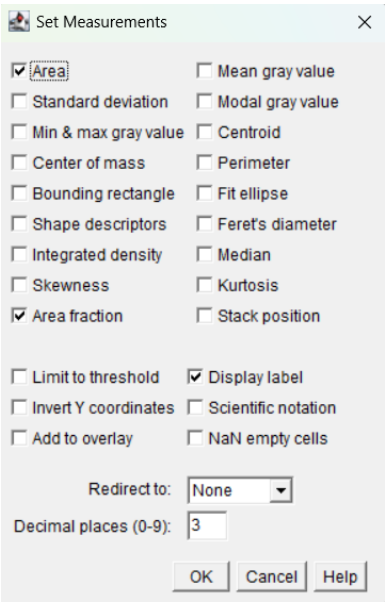

Figure 32: ImageJ Set Measurements window.

Recording the Macro (a macro is a script that automates repetitive tasks within a software): We open the macro recorder in ImageJ to record all the subsequent steps. This macro will then be used to automate the process for all the images.

Processing a Representative Image: We load a representative image and crop it to focus on the area of interest thus excluding the sides of the root container for the scans. Then we find and apply an appropriated threshold to distinguish the roots from the background as shown on the following figure.

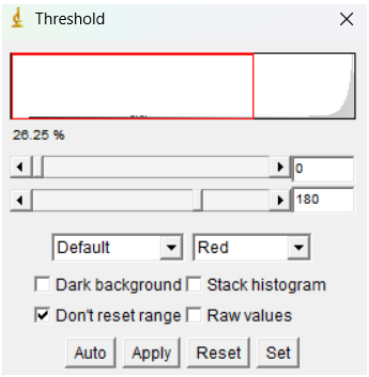

Figure 33: ImageJ setting threshold window.

If necessary we can use the “despeckle” option to remove noise and refine the image, ensuring that the root areas are clearly defined. And last we apply the measurement. Then we save the recorded macro. This macro captures all the steps: cropping, thresholding, noise removal and measurement. The macro will look like the following figure.

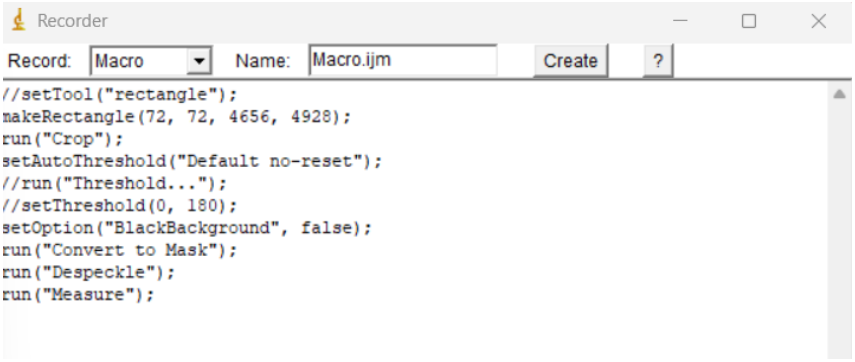

Figure 34: ImageJ Recorder window.

Once the macro is saved we can use it to process all the scanned images. The macro automatically applies the same steps to each image, ensuring uniformity and efficiency.

This batch processing will give us a CSV file containing for each image the name of the image, the corresponding area in number of pixels and the percentage of the area considered as root on the image. The result of this will look like the following figure.

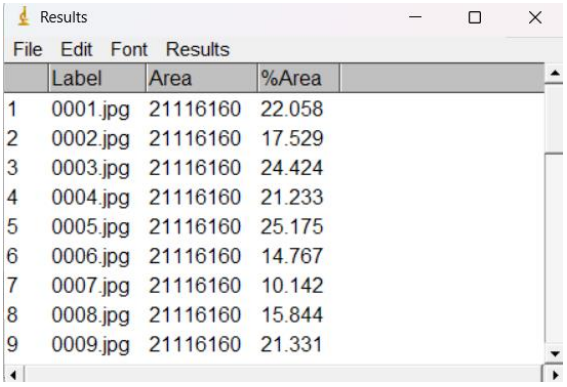

	Label	Area	%Area
1	0001.jpg	21116160	22.058
2	0002.jpg	21116160	17.529
3	0003.jpg	21116160	24.424
4	0004.jpg	21116160	21.233
5	0005.jpg	21116160	25.175
6	0006.jpg	21116160	14.767
7	0007.jpg	21116160	10.142
8	0008.jpg	21116160	15.844
9	0009.jpg	21116160	21.331

Figure 35: ImageJ Results window.

This automated process allows for efficient and accurate measurement of root areas across all images, providing a comprehensive dataset with the label, area, and percentage of area for each image.

Once the ImageJ analysis is done, a Python script handles the data to convert the percentage of area per image into root surface area in square centimetres. The entire pipeline process is structured around a folder system on the computer, which includes subfolders for storing the scans, processed images, and CSV files. The code is designed to operate within this folder structure, requiring only the folder details to locate and process the necessary files.

Based on the folder structure, the code imports CSV files containing the identifiers for images and associated plants. It also imports the CSV files with the image analysis results and calibration data from ImageJ.

Using the calibration measurements, the code calculates the number of pixels corresponding to a specific surface area, as determined during the calibration process. This pixel-to-surface area conversion factor is then applied to all subsequent calculations.

For each row in the ImageJ results CSV, the code converts the percentage of root area to a number of pixels. This pixel count is then multiplied by the conversion factor to obtain the root surface area in square centimetres for each image.

The code uses the image identifiers to match and sum the root surface areas for each plant. It creates a summary table that provides the total scanned root surface area for each plant.

There are two outputs of this code, as shown in the following figures. First, a summary table lists each plant along with its total root surface area in square centimetres. Then, a second summary table provides the surface area in square centimetres for each individual image.

Index	Plant Name	Number of Scans	Total cm2
0	x10	7	351.228
1	x11	7	274.099
2	x12	4	171.637
3	x5	3	120.185
4	x6	4	249.792
5	x7	3	145.464
6	x8	3	112.957
7	x9	5	220.607

Figure 37: Result summary list of plants and the corresponding root surface.

Index	label	area	%area	pixels	cm2	id
0	1	21612096	21.622	4.67297e+06	57.2273	x10
1	2	21612096	17.163	3.70928e+06	45.4256	x10
2	3	21612096	23.925	5.17069e+06	63.3227	x10
3	4	21612096	20.809	4.49726e+06	55.0756	x10
4	5	21612096	24.692	5.33646e+06	65.3528	x10
5	6	21612096	14.555	3.14564e+06	38.523	x10
6	7	21612096	9.937	2.14759e+06	26.3004	x10
7	8	21612096	15.496	3.34901e+06	41.0136	x11

Figure 36: : Result summary list of images and the corresponding root surface.

By following this structured approach, the code ensures accurate and efficient processing of the root surface area data, leveraging the predefined folder system and calibration data to produce reliable results. Both the Jupyter Notebook and the script are presented in “10.6. Annex 6: Pipeline 1 Jupyter notebook “ and “10.7. Annex 7: Pipeline 1 python script” for reference.

5.2.2. Pipeline 2 Transpiration pipeline

The scales are set to register the weight of the pots and the plants on top of them every 15 minutes for the entire duration of the experiment, generating a substantial amount of data. The datalogger records the date and time as well as the measured weight at that moment. The pipeline consists of a Python script, which can be found in "10.8. Annex 8: Pipeline 2 python script".

First, the data is imported from the files of the dataloggers. The data looks like the figure below, with one column for DateTime and one for the weight (in grams).

DateTime	weight
2023-05-19 16:15:00	1419.43
2023-05-19 16:30:00	1419
2023-05-19 16:45:00	1418.62
2023-05-19 17:00:00	1418.2
2023-05-19 17:15:00	1418
2023-05-19 17:30:00	1417.4
2023-05-19 17:45:00	1457.14
2023-05-19 18:00:00	1456.6
2023-05-19 18:15:00	1455.96
2023-05-19 18:30:00	1455.02
2023-05-19 18:45:00	1454.41

Figure 38: Screenshot of the weight measurements.

Next, since transpiration involves weight loss, the script calculates the difference between a weight measurement and the previous one to obtain the delta weight. This calculation is performed only if the time difference between the two measurements is as expected; otherwise, it indicates a datalogging failure, and the transpiration measurement cannot be assumed accurate. The resulting data includes a third column for the delta weight, as shown in the next figure.

DateTime	weight	delta_weight
2023-05-19 16:15:00	1419.43	-0.5
2023-05-19 16:30:00	1419	-0.43
2023-05-19 16:45:00	1418.62	-0.38
2023-05-19 17:00:00	1418.2	-0.42
2023-05-19 17:15:00	1418	-0.2
2023-05-19 17:30:00	1417.4	-0.6
2023-05-19 17:45:00	1457.14	39.74
2023-05-19 18:00:00	1456.6	-0.54
2023-05-19 18:15:00	1455.96	-0.64
2023-05-19 18:30:00	1455.02	-0.94
2023-05-19 18:45:00	1454.41	-0.61

Figure 39: Screenshot of the delta weight.

If a graph of the delta weight over time was generated, it would look similar to what is shown in the following figure.

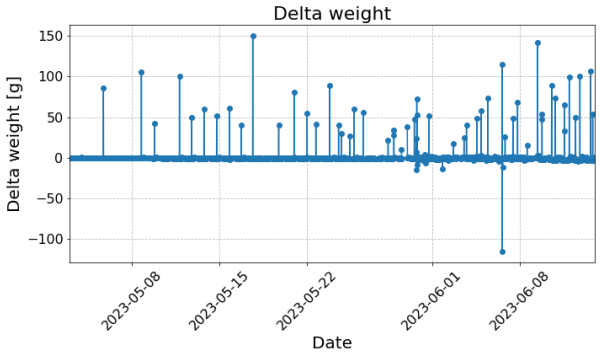

Figure 40: Graph of the delta weight.

The data shows both negative and positive delta weights. Negative delta weights could represent transpiration, while positive delta weights indicate an increase in the measured weight during the time span between two measurements. This means that the data needs to be separated between positive and negative delta weight for further processing. The following figure shows an example of the negative delta weight over time.

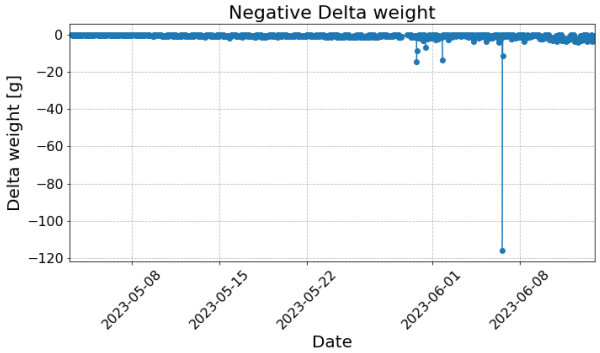

Figure 41: Graph of the negative delta weight.

Observing the negative delta weight, it seems that there are some outliers, which are unlikely to represent actual transpiration values and are probably due to measurement errors. Thus, the outliers need to be identified and flagged. To do so, a Z value is calculated for each data point. The Z value is calculated as follows:

$$Z = \frac{x - \mu}{\sigma}$$

where:

- x is the value of the data point.
- μ is the mean (average) of the dataset.
- σ is the standard deviation, which measures the spread or dispersion of the data.

A data point is considered an outlier if |Z| > 3, meaning it is more than 3 standard deviations away from the mean.

Since transpiration is linked to stomatal opening during photosynthesis, the negative delta weight values are separated based on whether the measurement was taken during the day or night. Additionally, because transpiration is influenced by plant size, a rolling mean and standard

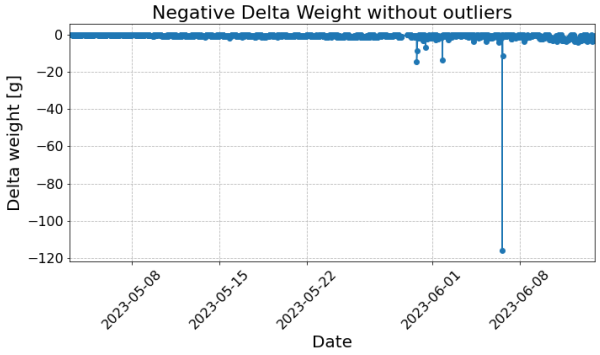

Figure 42: Graph of the negative delta weight after the first attempt to remove extreme values.

deviation for the Z value calculation are applied to obtain a more localized Z value. The window for the rolling mean and standard deviation is set to 7 days, so the rolling values are calculated from 3.5 days before to 3.5 days after the measurement. The graph of the data without the outliers detected by this first try is displayed in the next figure.

As we can see on the graph, bigger outliers are still there. After inspection, it seems to be due to the fact that a significant outlier can skew the rolling mean and standard deviation, causing outliers to go undetected. To address this issue, the calculation of the rolling mean and standard deviation is modified by excluding values that deviate more than 3 times the Median Absolute Deviation (MAD) from a rolling median. The rolling median is also calculated using a 7-day window, centered around the data point. The graph of the negative delta weight without the outliers detected by this second method is shown in the next figure.

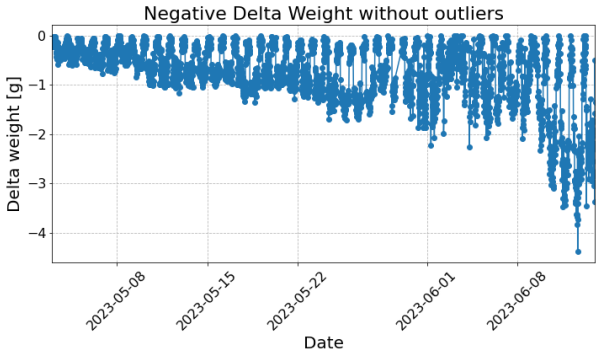

Figure 43: Graph of the negative delta weight after the second attempt to remove extreme values.

In this revised approach, the rolling statistics are calculated using only the data points that fall within a threshold based on the rolling median. This threshold is determined using the Median Absolute Deviation (MAD). By doing so, the pipeline ensures that extreme outliers do not influence the rolling statistics. The outliers are successfully flagged and set aside.

Once the negative delta weights have been sorted between outliers and non-outliers, the pipeline handles the positive delta weight. In the following figure, a graph of the positive delta weight over time is shown.

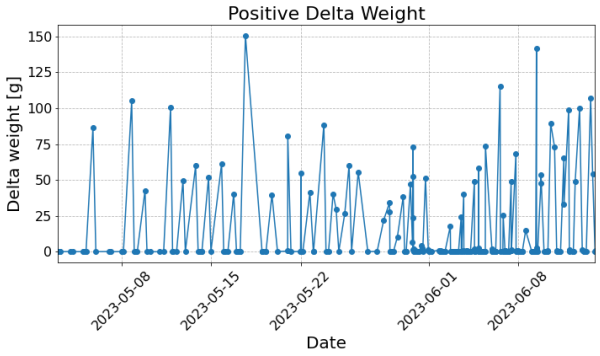

Figure 44: Graph of the positive delta weight.

Significant peaks, most likely corresponding to watering events, and smaller positive delta weight values, which could be due to ventilation or humidity spraying, causing an increase in the measured weight, are observed. It could also be due to leaf movements. To better handle these data, the two kinds of positive values are separated with a threshold. Values above the threshold are most likely watering events, whereas those below are due to other factors causing small measured weight increases.

Upon closer examination of the data, some values classified as watering events either preceded or followed a significant weight loss. This is due to a manipulation error where pressure was temporarily applied or lifted at the time the measurement was logged. The next figure displays an example of such an event.

DateTime	weight	delta_weight
2023-06-06 13:45:00	1337.19	-0.26
2023-06-06 14:00:00	1452.65	115.46
2023-06-06 14:15:00	1336.61	-116.04
2023-06-06 14:30:00	1336.36	-0.25

Figure 45: Example of a push pull anomaly.

As seen in the figure, a big positive delta weight is followed by a big negative one. Looking at the measured weight, it seems that the first value is the erroneous one, and the second is the return to the normal situation. These occurrences are flagged as push/pull events for correction.

The delta weight values are then categorized as transpiration, outliers, or push/pull events for the negative delta weights, and as watering, push/pull events, or small weight increases for the positive delta weights.

A weight correction algorithm for the push/pull events, outliers, and small weight increases is implemented. The correction is done by interpolating the previous correct weight and the next correct weight when possible. The resulting column, “Wcorr”, contains either the correct weight value (for correct values) or the corrected value.

With the corrected weight, the script calculates a corrected delta weight. This is done similarly to the initial delta weight calculation, ensuring no calculations are made over datalogging failures. The figure below illustrates the creation of the corrected weight and the corrected delta weight column.

DateTime	weight	delta_weight	Wcorr	corr_delta_weight
2023-06-06 13:45:00	1337.19	-0.26	1337.19	-0.26
2023-06-06 14:00:00	1452.65	115.46	1336.9	-0.29
2023-06-06 14:15:00	1336.61	-116.04	1336.61	-0.29
2023-06-06 14:30:00	1336.36	-0.25	1336.36	-0.25

Figure 46: Example of the corrected weight and delta weight.

The figure below shows the negative corrected delta weight over time.

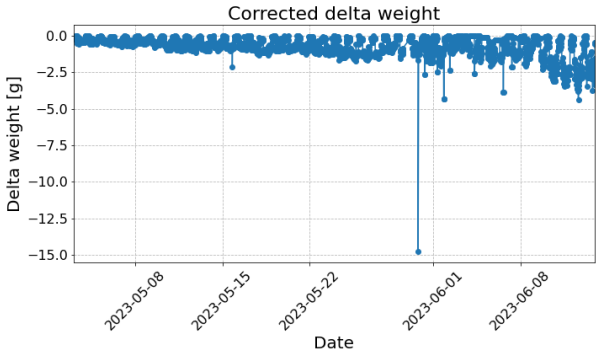

Figure 47: Graph of the corrected delta weight.

As observed in the graph, there are a few outliers among the corrected delta weight. Thus, the script detects outliers among the negative corrected delta weights. The data is separated into day and night measurements, and a rolling mean and standard deviation are used, similar to the previous approach. Values too far from a rolling median (more than 3 times the MAD) are excluded to calculate the outlier detection criteria. Additionally, corrected negative delta weights that were derived from corrections are not used to avoid error propagation.

Thus, the corrected delta weights are classified as either transpiration, outliers, values that could not be corrected, or watering events. The following figure shows the corrected delta weight over time that are considered to be transpiration weight variation.

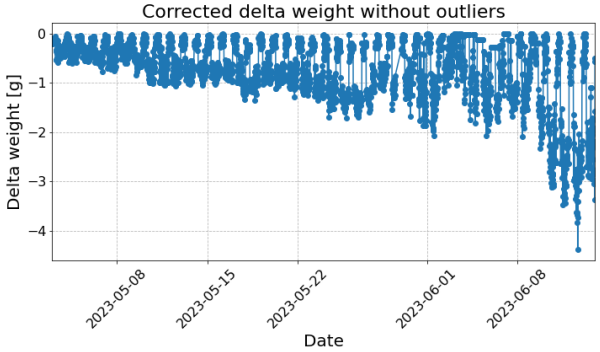

Figure 48: Graph of the corrected delta weight without outliers.

For values considered as transpiration, the transpiration rate is calculated by dividing the corrected delta weight (in grams) by the time span between two measurements (in minutes), yielding the transpiration rate in g/min. For all values that could not be corrected, the mean transpiration rate of the last 4 considered correct transpiration rates is used. The following figure displays the transpiration rate over time.

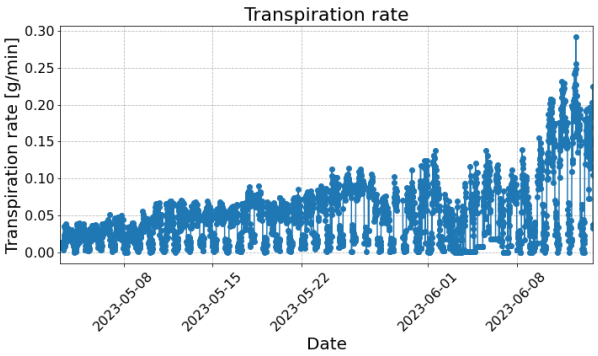

Figure 49: Graph of the calculated transpiration rate.

In summary, the transpiration pipeline does the following:

1. **Data Import**: Import weight data from datalogger files.
2. **Delta Weight Calculation**: Calculate the difference between consecutive weight measurements to obtain delta weight.
3. **Outlier Detection**: Among the negative delta weights, identify outliers using a Z-score method with a rolling mean and standard deviation, calculated by excluding values with a high median absolute deviation and separating day and night values.
4. **Detect Significant Weight Increases**: Among the positive delta weights, identify values that are higher than a defined threshold.
5. **Push/Pull Event Detection**: Identify and flag manipulation errors causing significant weight changes.
6. **Weight Correction**: Interpolate weights for push/pull events, outliers, and small weight increases to obtain corrected weights.
7. **Corrected Delta Weight Calculation**: Compute delta weight from corrected weights.
8. **Detect Outliers Among Corrected Delta Weights**: Identify outliers with a Z-score, excluding values with a high median absolute deviation and the corrected values from the calculation of the rolling mean and standard deviation.
9. **Transpiration Rate Calculation**: Calculate the transpiration rate from corrected delta weights and impute missing values with the mean of the last 4 correct values.

6. Discussion

In the following section the results and problem of the experiment will be discussed, focusing on the challenges and observations related to soil and leaf water potential, transpiration, root conductance, root surface and root conductivity. The variability in time required for plants to reach the desired stress level, difficulties in maintaining consistent soil water potential, and the occurrence of anomalous readings are explored in detail. These issues highlight the intricate interplay between plant physiology and environmental factors, such as lighting and soil water distribution. Additionally, the discussion addresses the limitations of the experimental setup, including pot size and data logging interruptions, which impacted the accuracy and consistency of the measurements. By reflecting on these challenges, the discussion proposes several improvements for future experiments, aiming to enhance the reliability of results and deepen the understanding of plant responses to water stress.

6.1. Soil water potential

In this section, we will discuss several key observations and challenges related to soil water potential as measured in our experiment. The focus will be on the time required for plants under stress treatment to reach the desired stress level, the difficulty in maintaining this level, the occurrence of unrealistically low values during the stress period, and the observed drops in soil water potential towards the end of the experiment.

Time to Reach Desired Stress Level:

One of the significant observations in our experiment was the variability in the time required for plants in the stress treatment to reach the desired soil water potential. The range was quite broad, with some plants taking approximately 3 days and others up to 7 days to achieve the target stress level. This disparity is likely due to differences in plant size and their respective transpiration rates; larger plants, which transpire more, reach the stress level quicker than smaller ones.

This variability could be attributed to uneven lighting within the phytotron, which led to differential growth rates. Plants in more illuminated areas grew larger, resulting in faster water consumption and quicker attainment of the stress level. To address this issue in future experiments, it would be beneficial to ensure a more uniform lighting setup. Additionally, normalizing plant size or measuring leaf area could help understand and mitigate this disparity, leading to more consistent results across different plants.

Difficulty in Maintaining Desired Stress Level:

Once the desired stress level was achieved, maintaining it proved to be a significant challenge. The strategy employed involved rewatering the pots to the weight corresponding to the initial stress level. However, this approach encountered several issues.

Firstly, during the treatment phase, some soil water potential values increased almost to control levels due to occasional overwatering errors. Conversely, other soil water potential values remained below, and sometimes well below, the targeted stress level. This discrepancy may be attributed to continued plant growth, which increased the water requirements not accounted for in subsequent water additions. Consequently, the initial weight used to determine the stress level no longer accurately reflected the growing plants' increased water needs.

Additionally, the method and frequency of top watering might have contributed to the issue. Frequent, small quantities of water applied to the surface may not have had sufficient time to reach the sensor level before being absorbed by the roots in the upper soil layers. This can result in sensor readings indicating lower soil water potential values than expected.

The literature suggests that high-frequency deficit irrigation (HFDI) is essential for maintaining a target soil water potential, though it often results in heterogeneous water distribution within the soil (Puértolas et al., 2017). Furthermore, as soil water content decreases, its hydraulic conductivity also diminishes (Lobet et al., 2014), which impedes water movement to deeper soil layers from the surface.

Turner's paper, "Imposing and Maintaining Soil Water Deficits in Drought Studies in Pots," highlights that small, shallow pots and frequent deficit irrigation are insufficient for effectively inducing and maintaining water deficits. Instead, larger, deeper pots with cycles of drying and rewetting more accurately replicate field water deficit conditions, thus enhancing the identification of drought-resistant traits (Turner, 2019).

For future experiments, establishing a water retention curve between soil water potential and soil water content would be advantageous. This curve would allow for more precise irrigation adjustments based on pot volume and the required water content to achieve the target soil water potential level. Utilising larger pots could also help sustain the targeted water deficit, although it may take longer to achieve. Additionally, re-evaluating the water deficit establishment method, such as incorporating cycles of gradual drying followed by complete rewetting, could prove beneficial. Implementing a more uniform and automated watering system could further ensure consistent stress levels and minimise human error.

Unrealistically Low Values During Stress Period:

During the stress period, some soil water potential measurements dropped to very low, and occasionally unrealistic, values, sometimes approaching pF 5. This level exceeds the permanent wilting point, which is commonly around pF 4.2 (Rai et al., 2017). Despite these extreme readings, the plants did not exhibit signs of irreversible stress and recovered upon rewatering, suggesting that the actual soil water potential did not reach such extreme levels.

As previously discussed, these unusually low readings could be attributed to soil water heterogeneity (Puértolas et al., 2017). Variations in water distribution within the soil can lead to inconsistent sensor readings. Another likely cause of these anomalies is soil cracking. As the soil dries, it contracts and forms cracks, which can disrupt the contact between the TEROS21 sensors and the soil. This disruption can result in erroneous readings that do not accurately reflect the true soil water potential.

To address these issues, it may be necessary to explore alternative methods for measuring soil water potential or to adjust the experimental setup to mitigate the impact of soil cracking. Ensuring better contact between sensors and the soil could improve measurement accuracy. Additionally, incorporating measures to reduce soil cracking, such as adjusting watering techniques, using soil with a lower clay content, or adding soil amendments, might enhance the reliability of soil water potential data.

Difficulty Maintaining High Soil Water Potential Towards Experiment End:

Towards the end of the experiment, maintaining a high soil water potential became increasingly difficult, with values dropping to around pF 3 during the day and rising again upon watering. This

fluctuation is primarily attributed to the increased water demand from the larger plants and the limited water-holding capacity of the pots.

The challenge arises chiefly because the small size of the pots restricts the soil volume, limiting the amount of water available for transpiration and leading to rapid depletion. Additionally, as the plants grew significantly over the course of the experiment, their increased weight further compounded the issue. Although an initial adjustment for plant biomass was made, it was based on a mean weight measured at the end of the growing phase. This correction became less effective as the plants continued to grow, with the mean weight increasingly underestimating the actual biomass of the larger plants.

These factors combined to create a dynamic where maintaining a high soil water potential became more challenging as the experiment progressed.

6.2. Leaf water potential with Psychrometer

While using psychrometers from ICT International to measure leaf water potential, two primary issues were encountered: zero readings (where the measured leaf water potential curve remained flat at zero) and data logging interruptions. However, one sensor provided valid measurements without exhibiting these problems. In this section, we will discuss these three points: the causes and implications of zero readings, the reasons behind data logging interruptions, and the comparison between psychrometer and Scholander pressure chamber measurements to evaluate the accuracy of the psychrometer readings.

Constant Zero Readings:

The constant zero readings observed in some measurements can be attributed to various factors. If the thermocouples are in contact with each other or both are touching the chamber walls, they may register the same temperature, resulting in a differential voltage of zero. This effectively means no potential difference is recorded. Additionally, improper calibration of the sensors can lead to inaccurate readings, including constant zero values. Physical damage to the thermocouples or the psychrometer unit can also result in erroneous zero readings.

Data Logging Interruptions:

Interruptions in data recording can be due to several reasons. The data logger might stop functioning properly, halting data collection. There could be problems in the communication link between the sensor and the data logger, leading to data loss. Furthermore, connectivity issues or software bugs can interrupt the download or recording of data.

Comparison of Psychrometer and Other Measurements:

One psychrometer provided non-zero leaf water potential readings without data logging interruptions, monitoring a plant under stress treatment. The values oscillated between 0 MPa at night and around -0.3 MPa at the lowest peaks during the day. In comparison, the Scholander pressure chamber measured values between -0.95 to -1.35 MPa for the same group, taken in the morning. Literature shows that maize in well-watered conditions has a leaf water potential around -0.5 MPa (Foyer et al., 1998), and maize under water deficit can reach a leaf water potential below - 1.4 MPa (Riboldi et al., 2016). Additionally, soil water potential during the treatment phase sometimes reached pF 4, equivalent to -1 MPa. Given that the transpiration rate decreased but did not drop to zero during stress, and the psychrometer readings did not reflect the expected lower

leaf water potential necessary for water uptake from the soil, the psychrometer measurements appear unreliable and inconsistent with expected values, suggesting potential calibration issues.

To address the problem of zero readings, a thorough check of the thermocouple placement is necessary before using the psychrometers. More generally, these discussions highlight the importance of proper setup, maintenance, and calibration of equipment to obtain accurate measurements of leaf water potential using psychrometers.

6.3. Transpiration

Data Gaps and Solutions:

In the results section, gaps in the transpiration data were observed, primarily due to datalogger failures. Upon detection, the dataloggers were reinitialized and restored. To avoid such issues in future experiments, it is essential to explore alternative data logging methods that ensure continuous measurement without gaps.

Transpiration Variations:

At the beginning of the experiment, total transpiration was similar across all plants, but differences emerged towards the end. These variations are likely linked to differences in plant size due to uneven lighting in the phytotron. Future experiments should aim for more uniform environmental conditions. Additionally, early water deficits in maize reduce plant height and biomass ((Abrecht & Carberry, 1993). As larger leaf areas lead to higher transpiration rates (Kozlowski & Pallardy, 1997), it would be beneficial to continuously evaluate leaf area to normalise and compare transpiration rates ($g/m^2/s$).

Soil Water Potential and Transpiration:

By comparing soil water potential with transpiration over the experiment, it was observed that transpiration decreased in response to changes in soil water potential, as suggested by Jerszurki et al. (2017).

Evaluating Transpiration Models:

If reliable measurements for soil and leaf water potential are obtained in future experiments, we can assess the accuracy of the classical tension-cohesion model (Steudle, 2001) for predicting transpiration rates. Alternatively, as suggested by Couvreur et al. (2018), models that include osmotic gradients might provide better predictions of observed transpiration rates.

Transpiration Estimation Methods:

Transpiration was estimated using a pipeline based on weight variations. Comparing this method with other techniques, such as porometer measurements (Pearcy et al., 2000), could validate the pipeline's accuracy and offer insights into improving measurement techniques.

Addressing Outliers:

Future studies should consider factors like ventilation and moisture spray that may induce ripple effects, causing outliers. Evaluating the impact of pot manipulation during watering on data accuracy is also crucial.

Preventing Soil Water Evaporation:

In our data processing, we assumed that all weight variations were due to plant transpiration, with aluminium foil used to prevent direct evaporation from the soil. However, if the aluminium foil does not completely prevent evaporation, it will be necessary to account for this factor in future measurements. Assessing the effectiveness of the aluminium foil is crucial to minimize external variables, ensuring that observed weight changes more accurately reflect actual transpiration rates and improving the reliability of our data.

6.4. Root conductance

The ANOVA analysis revealed significant differences in root hydraulic conductance between different experimental stages, which aligns with expectations. As the plants grew, their root systems expanded, leading to increased hydraulic conductance.

However, no significant differences were found between treatments, suggesting that the maize roots did not exhibit adaptive changes within the experimental period. While literature suggests that water deficit can affect root conductance (Alsina et al., 2010; Jafarikouhini & Sinclair, 2023), the lack of significant changes in this experiment could be due to the treatment period being too short, insufficiently maintained water deficit, or limited sample size. Future experiments with longer durations, better-maintained conditions, and more repetitions could provide more robust results for comparison.

6.5. Root surface

The ANOVA analysis of root surface area during the experiment revealed no significant differences between treatments, stages, or their interactions. This is somewhat unexpected, as literature often reports that plants under water stress tend to allocate more resources to root development. For example, Gregory (2006) found that plants in dry soils develop more extensive root systems, including deeper rooting and greater root length. Other studies, such as Benjamin et al. (2014) have shown a linear decline in both root and shoot growth under water deficit stress, with shoot growth being more severely affected, leading to an increase in the root-to-shoot ratio.

The lack of significant differences in our experiment might be due to the limited pot size, which could have constrained root growth as the plants developed. Under normal conditions, maize roots would continue expanding with plant growth, leading to increased root surface area. However, the confined space likely inhibited this natural process. Additionally, the difficulty we encountered in maintaining the desired soil water potential for the stress treatment, along with the time it took for the plants to reach this threshold, might have prevented a measurable adaptation in root growth. The small sample size may also have limited the statistical power to detect subtle differences.

To better understand how maize root systems respond to water stress, future experiments should use larger pots to allow unrestricted root growth, better manage the water deficit treatments, and increase the number of replicates. Measuring the total leaf surface area and the weight of both the shoot and root systems would enable the calculation of the shoot-to-root ratio, a key metric for determining whether there is a shift in resource allocation between above-ground and below-

ground structures in response to different treatments. This would provide a clearer understanding of plant adaptation strategies under varying environmental conditions.

6.6. Root conductivity

We observed significant differences in root hydraulic conductivity, notably in the "Treatment Stressed" group, where an increase was detected. This aligns with findings by Hose et al. (2000), which link increased abscisic acid (ABA) levels under stress to enhanced maize root conductivity.

The variation between the "Treatment Stressed" and "Rewatering Stressed" groups suggests that these changes are reversible, with conductivity rising under stress and falling upon rehydration.

The unexpected difference between the "Treatment Control" and "Rewatering Control" groups might be attributed to the observed drop in soil water potential towards the experiment's end, potentially triggering a stress response in the control plants.

It's important to note that these statistical analyses were based on only four replicates per group, which limits the robustness of the findings. In future experiments, increasing the number of replicates would help to ensure more reliable and accurate results.

6.7. Leaf water potential with Scholander pressure chamber

The ANOVA analysis reveals a significant interaction effect between treatment and stage on leaf water potential, suggesting that the influence of treatment varies depending on the stage of the experiment. This could imply inconsistencies in how soil water potential was maintained or applied for the control treatment across different phases of the experiment.

The significant differences found through Tukey's HSD test further elaborate on this interaction. For instance, both the "Control Treatment" and "Stressed Treatment" groups showed significantly lower leaf water potential compared to their respective control groups during the growth stage.

This suggests that plants subjected to stress treatments experienced a notable decline in leaf water potential, which is consistent with expectations under water deficit conditions. Lower leaf water potential in the "Stressed Treatment" group aligns with stress-induced reductions in water availability, leading to more negative water potential values.

It's surprising not to observe a significant difference between the "Treatment Control" and "Treatment Stressed" groups in leaf water potential. Typically, we would expect the leaf water potential in the "Treatment Control" group not to drop, suggesting that the stress application might not have been fully controlled. This raises the possibility that some level of stress was inadvertently applied to the control group. Another possible explanation of such an observation is that the plant in the group "Treatment Control" have an increased transpiration rate due to a larger leaf area and thus the leaf water potential might be lower depending on the air humidity and temperature when the sampling was conducted as suggested by Couvreur et al. (2014).

By comparing this with the soil water potential data at the end of the treatment phase, it is noticeable that some control plants experienced lower soil water potential during certain times of the day. This suggests that these control plants might have undergone a slight stress, which could explain the lower leaf water potential observed.

The increase in leaf water potential during the rewatering phase in the "Stressed Rewatering" group compared to the "Stressed Treatment" group indicates a recovery effect, reflecting the plant's ability to regain water status upon rehydration. This recovery is a positive sign that the plants were able to respond to the alleviation of stress and is consistent with what has been already observed (Parent et al., 2009).

In future experiments, it's crucial to improve the monitoring and application of soil water potential in the control treatment group. Any lapses could inadvertently introduce mild water stress, which, as shown by (Zhang et al., 2023), can significantly alter leaf water potential. (Parent et al., 2009)

7. Perspectives

Ensuring uniform experimental conditions, such as consistent light, is critical to minimise the variability in plant responses. To enhance statistical power, increasing the number of replicates per treatment group is recommended, reducing the influence of outliers and yielding more robust results.

Several improvements could enhance the experimental protocol. Using larger pots would facilitate more natural root growth, avoiding constraints that may impact plant development and water uptake measurements. Additionally, adding measurements like leaf surface area and fresh and dry weights of leaves and roots would enable a more comprehensive analysis, helping to normalise other measurements and assess the effects of stress and rewatering on biomass allocation.

Investigating water potential further by measuring osmotic potential is also important. This could be done by collecting leaf sap from pressure chambers for osmometer analysis or assessing soil osmotic potential through diluted soil samples.

For better soil water management, establishing a relationship curve between soil water content and water potential, rather than relying on target weights, would ensure consistent soil water potential throughout the experiment, particularly for the control group. Implementing an automated watering system could maintain desired soil water potential levels and prevent issues arising from manual watering.

Refining and validating existing data analysis pipelines will allow for more effective handling of large datasets, ensuring accurate estimations of transpiration rates and verifying assumptions like negligible pot evaporation. By implementing these changes, future experiments will be better equipped to investigate plant responses to stress, leading to more reliable and insightful outcomes.

8. Conclusion

This master's thesis had two main objectives: to quantify maize's response to water deficit through an experimental protocol and to establish reliable data management pipelines. The ANOVA analysis revealed some significant findings, particularly in root hydraulic conductance and leaf water potential, which provide partial insights into the plant's response under the experimental conditions.

Significant differences in root hydraulic conductance were observed across various experimental stages, reflecting the expected increase as the plants grew. However, no significant differences were found between the water-stressed and well-watered treatments, indicating that the maize roots did not exhibit notable adaptive changes during the experiment. This suggests that the treatment period may have been too short or the water deficit insufficiently maintained to induce such changes.

The analysis of root surface area showed no significant differences between treatments, stages, or their interactions. This was unexpected, given that literature often reports an increase in root development under water stress. The lack of observed differences may be attributed to constraints imposed by the limited pot size and the challenges in maintaining consistent soil water potential during the experiment.

In terms of root hydraulic conductivity, significant increases were noted in the "Treatment Stressed" group, aligning with existing research that links stress-induced abscisic acid (ABA) production to enhanced root conductivity. These changes appear to be reversible, with conductivity rising under stress and decreasing upon rehydration, emphasising the dynamic response of maize roots to water availability.

Lastly, the significant interaction effect between treatment and stage on leaf water potential underscores the variability in treatment application across different experimental stages. Lower leaf water potential in stressed plants during the treatment stage was consistent with expectations, although some anomalies were observed in the control group, likely due to unintentional stress or variations in environmental conditions.

While these findings provide valuable insights, the experiment's limitations—such as the small sample size and non-uniform environmental conditions—highlight the need for further refinement in future studies. As discussed in the "Perspectives" section, these improvements will be essential for enhancing the precision and reliability of future research on crop responses to water stress.

Despite these challenges, this initial experiment has laid important groundwork for future research. Two crucial data management pipelines were developed: one for efficiently measuring root surface area and another for accurately determining transpiration rates from scale measurements. These tools represent a significant step forward in managing and analysing the complex data generated in plant physiology experiments.

The insights and methodologies developed in this thesis will guide future studies, helping to ensure that subsequent research is carried out with improved precision and effectiveness. While the experiment faced certain limitations, these have also highlighted areas for improvement, which will be addressed in future work to produce more reliable and informative results in the study of plant responses to water stress.

9. References

Abrecht, D. G., & Carberry, P. s. (1993). The influence of water deficit prior to tassel initiation on maize growth, development and yield. *Field Crops Research*, *31*(1), 55–69. https://doi.org/10.1016/0378-4290(93)90050-W

Alsina, M. M., Smart, D. R., Bauerle, T., de Herralde, F., Biel, C., Stockert, C., Negron, C., & Save, R. (2010). Seasonal changes of whole root system conductance by a drought-tolerant grape root system. *Journal of Experimental Botany*, *62*(1), 99–109. https://doi.org/10.1093/jxb/erq247

Bai, X.-F., Zhu, J.-J., Zhang, P., Wang, Y.-H., Yang, L.-Q., & Zhang, L. (2007). Na+ and Water Uptake in Relation to the Radial Reflection Coefficient of Root in Arrowleaf Saltbush Under Salt Stress. *Journal of Integrative Plant Biology*, *49*(9), 1334–1340. https://doi.org/10.1111/j.1744-7909.2007.00529.x

Benjamin, J. G., Nielsen, D. C., Vigil, M., Mikha, M., & Calderon, F. (2014). Water Deficit Stress Effects on Corn (Zea mays , L.) Root:Shoot Ratio. *Open Journal of Soil Science*, *04*, 151–160. https://doi.org/10.4236/ojss.2014.44018

Brown, H. R. (2013). The Theory of the Rise of Sap in Trees: Some Historical and Conceptual Remarks. *Physics in Perspective*, *15*(3), 320–358. https://doi.org/10.1007/s00016-013-0117-1

Buck, A. L. (1981). New equations for computing vapor pressure and enhancement factor. *Journal of Applied Meteorology (1962-1982)*, 1527–1532.

Chavarria, G., & dos Santos, H. P. (2012). *Plant water relations: Absorption, transport and control mechanisms*.

Chaves, M. M., Maroco, J. P., & Pereira, J. S. (2003). Understanding plant responses to drought—From genes to the whole plant. *Functional Plant Biology : FPB*, *30*(3), 239–264. https://doi.org/10.1071/FP02076

Cirelli, D., Lieffers, V. J., & Tyree, M. T. (2012). Measuring whole-plant transpiration gravimetrically: A scalable automated system built from components. *Trees*, *26*(5), 1669–1676. https://doi.org/10.1007/s00468-012-0731-6

Couvreur, V., Faget, M., Lobet, G., Javaux, M., Chaumont, F., & Draye, X. (2018). Going with the Flow: Multiscale Insights into the Composite Nature of Water Transport in Roots. *Plant Physiology*, *178*(4), 1689–1703. https://doi.org/10.1104/pp.18.01006

Couvreur, V., Heymans, A., Lobet, G., & Draye, X. (2021). Evidence for a multicellular symplasmic water pumping mechanism across vascular plant roots. *BioRxiv*. https://dial.uclouvain.be/pr/boreal/fr/object/boreal%3A251387

Couvreur, V., Vanderborght, J., Draye, X., & Javaux, M. (2014). Dynamic aspects of soil water availability for isohydric plants: Focus on root hydraulic resistances. *Water Resources Research*, *50*(11), 8891–8906.

CR1000—Measurement and Control Datalogger. (n.d.). Retrieved 22 September 2023, from https://www.campbellsci.com/cr1000

De Swaef, T., Pieters, O., Appeltans, S., Borra-Serrano, I., Coudron, W., Couvreur, V., Garré, S., Lootens, P., Nicolaï, B., Pols, L., Saint Cast, C., Šalagovič, J., Van Haeverbeke, M., Stock, M., & wyffels, F. (2022). On the pivotal role of water potential to model plant physiological processes. *In Silico Plants*, *4*(1), diab038. https://doi.org/10.1093/insilicoplants/diab038

Dobra, J., Motyka, V., Dobrev, P., Malbeck, J., Prasil, I. T., Haisel, D., Gaudinova, A., Havlova, M., Gubis, J., & Vankova, R. (2010). Comparison of hormonal responses to heat, drought and combined stress in tobacco plants with elevated proline content. *Journal of Plant Physiology*, *167*(16), 1360–1370. https://doi.org/10.1016/j.jplph.2010.05.013

Draye, X., Kim, Y., Lobet, G., & Javaux, M. (2010). Model-assisted integration of physiological and environmental constraints affecting the dynamic and spatial patterns of root water

uptake from soils. *Journal of Experimental Botany*, *61*(8), 2145–2155. https://doi.org/10.1093/jxb/erq077

Enns, L. C., Canny, M. J., & McCully, M. E. (2000). An investigation of the role of solutes in the xylem sap and in the xylem parenchyma as the source of root pressure. *Protoplasma*, *211*(3), 183–197. https://doi.org/10.1007/BF01304486

Erenstein, O., Jaleta, M., Sonder, K., Mottaleb, K., & Prasanna, B. M. (2022). Global maize production, consumption and trade: Trends and R&D implications. *Food Security*, *14*(5), 1295–1319. https://doi.org/10.1007/s12571-022-01288-7

FAO. (2023a). *The Impact of Disasters on Agriculture and Food Security 2023 – Avoiding and reducing losses through investment in resilience.*

FAO. (2023b). *World Food and Agriculture – Statistical Yearbook 2023*.

FAO, IFAD, UNICEF, WFP, & WHO. (2024). *The State of Food Security and Nutrition in the World 2024 – Financing to end hunger, food insecurity and malnutrition in all its forms*.

Farooq, M., Wahid, A., Kobayashi, N., Fujita, D., & Basra, S. M. A. (2009). Plant drought stress: Effects, mechanisms and management. *Agronomy for Sustainable Development*, *29*(1), 185–212. https://doi.org/10.1051/agro:2008021

Flexas, J., Bota, J., Loreto, F., Cornic, G., & Sharkey, T. D. (2004). Diffusive and Metabolic Limitations to Photosynthesis under Drought and Salinity in C3 Plants. *Plant Biology*, *6*(3), 269–279. https://doi.org/10.1055/s-2004-820867

Flexas, J., Scoffoni, C., Gago, J., & Sack, L. (2013). Leaf mesophyll conductance and leaf hydraulic conductance: An introduction to their measurement and coordination. *Journal of Experimental Botany*, *64*(13), 3965–3981. https://doi.org/10.1093/jxb/ert319

Foyer, C., Valadier, M., Migge, A., & Becker, T. (1998). Drought-Induced Effects on Nitrate Reductase Activity and mRNA and on the Coordination of Nitrogen and Carbon Metabolism in Maize Leaves. *Plant Physiology*, *117*, 283–292.

Gregory, P. J. (2006). Roots and the Physico-Chemical Environment. In *Plant Roots: Growth, Activity, and Interaction with Soils* (pp. 131–173). Blackwell Publishing.

HCFM-XP Gen 3 Hydraulic Conductance Flow Meter—Dynamax. (n.d.). Retrieved 18 September 2023, from https://dynamax.com/products/plant-hydraulic-conductance/hcfm-xp-gen-3-hydraulic-conductance-flow-meter

Hillel, D. (2013). *Introduction to Soil Physics*. Academic Press.

Hose, E., Steudle, E., & Hartung, W. (2000). Abscisic acid and hydraulic conductivity of maize roots: A study using cell- and root-pressure probes. *Planta*, *211*(6), 874–882. https://doi.org/10.1007/s004250000412

Hsiao, T. C., & Acevedo, E. (1974). Plant responses to water deficits, water-use efficiency, and drought resistance. *Agricultural Meteorology*, *14*(1), 59–84. https://doi.org/10.1016/0002-1571(74)90011-9

ICT - PSY1—Plants—Stem Psychrometers By ICT International. (n.d.). Retrieved 20 November 2023, from https://www.agriculture-xprt.com/products/ict-model-psy1-stem-psychrometers-182474

IPCC. (2023). *Climate Change 2023 Synthesis Report*.

Jafarikouhini, N., & Sinclair, T. R. (2023). Hydraulic conductance and xylem vessel diameter of young maize roots subjected to sustained water-deficit. *Crop Science*, *63*(4), 2458–2464. https://doi.org/10.1002/csc2.21023

Jerszurki, D., Couvreur, V., Maxwell, T., Silva, L. de C. R., Matsumoto, N., Shackel, K., de Souza, J. L. M., & Hopmans, J. (2017). Impact of root growth and hydraulic conductance on canopy carbon-water relations of young walnut trees (*Juglans regia* L.) under drought. *Scientia Horticulturae*, *226*, 342–352. https://doi.org/10.1016/j.scienta.2017.08.051

Jones, H. (2013). Plants and Microclimate: A Quantitative Approach to Environmental Plant Physiology. *Plants and Microclimate: A Quantitative Approach to Environmental Plant Physiology*, 1–407. https://doi.org/10.1017/CBO9780511845727

Jones, H. G., & Corlett, J. E. (1992). Current topics in drought physiology. *The Journal of Agricultural Science*, *119*(3), 291–296. https://doi.org/10.1017/S0021859600012144

King-Okumu, C. (2021). *A rapid review of drought risk mitigation measures*. FAO ; https://openknowledge.fao.org/handle/20.500.14283/cb7085en

Kirkham, M. B. (2005). 8—Field Capacity, Wilting Point, Available Water, and the Non-Limiting Water Range. In M. B. Kirkham (Ed.), *Principles of Soil and Plant Water Relations* (pp. 101–115). Academic Press. https://doi.org/10.1016/B978-012409751-3/50008-6

Kozlowski, T. T., & Pallardy, S. G. (1997). CHAPTER 12—Transpiration and Plant Water Balance. In T. T. Kozlowski & S. G. Pallardy (Eds.), *Physiology of Woody Plants (Second Edition)* (Second Edition, pp. 269–308). Academic Press. https://doi.org/10.1016/B978-012424162-6/50029-6

Kramer, P. J., & Boyer, J. S. (1995). *Water relations of plants and soils*. Academic Press.

Lisar, S. Y., Motafakkerazad, R., Hossain, M., & M M Rahman, I. (2012). *Water Stress in Plants: Causes, Effects and Responses* (pp. 1–14). https://doi.org/10.5772/39363

Lobet, G., Couvreur, V., Meunier, F., Javaux, M., & Draye, X. (2014). Plant Water Uptake in Drying Soils. *Plant Physiology*, *164*, 1619–1627. https://doi.org/10.1104/pp.113.233486

Mittler, R. (2002). Oxidative stress, antioxidants and stress tolerance. *Trends in Plant Science*, *7*(9), 405–410. https://doi.org/10.1016/s1360-1385(02)02312-9

Monteith, J., & Unsworth, M. (2013). *Principles of Environmental Physics: Plants, Animals, and the Atmosphere*. Academic Press.

Mullins, M. G., Bouquet, A., & Williams, L. E. (1992). *Biology of the Grapevine*. Cambridge University Press.

Nobel, P. S. (2009). *Physicochemical \& environmental plant physiology* (4th ed.). Academic press.

Parent, B., Hachez, C., Redondo, E., Simonneau, T., Chaumont, F., & Tardieu, F. (2009). Drought and Abscisic Acid Effects on Aquaporin Content Translate into Changes in Hydraulic

Conductivity and Leaf Growth Rate: A Trans-Scale Approach. *Plant Physiology*, *149*(4), 2000–2012. https://doi.org/10.1104/pp.108.130682

Pearcy, R. W., Schulze, E.-D., & Zimmermann, R. (2000). Measurement of transpiration and leaf conductance. In R. W. Pearcy, J. R. Ehleringer, H. A. Mooney, & P. W. Rundel (Eds.), *Plant Physiological Ecology: Field methods and instrumentation* (pp. 137–160). Springer Netherlands. https://doi.org/10.1007/978-94-010-9013-1_8

Pirasteh-Anosheh, H., Saed-Moucheshi, A., Pakniyat, H., & Pessarakli, M. (2016). Stomatal responses to drought stress. In *Water Stress and Crop Plants* (pp. 24–40). John Wiley & Sons, Ltd. https://doi.org/10.1002/9781119054450.ch3

Psychrometer PSY1 for Plant Water Potential and Water Stress. (n.d.). *ICT International*. Retrieved 20 November 2023, from https://ictinternational.com/product/psy1-psychrometer-for-plant-water-potential/

Puértolas, J., Larsen, E. K., Davies, W. J., & Dodd, I. C. (2017). Applying 'drought' to potted plants by maintaining suboptimal soil moisture improves plant water relations. *Journal of Experimental Botany*, *68*(9), 2413–2424. https://doi.org/10.1093/jxb/erx116

Rai, R. K., Singh, V. P., & Upadhyay, A. (2017). Chapter 17—Soil Analysis. In R. K. Rai, V. P. Singh, & A. Upadhyay (Eds.), *Planning and Evaluation of Irrigation Projects* (pp. 505–523). Academic Press. https://doi.org/10.1016/B978-0-12-811748-4.00017-0

Riboldi, L., Oliveira, R., & Angelocci, L. (2016). Leaf turgor pressure in maize plants under water stress: *Australian Journal of Crop Science*, *10*, 878–886. https://doi.org/10.21475/ajcs.2016.10.06.p7602

Rowan, A., McCully, M. E., & Canny, M. J. (2000). The origin of the exudate from cut maize roots. *Plant Physiology and Biochemistry*, *38*(12), 957–967. https://doi.org/10.1016/S0981-9428(00)01205-5

Sage, R. F. (2004). The evolution of C4 photosynthesis. *New Phytologist*, *161*(2), 341–370.

Schenk, H. J., Jansen, S., & Hölttä, T. (2021). Positive pressure in xylem and its role in hydraulic function. *New Phytologist*, *230*(1), 27–45. https://doi.org/10.1111/nph.17085

Scholander, P. F., Bradstreet, E. D., Hemmingsen, E., & Hammel, H. (1965). Sap Pressure in Vascular Plants: Negative hydrostatic pressure can be measured in plants. *Science*, *148*(3668), 339–346.

Seleiman, M. F., Al-Suhaibani, N., Ali, N., Akmal, M., Alotaibi, M., Refay, Y., Dindaroglu, T., Abdul-Wajid, H. H., & Battaglia, M. L. (2021). Drought Stress Impacts on Plants and Different Approaches to Alleviate Its Adverse Effects. *Plants (Basel, Switzerland)*, *10*(2). https://doi.org/10.3390/plants10020259

Shackel, K. (2022, June 27). *The Pressure Chamber (The Bomb)*. Fruit & Nut Research & Information Center. https://fruitsandnuts.ucdavis.edu/pressure_chamber

Software & Downloads—Dynamax. (n.d.). Retrieved 18 September 2023, from https://dynamax.com/technical-center/software

Steudle, E. (2001). THE COHESION-TENSION MECHANISM AND THE ACQUISITION OF WATER BY PLANT ROOTS. *Annual Review of Plant Physiology and Plant Molecular Biology*, *52*, 847–875. https://doi.org/10.1146/annurev.arplant.52.1.847

Tadesse, A., & Anteneh, M. (2018). *Drought Tolerance Mechanisms in Field Crops*.

Taiz, L., Zeiger, E., Møller, I. M., & Murphy, A. (2015). *Plant physiology and development* (6th ed.). Sinauer Associates.

Tardieu, F. (2012). Any trait or trait-related allele can confer drought tolerance: Just design the right drought scenario. *Journal of Experimental Botany*, *63*(1), 25–31. https://doi.org/10.1093/jxb/err269

Tardieu, F., Granier, C., & Muller, B. (2011). Water deficit and growth. Co-ordinating processes without an orchestrator? *Current Opinion in Plant Biology*, *14*(3), 283–289. https://doi.org/10.1016/j.pbi.2011.02.002

Tardieu, F., & Simonneau, T. (1998). Variability among species of stomatal control under fluctuating soil water status and evaporative demand: Modelling isohydric and anisohydric behaviours. *Journal of Experimental Botany*, *49*(Special_Issue), 419–432. https://doi.org/10.1093/jxb/49.Special_Issue.419

TEROS 21. (2021, July 28). METER. https://www.metergroup.com/en/meter-environment/products/teros-21-soil-water-potential-sensor

Turner, N. (2019). Imposing and maintaining soil water deficits in drought studies in pots. *Plant and Soil*, *439*, 1–11. https://doi.org/10.1007/s11104-018-3893-1

Tyree, M. T., Patiño, S., Bennink, J., & Alexander, J. (1995). Dynamic measurements of roots hydraulic conductance using a high-pressure flowmeter in the laboratory and field. *Journal of Experimental Botany*, *46*(1), 83–94. https://doi.org/10.1093/jxb/46.1.83

Tyree, M. T., & Zimmermann, M. H. (2013). *Xylem structure and the ascent of sap*. Springer Science & Business Media.

UNESCO World Water Assessment Programme. (2024). *The United Nations World Water Development Report 2024: Water for prosperity and peace*.

Vetterlein, D., Lippold, E., Schreiter, S., Phalempin, M., Fahrenkampf, T., Hochholdinger, F., Marcon, C., Tarkka, M., Oburger, E., Ahmed, M., Javaux, M., & Schlüter, S. (2021). Experimental platforms for the investigation of spatiotemporal patterns in the rhizosphere—Laboratory and field scale. *Journal of Plant Nutrition and Soil Science*, *184*(1), 35–50. https://doi.org/10.1002/jpln.202000079

WMO. (2022). *Drought and Water Scarcity*.

Zhang, Y., Xiaowei, D., Chen, Z., & Hou, G. (2023). A study on the physiological parameters of corn during the jointing stage of growth under soil water stress based on the PSII light quantum yield (QY). *HydroResearch*, *6*, 177–183. https://doi.org/10.1016/j.hydres.2023.04.002

10. Annexes

10.1. Annex 1: Experiment 2 methodology

Experimental design:

In this experiment, we followed the same methodology as in the first, wherein plants were divided into two treatments: a well-watered control group and a stress treatment subjected to water deficit.

Treatments:

The treatment conditions remained consistent between the two experiments, with plants in the control treatment maintained under regular watering conditions to sustain soil water potential close to field capacity. However, in the stress treatment, the level of water deficit was intensified in the second experiment, resulting in a soil water potential of approximately -800 kPa compared to -400 kPa in the first experiment.

Replication and Sample Size:

In this experiment, a total of twenty-four plants were cultivated. Initially, four plants were designated for pre-treatment destructive measurements. Following this, ten plants were allocated to receive the stress treatment, while another ten were assigned to the control treatment. Subsequently, within each treatment group, five plants underwent post-treatment destructive measurements, while the remaining five underwent a rewatering phase before subsequent destructive measurements.

Randomization:

The plants were arranged in 6 blocs, with the treatments alternated within the bloc to minimize potential spatial effects.

Experimental Timeline:

As in the first experiment, this study consisted of three phases:
1) Growing Phase: Plants were grown for six weeks with regular watering (July 11th - August 31st, 2023).

2) Treatment Phase: Specific treatments were applied to plant groups for two weeks (August 31st - September 19th, 2023).

3) Rewatering Phase: Plants underwent rewatering to recover from stress (September 19th - September 26th, 2023).

Plant material:

The second experiment utilized the same maize variety as the first (Maize B104, obtained from the Louvain Institute of Biomolecular Science and Technology). Seed sterilisation and germination procedures were replicated precisely.

Environment:

The experiment was conducted within the greenhouse facilities of the UCLouvain. Temperature and humidity levels naturally fluctuated within the greenhouse environment. Throughout the

study, the average temperature recorded was 24.73°C, with a range between 20.15°C and 35.98°C. Humidity levels varied with an average of 69.06%, ranging from 33.70% to 91.21%.

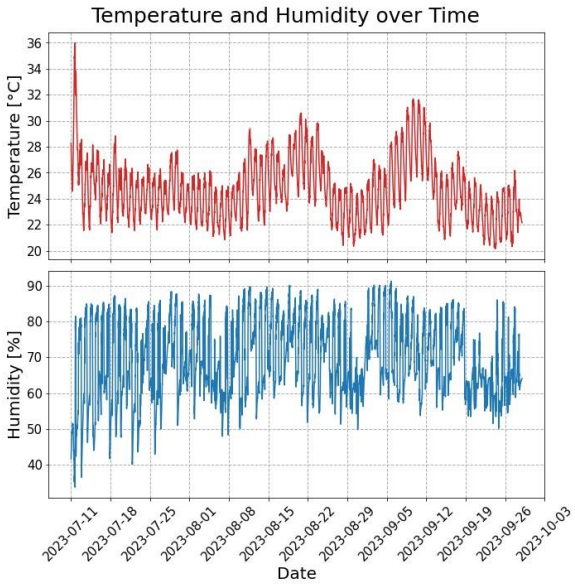

Substrate:

The substrate used in this experiment was different than the one used in the first one. The substrate was obtained through the University of Bayreuth in Germany. We used the loam that was obtained as described in the article “Experimental platforms for the investigation of spatiotemporal patterns in the rhizosphere—Laboratory and field scale” (Vetterlein et al., 2021).

Pots:

In this experiment, MXC 14 circular pots manufactured by Pöppelmann were employed. The diameter and height of these pots were respectively 14 cm and 10.9 cm, providing an approximate capacity of 1 litre. Each pot was filled with 1145 grams of soil. Similarly to the first experiment, an aluminium sheet was utilised to mitigate direct evaporation.

Watering:

The plants were nurtured with a Hoagland solution. Throughout the growing phase, each plant was monitored and watered to maintain its field capacity weight. Field capacity, determined to be 333 ml per pot using methods consistent with the first experiment, served as the benchmark for watering adjustments.

As the plants matured, watering frequency increased accordingly, mirroring the protocol established in the first experiment. During the treatment phase, plants subjected to stress were carefully watered with the aim of maintaining soil water potential around -800 kPa which is equivalent to pF 3.9. The watering regimen for stressed plants was tailored to ensure soil conditions remained within the desired range, with each plant's water weight adjusted based on the initial scale measurements taken upon reaching -800 kPa.

Measurements:

<u>Continuous measurements :</u>

Transpiration rate – scale

All the plants were placed on weighing scales to monitor their total transpiration and transpiration rate. The scales used were the EK-15KL model, accompanied by the Win CT software operating on a computer as a datalogger, both supplied by A&D company. Consistent with the approach in the first experiment, the software was programmed to record weight measurements every 15 minutes. The collected data were then processed to extract the total transpiration between two watering events and calculate the transpiration rate.

Soil water potential – TEROS 21

The procedures for monitoring soil water potential using Teros 21 sensors were identical to those described in the first experiment. The sensors were installed in the soil of each pot, positioned at a depth of approximately half the pot height. Data collection was facilitated by a CR800 data logger.

Leaf water potential - Psychrometer

The leaf water potential was measured using PSY1-Stem psychrometers from ICT International, with procedures identical to the first experiment. Psychrometers were placed on the sixth or seventh fully ligulated leaves and connected to a data logger during both treatment and rewatering phases.

10.2. Annex 2: Experiment 1 Soil water potential graphs

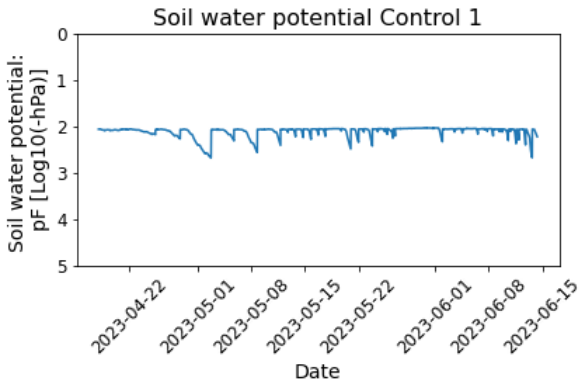

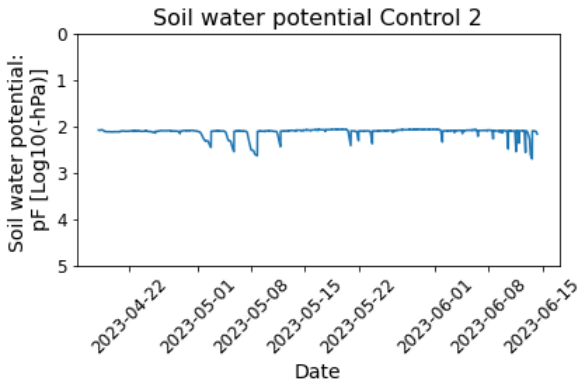

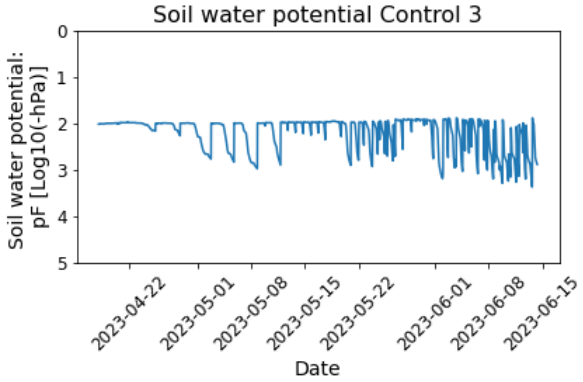

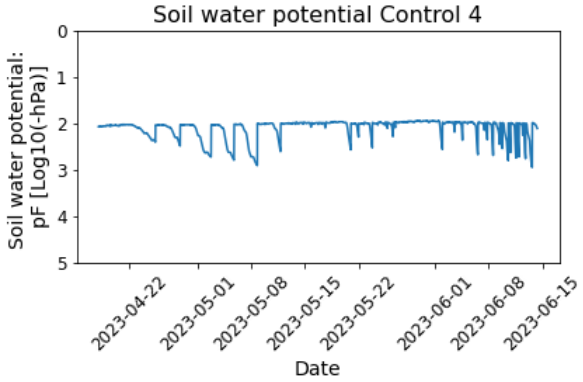

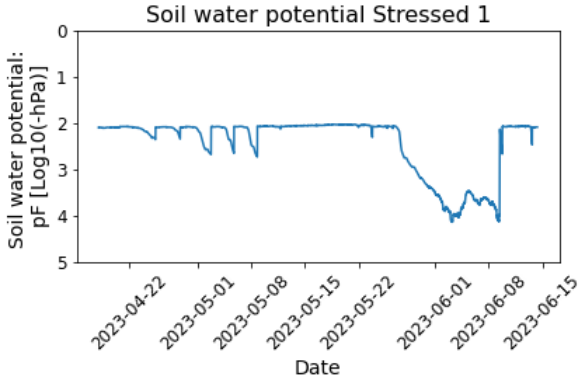

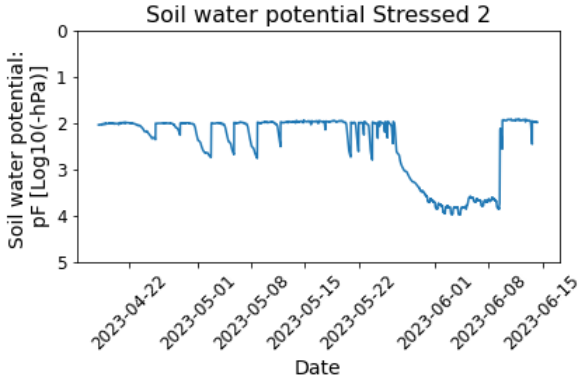

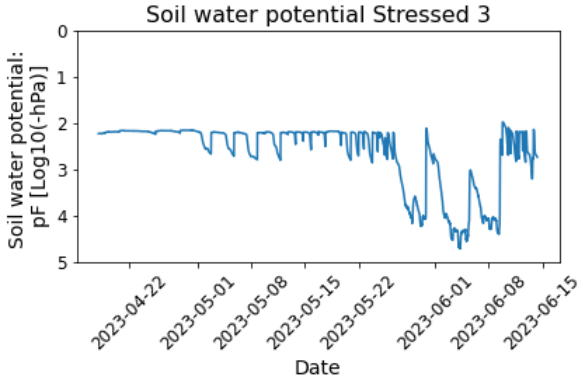

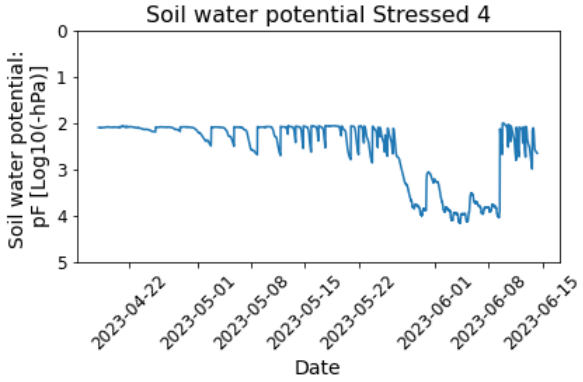

10.3. Annex 3: Experiment 1 Leaf water potential measured with psychrometer graphs

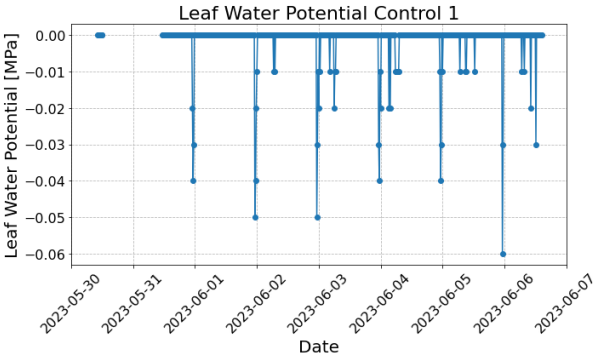

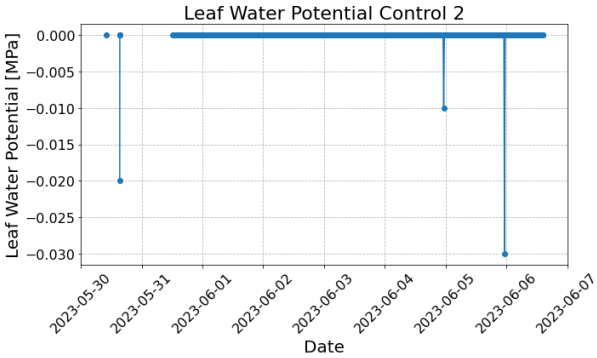

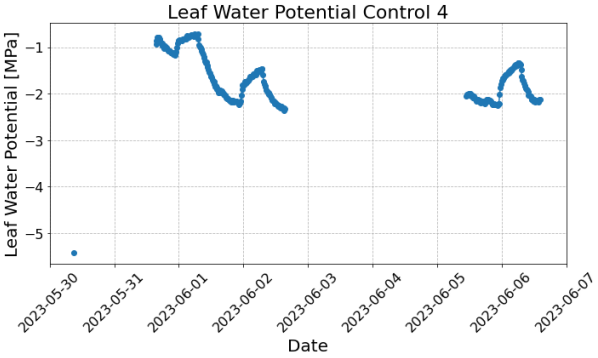

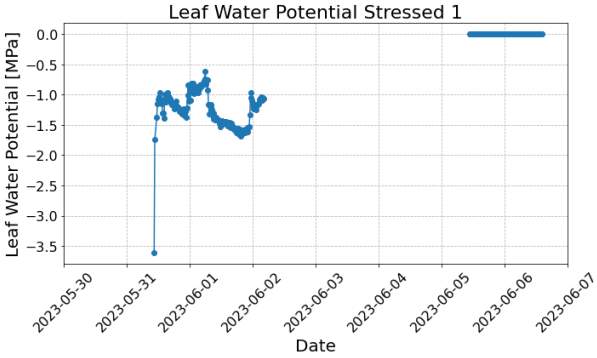

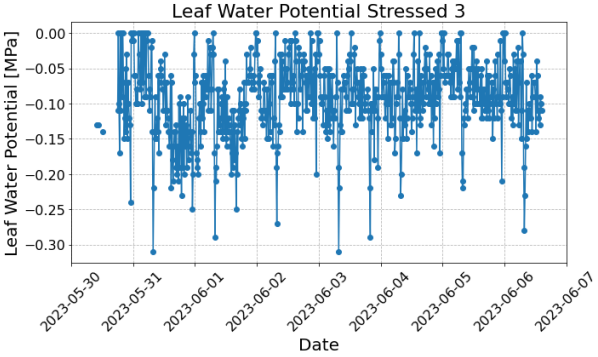

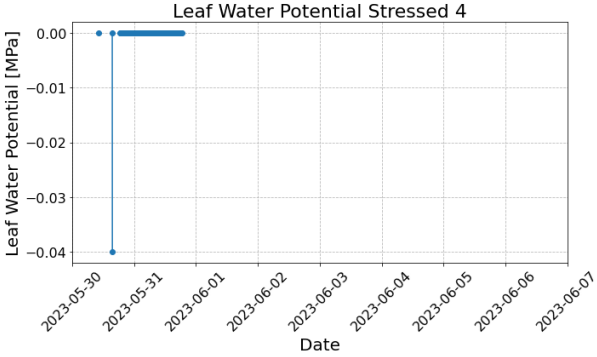

10.4. Annex 4: Experiment 1 Transpiration graphs

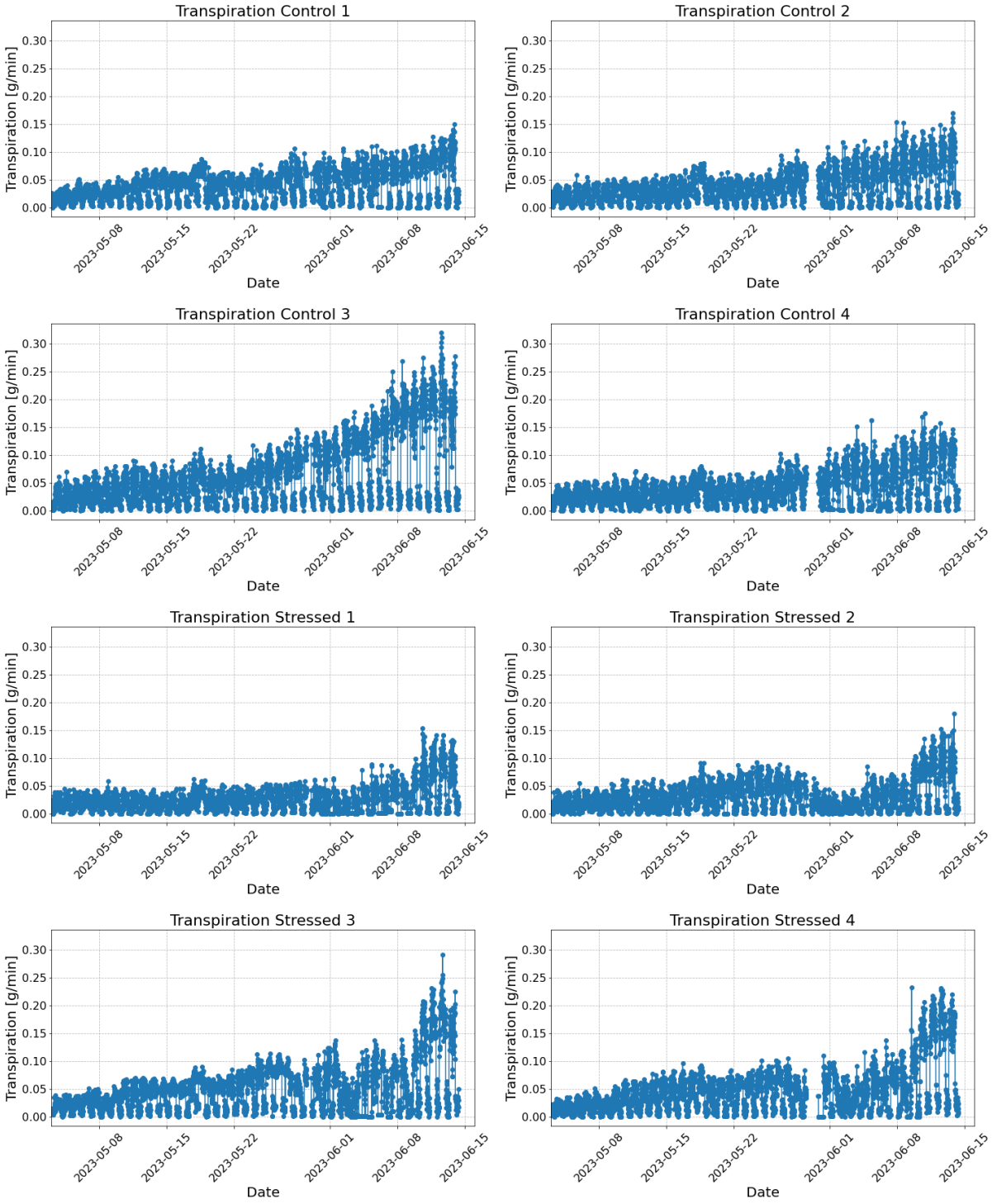

10.5. Annex 5: Pipeline 1 protocol

Root surface

General information

This protocol will guide you through the different steps that you need to follow in order to obtain the root surface. The root surface can be used to normalise other measurement or directly to compare your plants.
From your plants to the root surface you will need to follow 4 steps:

1) Extracting/cleaning the roots
2) Scanning the roots
3) Image treatment with ImageJ
4) Conversion of pixels into cm^2

Start by downloading the folder "root_to_surface".

Step 1: Extracting/cleaning the roots

Starting from plants in pots you will obtain a cleaned root system for each plant.

Material

- Your plants;
- Gardening hose with adjustable spray nozzle;
- Grid table;
- One water container for each plant;

Preparation

For each plant prepare a container and mark it with the identification of your plant.
Prepare the grid table usually behind the greenhouse, and the hose.
Bring your plants in their pots and, if it is not already done, cut the plant at the collar.

Cleaning

Always use a "gentle" spray type to avoid damaging the roots.
Start by spraying the top of your pot while rotating it and inclining it or putting it on its side in order to get rid of the substrate on the top. Then if possible spray from the bottom to erode the substrate in the bottom or pushing the content of the pot out of it. And when it is possible extract the roots and substrate from the pot, then spray the content on the sides to erode all the substrate. Ensure to get rid of a maximum of the substrate, and try to have the cleanest root as possible, then place the root system in the container prepared for this plant. Proceed like this for all your plants.

Step 2: Scanning the roots

From your cleaned root systems you will obtain images from the roots.

Material

- Your root systems;
- A calibration shape of known surface (ex: 10 cm² metal disk);
- A scanner (Epson Perfection V850 Pro);
- A computer with the scanner software (Epson Scan) and Excel and the downloaded folder "roots_to_surface";
- A transparent container for the scans with high sides;
- A blade or knife;

Scanner configuration

- Install the corresponding software on your computer (Epson Scan);
- Unlock the 2 locks;
- Unsure that the hinges are placed correctly in the holes;
- Connect the scanner to your computer (USB cable);
- Switch on the scanner;
- Start Epson Scan;
- Choose the professional mode ("Mode professionnel");
- Use the following configuration shown on figure1, you might need to adjust the resolution depending on the kind of root you are scanning (600ppi for maize, 1200ppi for tomatoes);

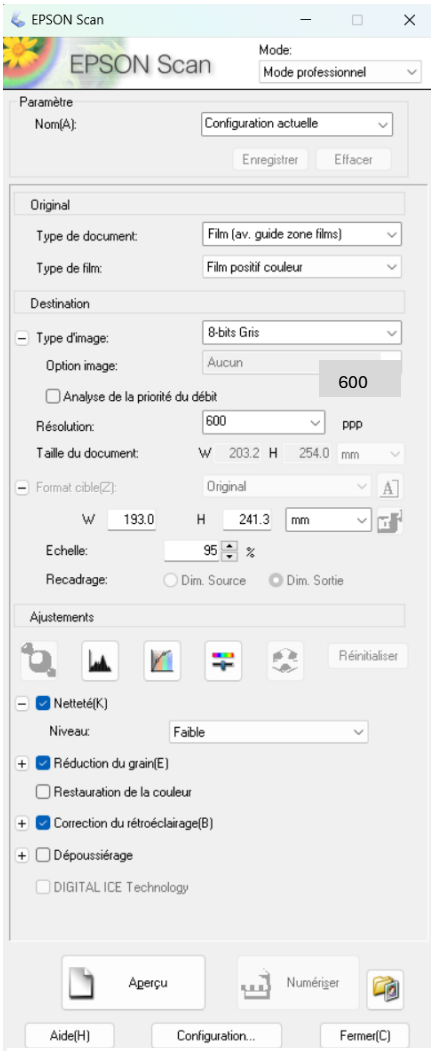

Figure 50: Scanner configuration

Calibration scans
The calibration scans need to be saved in the subfolder "calibration_scans" located in the "roots_to_surface" and "task_folder" folders.
Before scanning place correctly the transparent container in the scanner (use the visual marks on the sides of the scanner), then you can proceed with 3 scans of your calibration shape. For the first scan, place your shape in the middle of your container then click on the preview button ("Aperçu") and then click on the digitise button ("Numériser"). You should obtain a scan with your shape in the middle, call this scan "middle". Then you will place your calibration shape on the left and call this scan "left" then do the same on the right, make sure that your calibration shape is at least 1 cm away from the recipient lateral edge.

On figure 2 there is a view of the four scans you should have in your calibration_scans folder:

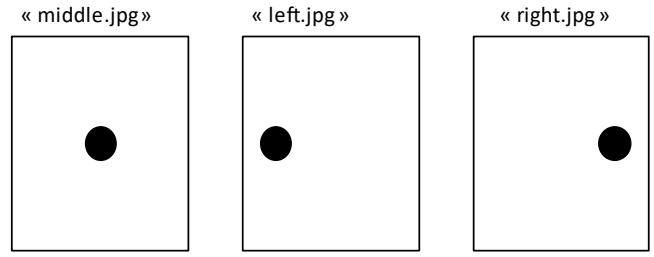

Figure 51: Calibration scans

Root preparation
Use the blade or knife to cut your root systems into smaller bits that cand be scanned.
Be careful to keep separated the roots from different plants.

Root scans
First, place your container in the scanner (be careful to put it correctly and follow the visual marks) and fill it partially with water.
Then place some roots in the container, put them in a visible way (not too packed together and not too close to the edges of the container, at least 1 cm away from it). Make sure there is no bubbles, add water if needed then you can scan.
Save your root scans in the subfolder "root_scans" and name each scan with a number from 0001 to x (with x your total number of scans).
While scanning update the Excel file located in the folder "id_tab" by completing the columns "Scan" and "ID", the column Scan should contain the number of the scan and the column ID should contain your plant ID.
Once your scan is done and saved, you can empty the container and proceed with the following scan and repeat this procedure for all the remaining scans.
Then save the Excel file containing the Scan and associated ID.

Step 3: Image treatment with ImageJ

ImageJ treatment will convert your scans into black and white images and count the percentage of black pixels thus the percentage of pixels that the roots recover.

Material

- Your scan images (calibration and root scans);
- A computer with the ImageJ software;

Preparation

- Open ImageJ;
- Click on "Analyze" > "Set Measurements…"
- In the new window select the option as shown on figure 3 and click on ok;

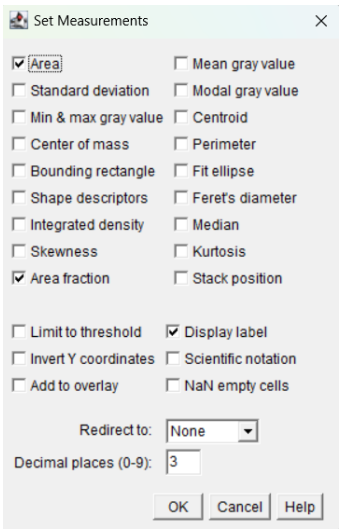

Figure 52: ImageJ set measurement window

- Click on "File" > "Open…" and open one of your roots scan (in the folder "root_scans");
- Click on "Plugins" > "Macros" > "Record…";
- Click on the rectangle below the "File" button and select a rectangle on your image (to exclude the container sides);
- Click on "Image" > "Crop";
- Click on "Image" > "Adjust" > "Threshold…"
- On the window that appeared select the superior threshold (the second cursor line) that is the best to see your roots in the example on the figure 4 the threshold has been set to 180.

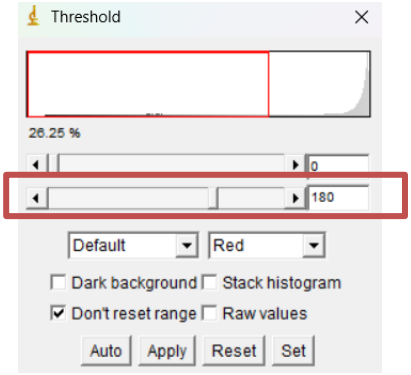

Figure 53: ImageJ treshold window

- When you have found the adequate threshold and selected the option as shown on the figure 3, click on "Apply";
- Click on "Process" > "Noise" > "Despeckle";

- If there is a lot of noise you can repeat the previous process;
- Click on “Analyze” >“Measure” you should get a window results that looks like the figure 5;

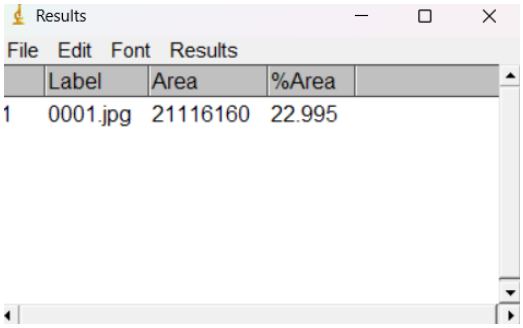

Figure 54: ImageJ result window

- The recorder window should look like the figure 6;

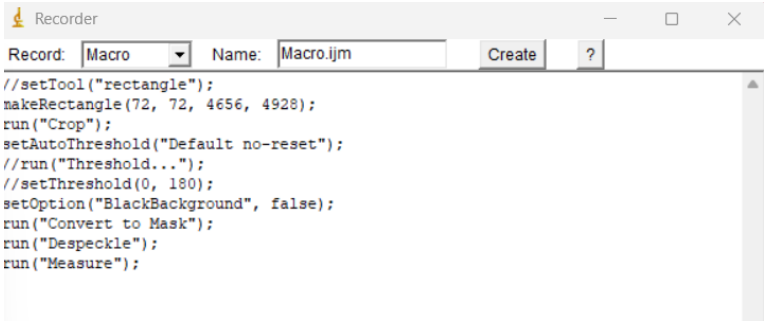

Figure 55: ImageJ recorder window

- On the recorder window click on the “Create” button;
- On the Macro.ijm window click on “File” > “Save As…” and save the Macro in the instruction folder;
- You can then close ImageJ, do not save anything after saving your Macro;

ImageJ image treatment

- Open ImageJ;
- Click on “Procees” > “Batch” > “Macro”;
- In the Batch Process window (figure 7) select your input folder(root_scans) and output folder (root_image);
- Click on open and select the macro you just created and saved in the instruction folder;

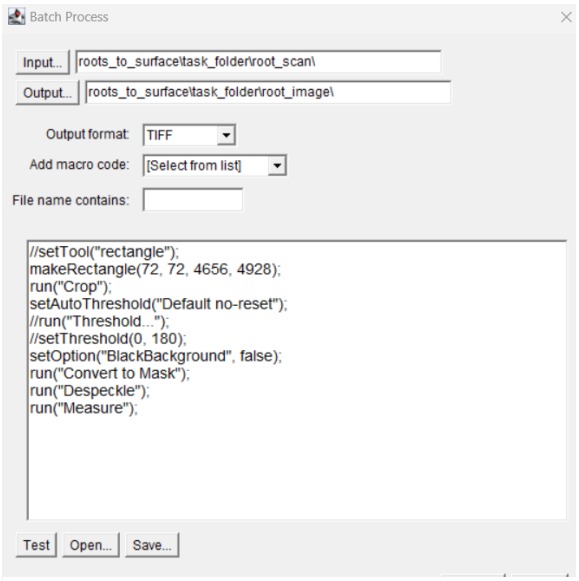

Figure 56: ImageJ batch process window

- Click on process;
- You will get a new window of result (figure 8);

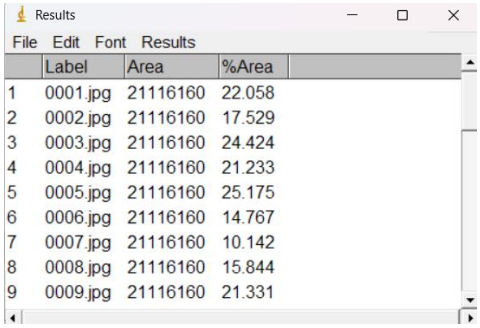

Figure 57: ImageJ result window after the batch process

- On the result window, click on "File" > "Save As…" select the destination folder to be root_tab and name your CSV as you wish;

Repeat the same process for the calibration scan, except this time use the calibration_scans, calibration_image and calibration_tab folders.

Step 4: Pixels to surface with Jupyter notebook

The Jupyter notebook called pix_to_surf will use your CSV files from the previous step and calculate the surface of the root projection on the scans. It will give you two CSV files, one giving you the result image by image and the other one giving you the result for each plant.

Material

- Your tabs from the previous steps;
- A computer with python (jupyter notebook);

Preparation

- Open the jupyter notebook code called pix_to_surf.ipynb placed in the instruction folder;
- Follow the instructions given in the jupyter notebook and then run the code;

Results

Once the code has done its job properly you should find the results in the subfolder "result_tab". There are two CSV files being generated, "combined_df" with all the information for each image and "summary_data" that sums up the result for each plant.

10.6. Annex 6: Pipeline 1 Jupyter notebook

Converting pixels into a surface after the imageJ treatment of root scans

This jupyter notebook is designed to process data from ImageJ. It converts the pixels into a surface in cm² and it groups your measurements by plants (in the case that you had more than one scan by plants).

In order for this code to work properly you need to have followed the protocols for the scan and the imageJ treatment properly.

Now, follow the two steps below, and everything should work smoothly (hopefully)!

Step 1: Preparing the Data and Folders

Inside the prepared folder named "task_folder," among the subfolders you should find four subfolders precisely named as written here:

- *root_tab*
- *result_tab*
- *calibration_tab*
- *id_tab*

In the *root_tab* folder, you should have your CSV file generated by the ImageJ treatment. This file should contain four columns (, `Label`, `Area`, `%Area`):

1. The first column has no name and serves as the index.
2. The second column is labeled `Label` and contains the name of the image with the extension (for example: "0001.jpg").
3. The third column is labeled `Area` and contains the total number of pixels in the image.
4. The fourth column is labeled `%Area` and contains the percentage of black pixels in the image.

Ensure the *result_tab* folder is empty.

In the *calibration_tab* folder, you should have your CSV file with the calibration data obtained from ImageJ. It should have five columns (, `Label`, `Area`, `%Area`, `cm2`). You have to add yourself the last column and complete the corresponding surface in cm² for each line. Once you have added the last column save the CSV file.

In the *id_tab* folder, put the CSV file containing the list of scans and associated plants. It should contain two columns (`Scan`, `ID`):

1. The first column is named `Scan` and contains the scan name without the extension (for example: "0001").
2. The second column is named `ID` and contains the plant ID.

Step 2: Specify the Working Directory and Run the Code

In the code below, specify the directory of your task folder by modifying the line: `base_dir = r'/path/to/your/task_folder'`.
Then, just run the code, sit back, relax, and enjoy the result! Check the *output* folder to see if it worked properly.
If it didn't, verify that you have followed the instructions in all the protocols properly.
If, even after following the instructions, it is still not working properly, then you can try to analyze the `pixtosurf_backcode.py` file.

```
# Define the base directory by replacing the path with the path to your task
folder
base_dir = r'/path/to/your/task_folder'

# Here is an example of what it should look like :
# base_dir = r'C:\Users\...\...\roots_to_surface\task_folder'

#And then just run the code!

import os
script_dir = os.path.join(os.path.dirname(base_dir), 'instruction', 'code',
'pixtosurf_backcode.py')
exec(open(script_dir).read())
```

10.7. Annex 7: Pipeline 1 python script

```
# Import necessary libraries
import pandas as pd; import os
from fuzzywuzzy import process
from fuzzywuzzy import fuzz
import re

# Function to find the closest name using fuzzy string matching
def find_closest_name(target, choices):
    closest_match, score = process.extractOne(target, choices)
    return closest_match

# Function to find subfolders with close names
def find_subfolders(base_dir):
    expected_subfolders = ['root_tab', 'result_tab', 'calibration_tab',
'id_tab']
    available_subfolders = [folder for folder in os.listdir(base_dir) if
os.path.isdir(os.path.join(base_dir, folder))]

    closest_matches = {}
    for folder in expected_subfolders:
        closest_matches[folder] = find_closest_name(folder,
available_subfolders)

    return closest_matches

# Function to get directories for input, calibration, id, and output
def dir_folders (base_dir):
    subfolder_matches = find_subfolders(base_dir)
    input_dir = os.path.join(base_dir, subfolder_matches['root_tab'])
    calibration_dir = os.path.join(base_dir,
subfolder_matches['calibration_tab'])
    id_dir = os.path.join(base_dir, subfolder_matches['id_tab'])
    output_dir = os.path.join(base_dir, subfolder_matches['result_tab'])
    return input_dir,calibration_dir,id_dir,output_dir


# Function to check if folders exist
def check_folders(base_dir):
    subfolder_matches = find_subfolders(base_dir)
    paths = {
        'root_tab': os.path.join(base_dir, subfolder_matches['root_tab']),
        'calibration_tab': os.path.join(base_dir,
subfolder_matches['calibration_tab']),
        'id_tab': os.path.join(base_dir, subfolder_matches['id_tab']),
        'result_tab': os.path.join(base_dir, subfolder_matches['result_tab'])
    }
```

```
    # Check if folders exist
    for folder_name, folder_path in paths.items():
        if not os.path.exists(folder_path):
            raise FileNotFoundError(f"The folder '{folder_path}' does not
exist.")

    # Check if folders are unique
    if len(set(paths.values())) < len(paths):
        raise ValueError("It seems that at least one of the subfolders is not
named properly")
check_folders(base_dir)

# Function to find the closest match for a target column name in a DataFrame
def find_closest_match(target, df):
    target_name = target.lower()
    column_names = df.columns.tolist()
    best_match = max(column_names, key=lambda name: fuzz.ratio(target_name,
name.lower()))

    # Handle the case where the best_match is None
    if best_match is None:
        raise ValueError("No suitable match found.")

    # Rename the column in the DataFrame to lowercase
    df.rename(columns={best_match: best_match.lower()}, inplace=True)
    best_match = best_match.lower()
    return best_match, df

# Function to process the calibration data
def calibration_fct(directory):
    invent = [f for f in os.listdir(directory) if f.endswith('.csv')]
    if not invent:
        raise FileNotFoundError("No CSV files found in the calibration
folder.")
    elif len(invent) > 1:
        raise ValueError("Only one CSV file should be present in the
calibration folder.")
    file = os.path.join(directory, invent[0])
    df = pd.read_csv(file, sep=None)

    area_target_column_name = 'Area'
    area_col, df = find_closest_match(area_target_column_name, df)

    percent_area_target_column_name = '%Area'
    percent_area_col, df = find_closest_match(percent_area_target_column_name,
df)

    cm2_target_column_name = 'cm2'
    cm2_col, df = find_closest_match(cm2_target_column_name, df)
```

```
    # Calculate number of pixels and cm²
    df['pixels'] = df.apply(
        lambda row: row[area_col] * (row[percent_area_col] /100), axis=1
        )

    # Filter out rows with 0 cm² and calculate pixel/cm²
    valid_data = df[df[cm2_col] != 0]
    pixel_per_cm2 = valid_data['pixels'].mean() / valid_data[cm2_col].mean()

    # Calculate mean value and noise
    #noise_data = df[df[cm2_col] == 0]
    #noise = noise_data['pixels'].mean()
    #return df, pixel_per_cm2, noise
    return df, pixel_per_cm2

# Function to process the ID data
def id_fct(directory):
    invent = [f for f in os.listdir(directory) if f.endswith('.csv')]
    if not invent:
        raise FileNotFoundError("No CSV files found in the id folder.")
    elif len(invent) > 1:
        raise ValueError("Only one CSV file should be present in the id
folder.")
    file = os.path.join(directory, invent[0])
    df = pd.read_csv(file, sep=None)
    return df

def remove_hidden_characters(input_string):
    if isinstance(input_string, (str, bytes)):
        return re.sub(r'[^\x20-\x7E]', '', str(input_string))
    else:
        return input_string

# Main data processing function
def data_fct():
    # Get directory paths
    directory, calibration_dir, id_dir, output_dir = dir_folders(base_dir)

    # Process calibration data
    scan_plant_id = id_fct(id_dir)
    calib_df, calib_surf = calibration_fct(calibration_dir)

    # Process input data
    invent = [f for f in os.listdir(directory) if f.endswith('.csv')]
    dfs = {}  # Dictionary to store DataFrames for each plant ID
    summary_data = []
    for file in invent:
        df_name = os.path.splitext(file)[0]
```

```
        file_path = os.path.join(directory, file)
        df = pd.read_csv(file_path, index_col=0, sep=None)

        # Use fuzzy string matching to find the closest column name
        scan_target_column_name = 'Scan'
        scan_col, scan_plant_id = find_closest_match(scan_target_column_name,
scan_plant_id)

        ID_target_column_name = 'ID'
        ID_col, scan_plant_id = find_closest_match(ID_target_column_name,
scan_plant_id)

        label_target_column_name = 'Label'
        label_col, df = find_closest_match(label_target_column_name, df)

        area_target_column_name = 'Area'
        area_col, df = find_closest_match(area_target_column_name, df)

        percent_area_target_column_name = '%Area'
        percent_area_col, df =
find_closest_match(percent_area_target_column_name, df)

        df[label_col] = df[label_col].str.split('.').str[0]
        df['pixels'] = df.apply(lambda row: row[area_col] *
(row[percent_area_col] / 100), axis=1)
        df['cm2'] = df['pixels'].apply(lambda pixels: pixels / calib_surf)

        # Apply remove_hidden_characters to Label and Scan columns
        df[label_col] = df[label_col].apply(remove_hidden_characters)
        scan_plant_id[scan_col] =
scan_plant_id[scan_col].apply(remove_hidden_characters)
        scan_plant_id[ID_col] =
scan_plant_id[ID_col].apply(remove_hidden_characters)

        # Convert columns to a common data type (object) before merging
        df[label_col] = df[label_col].astype(int)
        scan_plant_id[scan_col] = scan_plant_id[scan_col].astype(int)

        # Merge based on the closest column name
        df = pd.merge(df, scan_plant_id, left_on=label_col, right_on=scan_col,
how='left')
        df = df.drop(columns=scan_col)

        # Separate data into dataframes for each plant
        plant_dfs = {}
        for name, group in df.groupby(ID_col):
            plant_dfs[name] = group
        dfs[df_name] = plant_dfs
```

```
        # Add data for the summary dataframe
        for plant_name, plant_df in plant_dfs.items():
            num_scans = len(plant_df)
            total_cm2 = plant_df['cm2'].sum()
            summary_data.append([plant_name, num_scans, total_cm2])

    summary_df = pd.DataFrame(summary_data, columns=['Plant Name', 'Number of
Scans', 'Total cm2'])
    # Concatenate all DataFrames in dfs into one DataFrame
    combined_df = pd.concat([df for df_list in dfs.values() for _, df in
df_list.items()], ignore_index=True)
    summary_df.to_csv(os.path.join(output_dir, 'summary_data.csv'),
index=False)
    combined_df.to_csv(os.path.join(output_dir, 'combined_df.csv'),
index=False)
    return combined_df, summary_df


# Run the data processing function and get the resulting DataFrames
combined_df, summary_df = data_fct()

# Print the first few rows of the resulting DataFrames
print(combined_df.head())
print(summary_df.head())
```

10.8. Annex 8: Pipeline 2 python script

```
import pandas as pd
import numpy as np
from datetime import timedelta
import os
from dateutil.parser import parse
import re

# Data import paths and settings
folder_path = r'C:\Users\franc\Documents\UNIF\UNIF 2023_2024\Master
thesis\exp1\Data exp\Balance\to_pipeline2/'
column_names = ['date', 'time', 'weight']
column_used = [0, 1, 2, 4]
light_schedule_path = r'C:\Users\franc\Documents\UNIF\UNIF 2023_2024\Master
thesis\exp1\Data exp\Balance\day_night.xlsx'
light_H_df = pd.read_excel(light_schedule_path)
light_H_df['Date'] = light_H_df['Date'].dt.strftime('%d/%m/%Y')

# Data handling settings
watering_treshold = 7.5
time_delta_min = 15

date1 = pd.to_datetime('2023-04-19 00:00:00')

#Data saving
output_dir_all = r'C:\Users\franc\Documents\UNIF\UNIF 2023_2024\Master
thesis\exp1\Data exp\pipeline2_exp1\transpiration'
output_dir_watering = r'C:\Users\franc\Documents\UNIF\UNIF 2023_2024\Master
thesis\exp1\Data exp\pipeline2_exp1\watering'


# Functions for data processing
def dir_fct(base_directory, csv_file):
    return os.path.join(os.path.dirname(base_directory), csv_file)

def detect_and_convert_date_format(sample_date):
    possible_formats = [
        '%d-%m-%y', '%d/%m/%Y', '%m/%d/%Y', '%Y-%m-%d', '%m-%d-%Y',
        '%Y/%m/%d', '%d.%m.%Y', '%Y.%m.%d', '%m/%d/%y', '%d/%m/%y'
    ]
    target_format = '%d/%m/%Y'
    for format in possible_formats:
        try:
            parsed_date = parse(sample_date, dayfirst=True)
            return parsed_date.strftime(target_format)
        except ValueError:
            pass
    return None
```

```
def split_filename(file):
    base_name = os.path.splitext(file)[0]
    match = re.match(r"([a-zA-Z]+)(\d*)", base_name)
    if match:
        return f"{match.group(1)} {match.group(2)}" if match.group(2) else
match.group(1)
    return base_name



def determine_day_or_night(row):
    time = row['DateTime']
    light_on = row['H light on']
    light_off = row['H light off']
    if light_on > light_off:
        return 'night' if time >= light_on or time <= light_off else 'day'
    return 'day' if light_on <= time <= light_off else 'night'

def find_next_correct_index(df_all_merged, current_index,
previous_correct_weight):
    for i in range(current_index + 1, len(df_all_merged)):
        if df_all_merged.loc[i, 'tag PP'] == 'watering':
            return None, None
        if df_all_merged.loc[i, 'tag PP'] in ['ok','PP2'] and
df_all_merged.loc[i, 'weight'] <= previous_correct_weight:
            return i, df_all_merged.loc[i, 'weight']
    return None, None


def detect_outliers(df, column_name, date_column, previous_tag_col, tag_col,
window_days=3, mad_threshold=1.5):
    df = df.copy()
    df[date_column] = pd.to_datetime(df[date_column])
    df = df.sort_values(by=date_column)

    # Create intermediary DataFrame for all rows
    intermediary_df = df[[date_column,
column_name]].copy().dropna(subset=[column_name]).set_index(date_column)

    # Filter out rows with specific tags for rolling statistics calculation
    if previous_tag_col in df.columns:
        df_filtered_for_stats = df[~df[previous_tag_col].isin(['smaller',
'PP1', 'outlier', 'datalogging failure'])]
        intermediary_df_filtered = df_filtered_for_stats[[date_column,
column_name]].copy().dropna(subset=[column_name]).set_index(date_column)

        # Calculate rolling statistics
```

```
        intermediary_df_filtered['rolling_median'] =
intermediary_df_filtered[column_name].rolling(window=7, center=True,
min_periods=1).median()
        intermediary_df_filtered['rolling_mad'] =
intermediary_df_filtered[column_name].rolling(window=7, center=True,
min_periods=1).apply(lambda x: np.median(np.abs(x - np.median(x))), raw=True)
        intermediary_df_filtered['threshold'] = mad_threshold *
intermediary_df_filtered['rolling_mad']

        # Apply these statistics to the original intermediary DataFrame
        intermediary_df =
intermediary_df.join(intermediary_df_filtered[['rolling_median',
'rolling_mad', 'threshold']], how='left')
    else:
        # Calculate rolling statistics for all data if no tag column is
specified
        intermediary_df['rolling_median'] =
intermediary_df[column_name].rolling(window=7, center=True,
min_periods=1).median()
        intermediary_df['rolling_mad'] =
intermediary_df[column_name].rolling(window=7, center=True,
min_periods=1).apply(lambda x: np.median(np.abs(x - np.median(x))), raw=True)
        intermediary_df['threshold'] = mad_threshold *
intermediary_df['rolling_mad']

    # Compute the mask for outliers
    intermediary_df['mask'] = np.abs(intermediary_df[column_name] -
intermediary_df['rolling_median']) <= intermediary_df['threshold']

    # Calculate rolling mean and std based on the filtered data
    filtered_df = intermediary_df[intermediary_df['mask']]
    filtered_df = filtered_df[~filtered_df.index.duplicated(keep='first')]

    rolling_mean = filtered_df[column_name].rolling(window=7, center=True,
min_periods=1).mean()
    rolling_std = filtered_df[column_name].rolling(window=7, center=True,
min_periods=1).std()

    # Reindex to match original DataFrame
    intermediary_df['rolling_mean'] =
rolling_mean.reindex(intermediary_df.index).fillna(method='ffill')
    intermediary_df['rolling_std'] =
rolling_std.reindex(intermediary_df.index).fillna(method='ffill')

    # Calculate z-scores and detect outliers
    intermediary_df['z_scores'] = (intermediary_df[column_name] -
intermediary_df['rolling_mean']) / intermediary_df['rolling_std']
    intermediary_df['is_outlier'] = (intermediary_df['z_scores'] > 3) |
(intermediary_df['z_scores'] < -3)
```

```
    # Update the tag column
    intermediary_df[tag_col] = intermediary_df['is_outlier'].map({True:
'outlier', False: 'ok'})

    # Reset index and merge results back to the original DataFrame
    intermediary_df = intermediary_df.reset_index()

    return df.merge(intermediary_df[[date_column, tag_col]], on=date_column,
how='left')

def scale_extract(base_dir, col_used, col_name, watering_treshold):
    # Get list of files in the base directory
    invent = [f for f in os.listdir(base_dir)]
    extract_data = {}
    watering_dfs = {}

    for file in invent:
        df_name = split_filename(file)
        file_path = dir_fct(base_dir, file)

        df = pd.read_csv(file_path, header=None, usecols=col_used,
index_col=0, sep=None, engine='python').reset_index(drop=True)
        df.columns = col_name
        df['converted_date'] =
df['date'].apply(detect_and_convert_date_format)
        df['DateTime'] = pd.to_datetime(df['converted_date'] + ' ' +
df['time'], format='%d/%m/%Y %H:%M:%S')
        df['date'] = df['converted_date']
        df = df.drop(columns=['converted_date'])

        # Round DateTime to the nearest 15 minutes and calculate time
differences
        df['DateTime'] = df['DateTime'].dt.round('15min')
        df = df.sort_values(by=['DateTime', 'weight'], ascending=[True,
False], na_position='last')
        df = df.drop_duplicates(subset=['DateTime'],
keep='first').reset_index(drop=True)
        df['time_diff'] = df['DateTime'].diff()
        condition = df['time_diff'] != pd.Timedelta(minutes=time_delta_min)
        df['delta_weight'] = df['weight'].diff()
        df.loc[condition, 'delta_weight'] = np.nan

        # Merge with light schedule and determine day/night
        df = pd.merge(df, light_H_df, left_on='date',
right_on='Date').drop(columns='Date')
        df['H light on'] = pd.to_datetime(df['date'] + ' ' + df['H light
on'].astype(str), format='%d/%m/%Y %H:%M:%S')
```

```
        df['H light off'] = pd.to_datetime(df['date'] + ' ' + df['H light
off'].astype(str), format='%d/%m/%Y %H:%M:%S')
        df['Day/Night'] = df.apply(determine_day_or_night, axis=1)

        # Separate day and night data for negative delta weights
        df_night = df[(df['Day/Night'] == 'night') & (df['delta_weight'] <=
0)].copy()
        df_day = df[(df['Day/Night'] == 'day') & (df['delta_weight'] <=
0)].copy()
        df_delta_positive = df[df['delta_weight'] > 0].copy()

        # Detect outliers in day and night data
        df_outliers_day = detect_outliers(df_day, 'delta_weight',
'DateTime','tag','tag', window_days=3, mad_threshold=1.5)
        df_outliers_night = detect_outliers(df_night, 'delta_weight',
'DateTime','tag','tag', window_days=3, mad_threshold=1.5)


        # Tag positive delta weights above threshold
        df_delta_positive['tag'] = df_delta_positive['delta_weight'].apply(
            lambda x: 'above threshold' if x > watering_treshold else
'smaller')

        #Tag nan data
        df_nan = df[pd.isna(df['delta_weight'])].copy()
        df_nan['tag'] = 'datalogging failure'

        # Merge positive and negative delta weights
        df_all_merged = pd.concat([df_outliers_day, df_outliers_night,
df_delta_positive,df_nan]).sort_values(by='DateTime').reset_index(drop=True)

        # Initial tag correction based on fraction threshold
        fraction_threshold = 0.75
        df_all_merged['tag PP'] = df_all_merged['tag'].map({
            'outlier': 'outlier',
            'above threshold': 'watering',
            'smaller': 'smaller',
            'ok': 'ok'
        })

        for i in range(len(df_all_merged) - 1):
            current_tag = df_all_merged.loc[i, 'tag']
            next_tag = df_all_merged.loc[i + 1, 'tag']
            current_delta_weight = df_all_merged.loc[i, 'delta_weight']
            next_delta_weight = df_all_merged.loc[i + 1, 'delta_weight']

            if (current_tag == 'outlier' and next_tag == 'above threshold') or
\
               (current_tag == 'above threshold' and next_tag == 'outlier'):
```

```
                abs_current = abs(current_delta_weight)
                abs_next = abs(next_delta_weight)
                smallest = min(abs_current, abs_next)
                largest = max(abs_current, abs_next)

                if smallest / largest >= fraction_threshold:
                    df_all_merged.loc[i, 'tag PP'] = 'PP1'
                    df_all_merged.loc[i + 1, 'tag PP'] = 'PP2'
                else:
                    if current_tag == 'above threshold':
                        df_all_merged.loc[i, 'tag PP'] = 'watering'
                        df_all_merged.loc[i + 1, 'tag PP'] = 'outlier'
                    elif current_tag == 'outlier':
                        df_all_merged.loc[i, 'tag PP'] = 'outlier'
                        df_all_merged.loc[i + 1, 'tag PP'] = 'watering'
            elif (current_tag == 'datalogging failure'):
                df_all_merged.loc[i, 'tag PP'] = 'datalogging failure'

        # Extract watering events
        condition = df_all_merged['tag PP'] == 'watering'
        df_water =
df_all_merged[condition].sort_values(by='DateTime').reset_index(drop=True)

        # Initialize columns for interpolation
        df_all_merged['Prev_W_corr'] = None
        df_all_merged['Prev_idx_corr'] = None
        df_all_merged['Next_W_corr'] = None
        df_all_merged['Next_idx_corr'] = None
        df_all_merged['Wcorr'] = df_all_merged['weight']
        df_all_merged['Tag corr'] = None

        # Initialize previous correct weight and index
        previous_correct_weight = None
        previous_correct_index = None

        for i in range(len(df_all_merged)):
            current_tag = df_all_merged.loc[i, 'tag PP']

            # Update the previous correct weight and index columns
            df_all_merged.loc[i, 'Prev_W_corr'] = previous_correct_weight
            df_all_merged.loc[i, 'Prev_idx_corr'] = previous_correct_index

            # Find the next correct index and weight if the previous correct
index is not None
            if previous_correct_index is not None:
                df_all_merged.loc[i, 'Next_idx_corr'], df_all_merged.loc[i,
'Next_W_corr'] = find_next_correct_index(df_all_merged, i,
previous_correct_weight)
```

```
            # Apply interpolation for 'smaller', 'PP1', and 'ok' when the
current value is larger than the previous correct value
            if current_tag in ['smaller', 'PP1','outlier'] or (current_tag ==
'ok' and previous_correct_weight is not None and df_all_merged.loc[i,
'weight'] > previous_correct_weight):
                if df_all_merged.loc[i, 'Prev_idx_corr'] is not None and
df_all_merged.loc[i, 'Next_idx_corr'] is not None:
                    prev_weight = df_all_merged.loc[i, 'Prev_W_corr']
                    next_weight = df_all_merged.loc[i, 'Next_W_corr']
                    prev_idx = df_all_merged.loc[i, 'Prev_idx_corr']
                    next_idx = df_all_merged.loc[i, 'Next_idx_corr']
                    if next_idx - prev_idx > 0:  # Ensure no division by zero
                        df_all_merged.loc[i, 'Wcorr'] = prev_weight -
((prev_weight - next_weight) / (next_idx - prev_idx)) * (i - prev_idx)
                        df_all_merged.loc[i, 'Tag corr'] = 'Corrected'

            # Update previous correct weight and index based on conditions
            if current_tag in ['watering']:
                previous_correct_weight = df_all_merged.loc[i, 'weight']
                previous_correct_index = i
            elif current_tag == 'ok':
                if previous_correct_weight is not None and
previous_correct_weight >= df_all_merged.loc[i, 'weight']:
                    previous_correct_weight = df_all_merged.loc[i, 'weight']
                    previous_correct_index = i
                elif i > 0 and df_all_merged.loc[i - 1, 'tag PP'] ==
'datalogging failure':
                    previous_correct_weight = df_all_merged.loc[i, 'weight']
                    previous_correct_index = i
                elif i == 0 or i == 1:
                    previous_correct_weight = df_all_merged.loc[i, 'weight']
                    previous_correct_index = i
            elif current_tag in ['datalogging failure'] and i != 0:
                df_all_merged.loc[i, 'Wcorr'] = np.nan
                previous_correct_weight = None
                previous_correct_index = None


        # Calculate corrected delta weights
        df_all_merged['corr_delta_weight'] = df_all_merged['Wcorr'].diff()
        df_all_merged.loc[condition, 'corr_delta_weight'] = np.nan


        # Separate day and night data for corrected delta weights
        df2_night = df_all_merged[(df_all_merged['Day/Night'] == 'night') &
(df_all_merged['corr_delta_weight'] <= 0)].copy()
        df2_day = df_all_merged[(df_all_merged['Day/Night'] == 'day') &
(df_all_merged['corr_delta_weight'] <= 0)].copy()
```

```
        # Detect outliers for corrected delta weights
        df2_outliers_day = detect_outliers(df2_day, 'corr_delta_weight',
'DateTime', 'tag', 'tag2', window_days=3, mad_threshold=1.5)
        df2_outliers_night = detect_outliers(df2_night, 'corr_delta_weight',
'DateTime', 'tag', 'tag2', window_days=3, mad_threshold=1.5)

        # Handle positive corrected delta weights
        df2_delta_positive = df_all_merged[(df_all_merged['corr_delta_weight']
> 0)].copy()
        df2_delta_positive['tag2'] =
df2_delta_positive['corr_delta_weight'].apply(lambda x: 'above threshold' if x
> watering_treshold else 'smaller')

        #Tag nan data
        df2_nan =
df_all_merged[pd.isna(df_all_merged['corr_delta_weight'])].copy()
        df2_nan.loc[df2_nan['tag'] != 'datalogging failure', 'tag2'] =
'watering'
        df2_nan.loc[df2_nan['tag'] == 'datalogging failure', 'tag2'] =
'datalogging failure'

        # Merge corrected positive and negative delta weights
        df2_all_merged = pd.concat([df2_outliers_day, df2_outliers_night,
df2_delta_positive,df2_nan]).sort_values(by='DateTime').reset_index(drop=True)

        # Filter data after the initial period
        df2_all_merged = df2_all_merged[df2_all_merged['DateTime'] > (date1 +
pd.DateOffset(weeks=2))].reset_index(drop=True)

        # Initialize transpiration column
        df2_all_merged['Transpiration [g/min]'] = np.nan

        # Compute transpiration rate for 'ok' tags
        for i in range(len(df2_all_merged)):
            if df2_all_merged.loc[i, 'tag2'] == 'ok':
                if df2_all_merged.loc[i, 'time_diff'] != 0:
                    df2_all_merged.loc[i, 'Transpiration [g/min]'] =
df2_all_merged.loc[i, 'corr_delta_weight'] / time_delta_min

        # Compute transpiration rate for other tags using mean of last 4 'ok'
values
        last_4_transpiration = []

        for i in range(len(df2_all_merged)):
            current_tag = df2_all_merged.loc[i, 'tag2']
            if current_tag != 'ok':
                if current_tag == 'datalogging failure':
                    df2_all_merged.loc[i, 'Transpiration [g/min]'] = np.nan
                elif last_4_transpiration:
```

```
                    mean_transpiration = np.mean(last_4_transpiration)
                    df2_all_merged.loc[i, 'Transpiration [g/min]'] =
mean_transpiration
            else:
                if not pd.isna(df2_all_merged.loc[i, 'Transpiration
[g/min]']):
                    last_4_transpiration.append(df2_all_merged.loc[i,
'Transpiration [g/min]'])

                if len(last_4_transpiration) > 4:
                    last_4_transpiration.pop(0)


        extract_data[df_name] = df2_all_merged
        watering_dfs[df_name] = df_water


    return extract_data, watering_dfs

extracted_data, watering_dfs = scale_extract(folder_path, column_used,
column_names, watering_treshold)




for df_name, df in extracted_data.items():
    output_file_path = os.path.join(output_dir_all, f"{df_name}.csv")
    df.to_csv(output_file_path, index=False)

for df_name, df in watering_dfs.items():
    output_file_path = os.path.join(output_dir_watering,
f"{df_name}_watering.csv")
    df.to_csv(output_file_path, index=False)
```

Maize (*Zea mays*) hydraulic responses to water deficit in controlled conditions

Maize (*Zea mays*) is a crucial global crop, dependent on water for optimal growth and productivity. With the increasing frequency and severity of droughts due to climate change, understanding maize's hydraulic responses to water deficit is becoming increasingly important.

The primary objectives of this study were twofold: first, to evaluate maize's hydraulic traits under controlled water deficit conditions, and second, to develop pipelines for processing and managing the resulting complex datasets. These objectives aimed to enhance the accuracy and reliability of future experiments investigating plant hydraulic responses to water stress.

The experimental protocol involved two treatments: well-watered (control) and water deficit, with the study structured into three phases: growing, treatment, and rewatering. Key measurements, including transpiration rate, soil and leaf water potential, root conductance, and root surface area, were recorded.

The results revealed significant differences in root hydraulic conductance across different experimental stages and in root conductivity within the stressed group, while no significant differences were observed between treatments in root surface area. Additionally, a significant interaction effect between treatment and stage was found in leaf water potential. Although partial, these findings provide valuable insights into maize's hydraulic responses under the experimental conditions.

The study also highlighted several challenges, such as maintaining consistent soil water potential, ensuring uniform stress across plants, and managing variations in environmental conditions within the controlled environment. These challenges underscored the complexity of studying maize's hydraulic responses under water deficit conditions and highlighted areas for improvement in experimental methodologies. This master thesis provides new pipelines for data management and insights for refining future experimental protocols, ultimately contributing to more reliable and accurate approaches for studying maize hydraulics under water stress.

Francis Mulligan

UNIVERSITÉ CATHOLIQUE DE LOUVAIN
Faculté des bioingénieurs
Croix du Sud, 2 bte L7.05.01, 1348 Louvain-la-Neuve, Belgique | **www.uclouvain.be/agro**